NASA Contractor Report 179573

Investigation of a GaAlAs Mach-Zehnder Electro-Optic Modulator

David M. Materna
Case Western Reserve University
Cleveland, Ohio

January 1987

Prepared for the
Lewis Research Center
Under Grant NCC 3-54

NASA

ACKNOWLEDGMENTS

I am especially grateful to Professor Altan M. Ferendeci for his for his guidance over the past year. I am indebted to Carl Radens and Professor Joseph T. Boyd of the University of Cincinnati for many enlightening discussions on optical waveguides. To Dr. Rainee Simons, for sharing his coplanar electrode programs and helping in many details of problem solution, I am grateful. I am grateful to Dr. Steven Marx and Andrew Dewa for their help in making the modulator mask. The work of Janis Hammonds on the optical test setup was also greatly appreciated.

Table of Contents

Chapter 1 : Introduction

Intensity modulation is a key element of optical communication systems. The intensity of light entering a fiber can be changed by varying the laser drive current (direct modulation) or by externally modulating light originating from a continuous wave laser. Direct modulation offers simplicity and low drive power but, is inherently limited at high frequencies due to laser relaxation resonance [1]. Also, modulation near the relaxation resonance requires that the laser be operated near its maximum output power resulting in accelerated degradation of the laser. External modulation requires greater microwave drive power, has added optical coupling power losses, and results in increased system complexity. However, external modulation is attractive because it does not have the the inherent bandwidth limitations of direct modulation. An external modulator fabricated on and using the electro-optic effect in Gallium Arsenide (GaAs) is even more attractive because it is potentially integrable with GaAs lasers. Integration of the laser with the modulator could reduce optical coupling losses and system complexity while allowing modulation at frequencies above the laser relaxation resonance.

The highest bandwidth external modulator reported is a lithium niobate ($LiNbO_3$) travelling wave Mach-Zehnder interferometer operating at 0.83 micron wavelength with a bandwidth of 17 GHz [2],[3],[4]. Recently, three electro-optic Mach-Zehnder modulators have been reported on GaAs at 1.3 micron wavelength [5],[6],[7]. The highest bandwidth achieved was 4.5 GHz [5] using bulk electrodes. The bandwidth of bulk electrode modulators is ultimately limited by the electrical RC time constant or the time required for the light to propagate through the modulator. Theoretically, these limitations can be overcome with transmission line electrodes. This was attempted by Lin [7] who obtained a bandwidth of 4.1 GHz. In the case of transmission line electrodes, the microwave signal propagates slower than the light and the bandwidth is limited by the "walkoff" between the two waves over the device length. Better matching of the microwave and light velocities offers a potential for higher bandwidth.

To integrate the modulator with a GaAs/GaAlAs heterostructure laser, it is necessary to have a modulator operating at 0.78-0.88 um wavelength. GaAs modulators and lasers could be integrated with other components on GaAs MMIC's (Monolithic Microwave Integrated Circuits) to form a fully integrated fiber

optic transmitter. This thesis will investigate for the first time a Mach-Zehnder electro-optic modulator fabricated on GaAs, operating at a wavelength of 0.82 um, and utilizing travelling-wave electrodes.

Some background information on fiber optic links, modulation techniques, and a review of previous work is provided in Chapter 2. Chapter 2 also describes some of the requirements of an integrable GaAs modulator. The electro-optic effect of GaAs is examined in chapter 3 along with the Mach-Zehnder intensity modulation scheme. Chapter 4 describes the investigation of low loss, single mode optical waveguides. The design of coplanar electrodes is discussed in Chapter 5 and a fully dimensioned modulator design is presented. The modulator bandwidth of 11.95 GHz is calculated along with its drive power requirement of 2.335 watts. The high drive power is an issue to be addressed in future experiments, but the theoretical bandwidth is higher than any reported GaAs modulator.

Chapter 2: Background

2.1 Motivation: Advantages of Fiber Optic Links

In the realm of high speed communications, fiber optic links offer several distinct advantages over traditional microwave electronics. These advantages encompass long distance communication links and short distance applications such as local area networks (LAN's) and antenna arrays. Low attenuation, low cost, immunity from electrical interference, light weight, and high bandwidth are all offered by fiber optic communications [1].

Long distance telephone communications can especially benefit from low attenuation, low cost, and the absence of electrical interference. These links usually operate at a laser wavelength of 1.3 microns where fused silica fibers exhibit their lowest attenuation. For example, silica based single-mode optical fibers offer losses of 0.47 dB/km at 1.3 - 1.6 microns [8]. This is three orders of magnitude smaller than RG-400 coaxial cable (1115 dB/km) and .141 semi-rigid coaxial cable (790 dB/km) when operating at 5 GHz [2]. This dramatically reduced attenuation means

fewer repeater stations over long hauls, resulting in lower system cost and complexity.

Short distance communication links are attracted by the light weight, reduced size, interference immunity, and high bandwidth of fiber optics [9]. Much space is occupied by copper cables used to interconnect computers in local area networks. Space is even more critical when trying to feed large antenna arrays. The hollow metal waveguides presently used in the 20 - 30 GHz satellite band are impractical for feeding the millions of elements engineers hope to use in the future. In addition, crosstalk between the closely spaced array elements can be reduced if not eliminated by using fiber optics. Weight is another major factor for antennas used on satellites which must be launched into space aboard rockets with limited payloads. Further reduction in size and weight is possible if the many copper cables can be replaced by a single optical fiber carrying frequency division multiplexed signals.

Fiber optics will not yet solve all of the problems mentioned above for antenna arrays. To date, no links above 17 GHz have been reported, making their application to the 20 - 30 GHz satellite band unrealizable. In addition, the power requirements of these short haul, high bandwidth links make them

impractical for satellite applications where the available power is limited. But, the tremendous advantages offered for high frequency communications by fiber optics make it an active area of research.

2.2 Direct vs. External Modulation

A typical fiber optic communication link is shown in figure 1. It shows the three major components of a communication link: the transmitter, the optical fiber as a transmission media, and the receiver. The light entering the fiber can be intensity modulated by either a direct or an external method. The definitions and advantages / disadvantages of these two methods will be examined in the following paragraphs.

A direct modulation scheme is shown in fig. 1b. Here, the RF signal is added to the laser diode bias current in a microwave matching network. In this way the laser intensity is modulated directly by changing the laser drive current. This method has the advantage of simplicity, but suffers from two disadvantages. First, the usable bandwidth is limited by the laser relaxation resonance which is determined by the laser cavity geometry and material parameters. To date, the

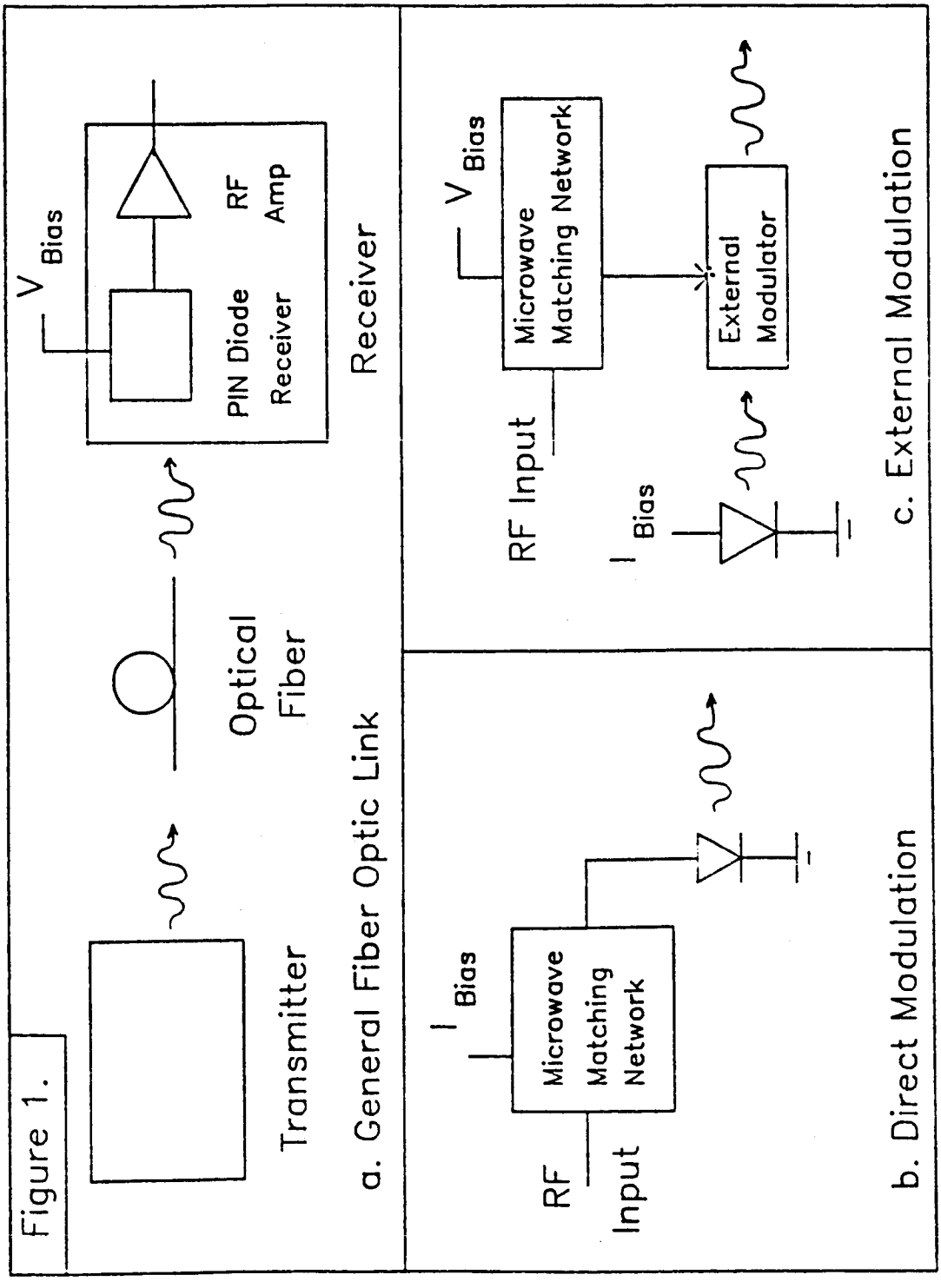
Figure 1.
Transmitter
Optical Fiber
PIN Diode Receiver
RF Amp
V Bias
Receiver
a. General Fiber Optic Link
I Bias
Microwave Matching Network
RF Input
b. Direct Modulation
V Bias
Microwave Matching Network
External Modulator
I Bias
c. External Modulation

highest direct modulation bandwidth reported is 16 GHz at room temperature, while up to 26.5 GHz has been achieved if the laser is cooled to -60^{o}C [10]. Second, the high bandwidths are only available when the lasers are operated at their maximum output power. This may result in faster degradation of the laser diode [1].

For operation above the laser relaxation resonance, an external modulation scheme (fig. 1c.) must be used. In this method, the laser is biased for continuous wave operation and the beam passes through an external "black box" for modulation. The "black box" can use any of a number of effects (electro-optic, acousto-optic, Franz-Keldysh effect, quantum wells, etc.) to achieve modulation. This thesis will approach only the linear electro-optic effect because it has shown the most promise in past modulator reportings. External modulation also suffers from two drawbacks. First, the system is made more complex by the addition of the external modulator element. Second, significant optical power losses result from coupling light into and out of the modulator. However, for modulation at frequencies above the relaxation resonance, there is no alternative to external modulation.

An external modulator integrated on the same chip as the laser source offers advantages over both direct

and external modulation. The laser resonances would not limit the modulation bandwidth because the laser would be operated as a continuous wave source. The optical coupling would be significantly improved by eliminating the laser-to-fiber and fiber-to-modulator junctions required by the conventional external modulator. System complexity would be reduced to the level of the direct modulator. This would be at the expense of a more complicated fabrication process to accomodate both the laser and modulator technologies. Overall, an "integrated external modulator" could combine the best of both worlds.

2.3 Review of Previous Work

As mentioned in the introduction, the highest bandwidth external modulator yet reported is a lithium niobate ($LiNbO_3$) device reported by Gee, Thurmond, and Yen [2],[3],[4]. This was a Mach-Zehnder modulator (fig. 2) utilizing the high (r_{33}) electro-optic coefficient of $LiNbO_3$ as well as travelling wave electrodes. It demonstrated a 3 dB bandwidth of 17 GHz and complete intensity modulation with 120 mW of drive power at 0.83 um wavelength. The change in electrode voltage required to swing from minimum light intensity

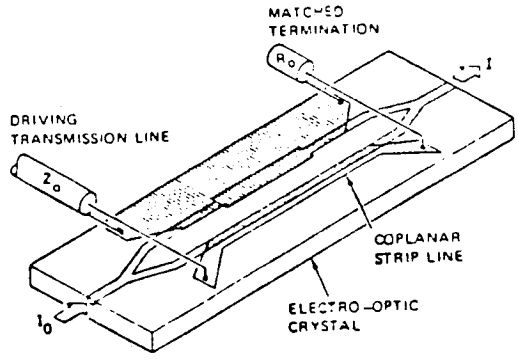

Figure 2. LiNbO3 Modulator [4]

at the output to maximum intensity was V_{Pi} = 5 V. Unfortunately, $LiNbO_3$ has limited optical power handling capabilities because it is a photorefractive material susceptible to optical damage [1]. Gee et. al. reported, "photo-induced optical throughput losses even at low optical power levels (<50 uW at 0.6328 um into 4 um channel waveguides)" [4]. In addition, questions have been raised about the DC bias stability of modulators fabricated on $LiNbO_3$. Ultimately, the technology barrier makes it impossible to grow $LiNbO_3$ on any semiconductor substrate. Therefore, integration of a $LiNbO_3$ modulator with a diode laser is also impossible.

The first high bandwidth GaAs modulator was reported by Donelly, Demeo, Ferrante, Nichols, and O'Donnell [11] in August of 1984. They demonstrated

modulation of 1.3 um light using a 2 mm interaction region [6]. They reported an extinction ratio* of 14.5 dB at the output with a V_{pi} of 22 V applied to one arm of the modulator. They reported a bandwidth of 2.2 GHz (~3.0 GHz small signal optical intensity bandwidth) which was limited by the RC time constant of the bulk electrodes used to establish the microwave field. One unusual feature of this modulator is that it used three guide couplers (fig. 3) to evenly couple light from the input guide into the modulator arms and then back into the output guide. While this is easier to fabricate than Y-branches, the interaction length for complete power transfer is critical and difficult to predict accurately.

The second high bandwidth GaAs modulator was reported by Buchmann, Kaufmann, Melchoir, and Grekos in March of 1985 [5]. It utilized the more traditional

---

*The extinction ratio is a measure of the ability of a modulator to change light intensity.

$$\text{extinction ratio} = \begin{cases} -10 \log (I_o - I_m)/I_o & I_m \leq I_o \\ -10 \log (I_m - I_o)/I_m & I_m \geq I_o \end{cases}$$

where I_o is the transmitted intensity when the maximum electrical signal is applied and I_m is the transmitted intensity when no electrical signal is applied [12].

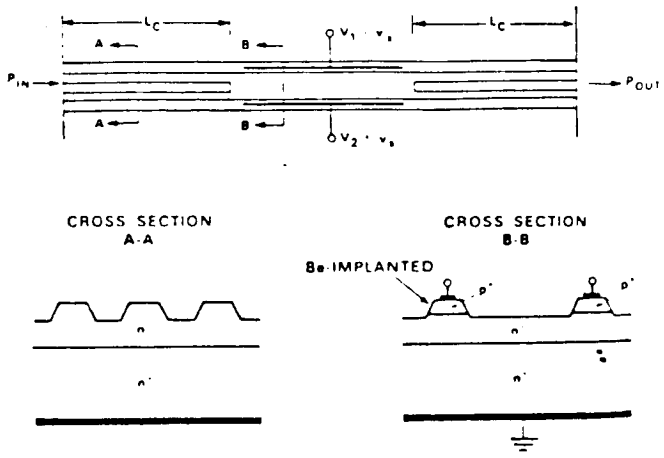

Figure 3. GaAs Modulator
using 3—Branch Couplers [6]

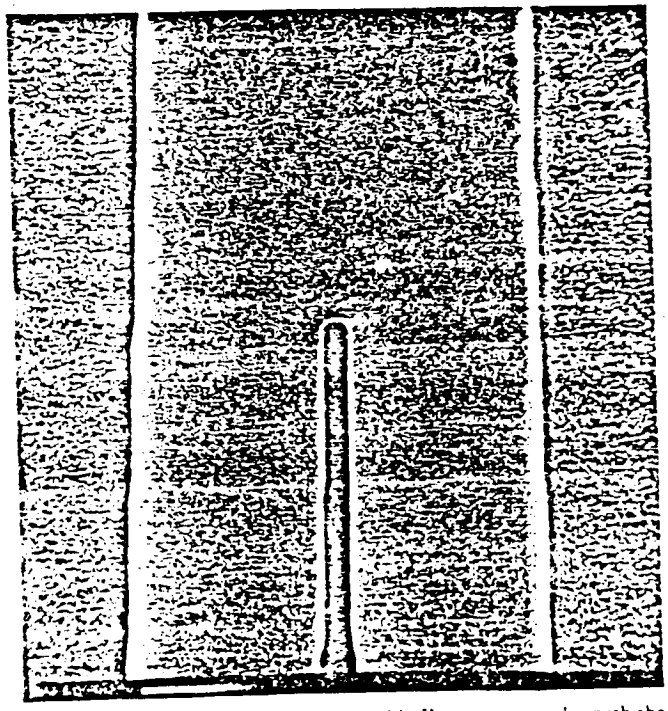

FIG 4. SEM picture of GaAs rib waveguide Y-junction coupler with sharp RIE formed branching tip. Mark is 2 μm. [5]

Y-branches for power splitting into (and combining out of) the modulator branches. The "Y" was fabricated by using reactive ion etching (RIE) to make a sharp tip with vertical waveguide sidewalls and thus reduce losses at the junction (fig 4). Their device demonstrated an extinction ratio of 12.7 dB using a V_{pi} of 13 V when operated in a push- pull configuration (opposite polarity voltages applied to each branch) at a wavelength of 1.3 um. The optical signal bandwidth was reported to exceed 4.5 GHz which is the highest yet reported for a GaAs modulator. As with the Donelly modulator, the bandwidth of this device was limited by the RC time constant of bulk electrodes.

Most recently, a GaAs modulator using travelling-wave electrodes was reported by Lin, Wang, and Houng in August of 1986 [7]. This device also operates at 1.3 um with an optical extinction ratio of 13 dB when a V_{pi} of 8 V is applied to one arm. It demonstrated an optical signal bandwidth of 4.1 GHz, limited by the "walkoff" between the microwave and optical fields. This "walkoff" is due to the fact that the microwave field propagates through the modulator's interaction region slower than the light. Though this modulator did not achieve a higher bandwidth than the Buchmann device, it is a milestone as the first travelling-wave GaAs

modulator. The travelling wave electrodes (with proper velocity matching) potentially offer a higher bandwidth than bulk electrodes [13].

2.4 Issues of Integration

All of the GaAs modulators reported have been designed to operate at a wavelength of 1.3 um. The motivation for this is best understood from a historical perspective on optical fibers. The earliest links operated exclusively near 0.8 um wavelength where fibers exhibited a local minimum in attenuation (fig. 5). In the mid 70's, improved fused silica fibers showed lower attenuation near 1.3 um and 1.6 um wavelengths.

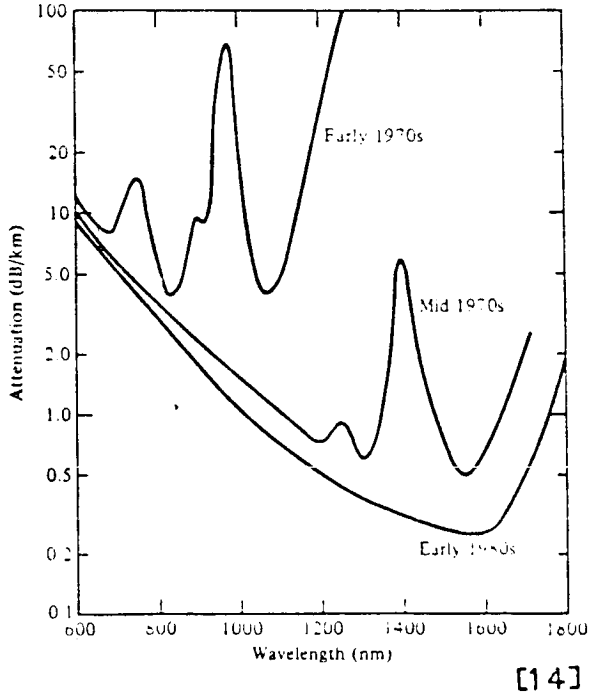

[14]

Figure 5. Fiber Attenuation vs. Wavelength

The choice of 1.3 um was driven by the availability of InGaAsP laser diodes operating at this wavelength. Some work at 1.6 um has more recently been undertaken to to take advantage of even lower attenuation at this wavelength in the 1980's. This historical evolution was directed by the need for extremely low losses in long distance communication links. However in short links, such as local area networks and antenna arrays, where the higher attenuation is tolerable, there are advantages to operating at shorter wavelengths (near 0.8 um).

Though no attempt to fabricate an integrated external modulator will be made in this thesis, it is an important long range technology goal. Lasers operating at a wavelength of 1.3 um are an InGaAsP technology grown epitaxially on InP substrates because there is good lattice matching between the InGaAsP layers and the InP substrate. Lattice matching is important to avoid thermal stresses when power is applied to the laser for long periods of time or near its threshhold current. The reported III-V modulators are either doped layers of GaAs or GaAs/GaAlAs heterostructures grown epitaxially on GaAs substrates. Before any attempt at integration is possible, both the modulator and laser must be fabricated on the same type of semiconductor substrate.

Poor lattice matching between InP and GaAs will make this difficult using the reported modulators and InGaAsP lasers. Semiconductor lasers using GaAs/GaAlAs heterostructures grown on a GaAs substrate are available in the wavelength range of 0.78 um - 0.88 um. If a modulator using films grown epitaxially on a GaAs substrate could be made to operate in this wavelength range, it would have the potential to be integrated with a laser on a GaAs substrate. In addition, GaAs MMIC (Monolithic Microwave Integrated Circuit) Technology is advancing rapidly. A GaAs modulator could be integrated with a laser and other transmitter components for a fully integrated fiber optic transmitter.

Unfortunately, making a modulator operate at the shorter wavelengths does not mean simply shining 0.82 um light into one of the previously reported modulators. In each of these modulators, the actual guiding layer carrying the light is GaAs. Figure 6 shows that GaAs has a high absorption coefficient at this wavelength [15]. This means that much of the light would simply be absorbed by the guide layer independent of the applied microwave field. This problem can be solved if GaAlAs layers are used to guide the light. The substitution of aluminum for gallium in the crystal lattice shifts the absorption edge to shorter wavelengths (fig. 6) giving

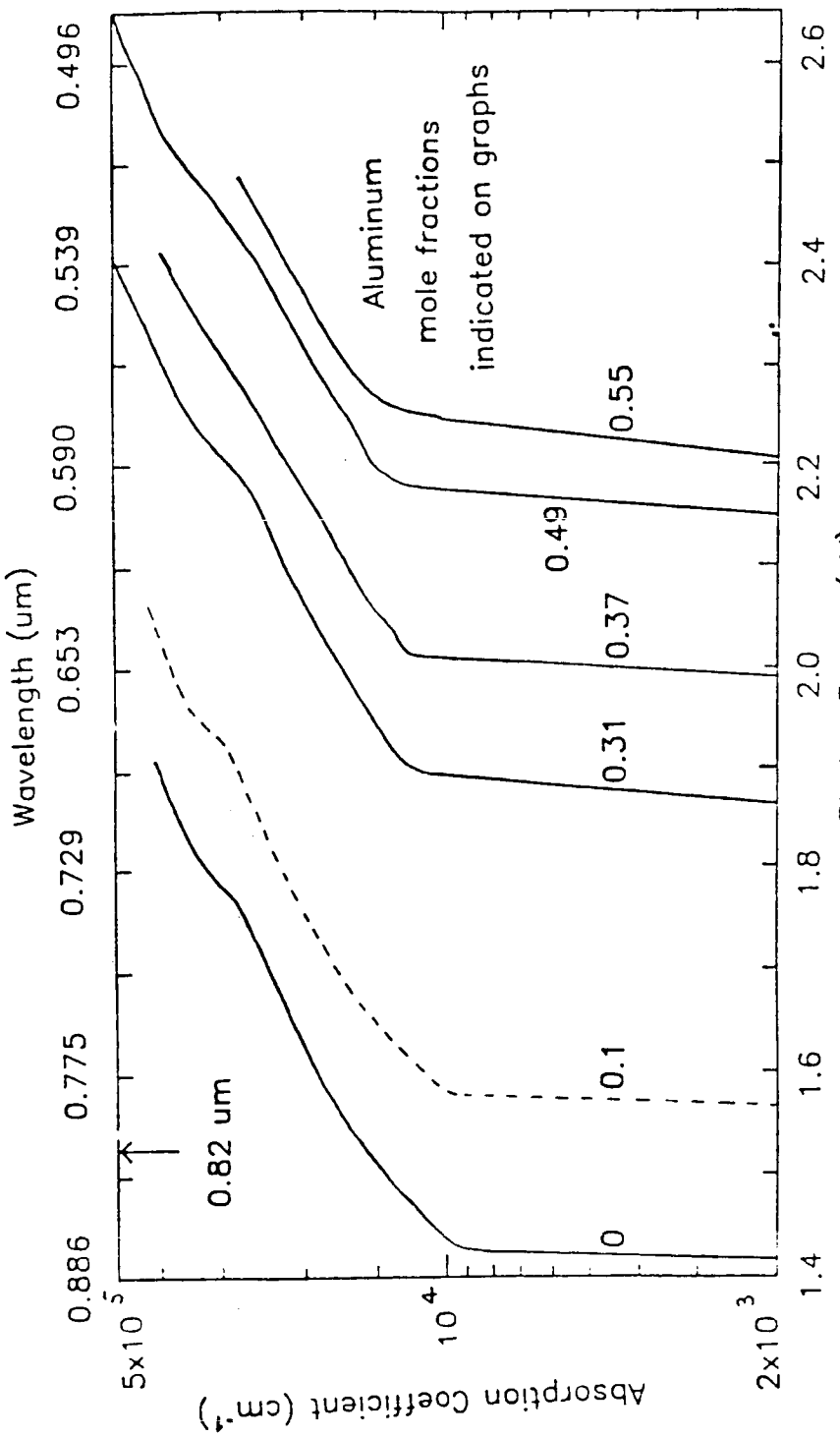

Figure 6. Absorption vs. Wavelength for GaAs & GaAlAs [15]

the GaAlAs layers low absorption coefficients at the wavelength of interest. This technique of using GaAlAs to reduce the absorption in a modulator has been demonstrated at low frequencies using a waveguide phase modulator operating at a wavelength of 0.88 um [16].

2.5 Problem Statement

Given the background presented in this chapter, it appears that before a laser and modulator can be integrated, a GaAs modulator operating at the wavelength of GaAs/GaAlAs heterostructure lasers must be designed. This thesis will investigate the design of a modulator fabricated on and using the electro-optic effect of GaAs while operating at a wavelength of 0.82 um. This includes utilization of the maximum electro-optic effect available in GaAs, the design of low loss single-mode optical waveguides, and travelling wave electrodes offering a potential for higher bandwidth. The required drive voltage and power of such a modulator will be theoretically determined along with the potential bandwidth.

Chapter 3: Electro-Optic Modulation in GaAs

3.1 Electro-Optic Effect of GaAs

In general, the electro-optic effect in a crystalline material is a change in its index of refraction in the presence of an externally applied electric field. This change can be proportional to the applied field (linear effect) or proportional to the square of the applied field (Kerr effect) [17]. GaAs, with its cubic lattice structure falls into the first category and exhibits the linear electro-optic effect [13].

The electro-optic effect in GaAs is a result of the fact that it is a birefringent material in the presence of an external field. That is, light propagating through the crystal can be decomposed into orthogonally polarized waves. These ordinary and extraordinary waves will propagate with different velocities. This results in a change in the direction (but not the magnitude) of the total optical field as it propagates through the material.

The change in the velocity of propagation can be described by a directionally dependent index of

refraction. This is because the velocity of propagation (v) in a material is related to the speed of light (c) through the index of refraction (n) by:

$$v = \frac{c}{n} \tag{3.1}$$

The index of refraction in any material can be fully described by an index ellipsoid.

$$\left[\frac{1}{n^2}\right]_1 x^2 + \left[\frac{1}{n^2}\right]_2 y^2 + \left[\frac{1}{n^2}\right]_3 z^2 + 2yz\left[\frac{1}{n^2}\right]_4 + 2xz\left[\frac{1}{n^2}\right]_5 + 2xy\left[\frac{1}{n^2}\right]_6 = 1 \tag{3.2}$$

Where the $(1/n^2)_i$ directional coefficients can be changed by the application af an external field. The equation is simplified (in the absence of an external field) if the x, y, and z coordinate axes are taken as the principal axes of the material. These are the orthogonal directions along which $\underline{D}$ and $\underline{E}$ remain parallel.

$$\frac{1}{n_x^2} + \frac{1}{n_y^2} + \frac{1}{n_z^2} = 1 \tag{3.3}$$

If the coordinate axes are defined as in (3.3), the principal planes will rotate relative to the fixed coordinate system and (3.2) must be used when the external field is applied. The six directional coefficients of the index ellipsoid change linearly with the applied field according to

$$\Delta \left[\frac{1}{n^2}\right]_i = \sum_{j=1}^{3} r_{ij} E_j \qquad (3.4)$$

where r_{ij} are the electro-optic coefficients of the material and j represents the 3 orthogonal components of the coordinate system (1=x, 2=y, 3=z).

To simplify the discussion, it is best to specify the crystal as GaAs at this point. GaAs falls into the zincblende class of cubic lattices where the only nonzero coefficients are $r_{41} = r_{52} = r_{63}$. Figure 7 shows the possible geometries with the corresponding index ellipsoids and relative phase shifts for zincblende crystals [18]. For the maximum phase shift, the geometry is repeated in figure 8 as it will be used for the modulator. The unprimed coordinates represent the principal system with no applied field, while the primed coordinates represent the principal system when the field is applied. The external applied field is:

$$\underline{E}_m = \frac{1}{\sqrt{2}} \left[\hat{a}_x + \hat{a}_y\right] E_m \qquad (3.5)$$

The equation of the index ellipsiod with the field applied is:

$$\left[\frac{x^2}{n_o^2}\right] + \left[\frac{y^2}{n_o^2}\right] + \left[\frac{z^2}{n_o^2}\right] + \frac{2r_{41}E_m}{\sqrt{2}}(yz + xz) = 1 \qquad (3.6)$$

	$E \perp (001)$ plane $E_x = E_y = 0 \quad E_z = E$	$E \perp (110)$ plane $E_x = E_y = \frac{E}{\sqrt{2}} \quad E_z = 0$	$E \perp (111)$ plane $E_x = E_y = E_z = \frac{E}{\sqrt{3}}$
index ellipsoid	$\frac{x^2+y^2+z^2}{n_0^2} + 2r_{41}Exy = 1$	$\frac{x^2+y^2+z^2}{n_0^2} + \sqrt{2}r_{41}E(yz+zx) = 1$	$\frac{x^2+y^2+z^2}{n_0^2} + \frac{2}{\sqrt{3}}r_{41}E(yz+zx+xy) = 1$
$n_{x'}$	$n_0 + \frac{1}{2}n_0^3 r_{41}E$	$n_0 + \frac{1}{2}n_0^3 r_{41}E$	$n_0 + \frac{1}{2\sqrt{3}}n_0^3 r_{41}E$
$n_{y'}$	$n_0 - \frac{1}{2}n_0^3 r_{41}E$	$n_0 - \frac{1}{2}n_0^3 r_{41}E$	$n_0 + \frac{1}{2\sqrt{3}}n_0^3 r_{41}E$
$n_{z'}$	n_0	n_0	$n_0 - \frac{1}{\sqrt{3}}n_0^3 r_{41}E$
$x'y'z'$ coordinate	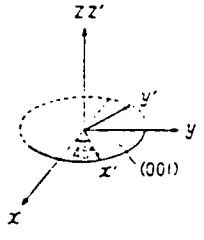	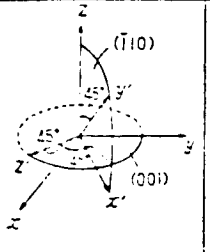	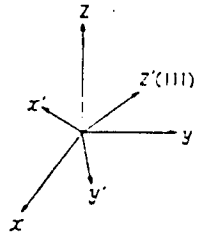
directions of optical path and axes of crossed polarizer	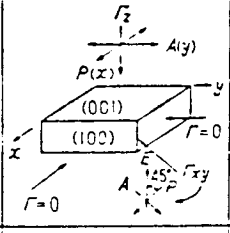	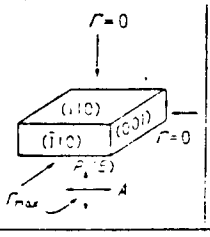	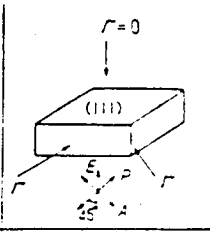
phase difference $\Gamma(V = Ed)$	$\Gamma_z = \frac{2\pi}{\lambda}n_0^3 r_{41}V$ $\Gamma_{xy} = \frac{\pi}{\lambda}\frac{l}{d}n_0^3 r_{41}V$	$\Gamma_{max} = \frac{2\pi}{\lambda}\frac{l}{d}n_0^3 r_{41}V$	$\Gamma = \frac{\sqrt{3}\pi}{\lambda}\frac{l}{d}n_0^3 r_{41}V$

Figure 7. Elecro-Optic Effect of Zincblende for 3 Geometries [18]

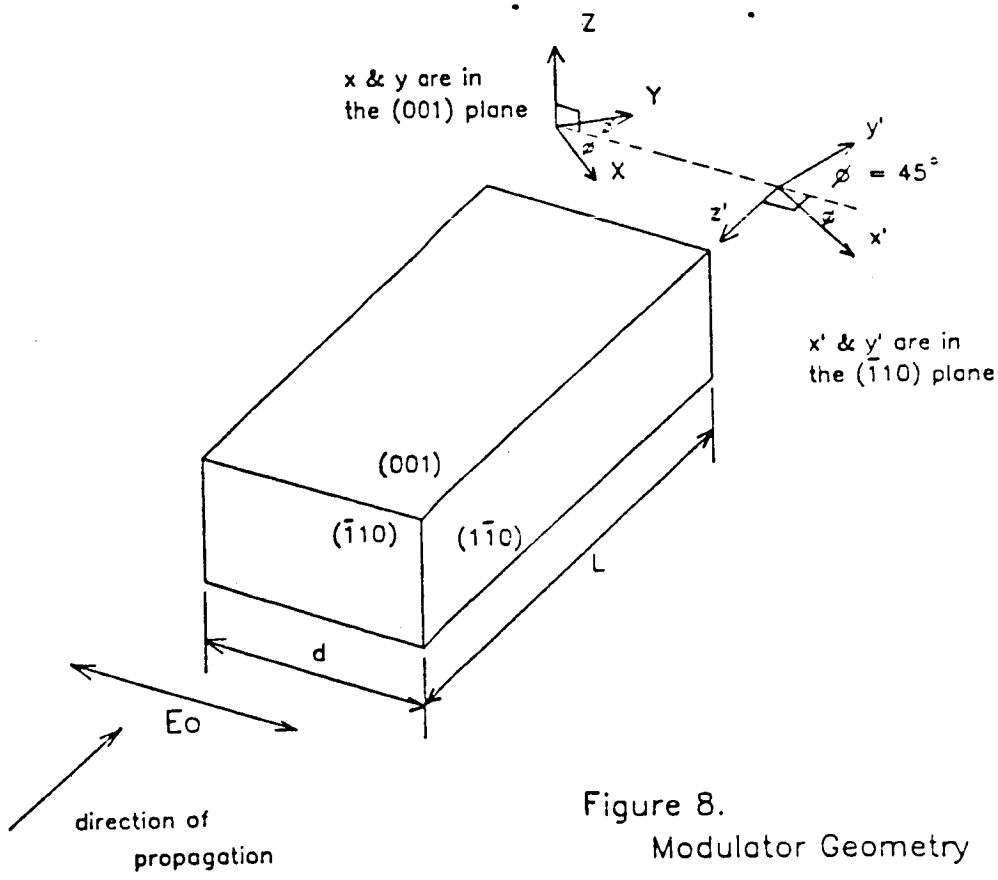

Figure 8.
Modulator Geometry

The equation shows that without any externally applied field, GaAs has the same index of refraction in all directions and is not birefringent at all. The coordinate systems are related by:

$$x = \frac{1}{\sqrt{2}}\left[\frac{x'+y'}{\sqrt{2}} + z'\right] \qquad (3.7.a)$$

$$y = \frac{1}{\sqrt{2}}\left[\frac{x'+y'}{\sqrt{2}} + z'\right] \qquad (3.7.b)$$

$$z = \frac{1}{\sqrt{2}}\left(y'-x'\right) \qquad (3.7.c)$$

If equations (3.7) are substituted into equation (3.6), the equation for the index ellipsoid becomes:

$$(x')^2\left[\frac{1}{n_o^2} - r_{41}E_m\right] + (y')^2\left[\frac{1}{n_o^2} + r_{41}E_m\right] + \frac{(z')^2}{n_o^2} = 1 \qquad (3.8)$$

The new $(1/n_x)^2$ can be read from the equation as:

$$\left(\frac{1}{n_{x'}}\right)^2 = \frac{1}{n_o^2} - r_{41}E_m \qquad (3.9)$$

If $n_{x'}$ is solved for and only the first term of a binomial expansion of n_o is used,

$$n_{x'} = n_o\left[1-n_o^2 r_{41}E_m\right]^{-\frac{1}{2}} \approx n_o\left[1+\frac{n_o^2 r_{41}E_m}{2}\right] \qquad (3.10)$$

similarly,

$$n_{y'} = n_o \left[1 - \frac{n_o^2 r_{41} E_m}{2} \right] \qquad (3.11)$$

while $n_{z'} = n_o$ is not effected by the applied field.

If an optical field (E_o) which is polarized parallel to the applied field is incident on the crystal,

$$\underline{E}_o = \frac{1}{\sqrt{2}} \left(\hat{a}_x + \hat{a}_y \right) E_o \qquad (3.12)$$

the relative phase shift induced by the crystal can be determined. For this particular field direction, the notation is independent of the coordinate system. That is:

$$\hat{a}_x + \hat{a}_y = \hat{a}_{x'} + \hat{a}_{y'} \qquad (3.13)$$

At the endface of the crystal, the optical field is:

$$\underline{E}_{out} = \frac{E_o}{\sqrt{2}} \left[\hat{a}_x e^{-jk_{x'}l} + \hat{a}_y e^{-jk_{y'}l} \right] \qquad (3.14)$$

and the relative phase shift of the orthogonal components is seen to be:

$$\Gamma = (k_{x'}l - k_{y'}l) = \frac{2\pi}{\lambda} l (n_{x'} - n_{y'}) \qquad (3.15.a)$$

$$= \frac{2\pi}{\lambda} l \left[(n_o + \tfrac{1}{2} n_o^3 r_{41} E_m) - (n_o - \tfrac{1}{2} n_o^3 r_{41} E_m) \right] \qquad (3.15.b)$$

$$\Gamma = \frac{2\pi l}{\lambda} n_o^3 r_{41} E_m \qquad (3.15.c)$$

These results are exactly those reported by Namba except for E_m. He chose to replace the general applied field with the field set up by parallel plate electrodes on the sides of the crystal. The more general expressions using E_m directly will be more useful in the Mach-Zehnder analysis of section 4.2.

In the foregoing analysis, GaAs has been analyzed as the electro-optic crystal. However, the absorption edge problem discussed in section 2.4 forces the use of GaAlAs for a modulator operating at 0.82 um wavelength. This discrepancy can be resolved by the following argument. The electro-optic effect is primarily determined by the structure of the crystal lattice. If the GaAlAs film layers are grown epitaxially on a GaAs substrate, these layers will have nearly the same crystallographic geometry, dimensions, and orientation of the GaAs substrate. Therefore, the electro-optic coefficient (r_{41}) and analysis of the epitaxially grown GaAlAs film layers will be taken as that of a bulk GaAs crystal. Data on the r_{41} coefficient of GaAs is included in Appendix A.

3.2 The Mach-Zehnder Modulator

The geometry used to determine the electro-optic effect in section 3.1 produces a phase shift between the primary orthogonal components of the optical field. This means that the intensity of the light is unchanged (neglecting losses in the crystal) while the polarization has been rotated through an angle $\Gamma / 2$ (fig. 9.a). For fiber optic communication systems, the easiest signal to detect is light intensity. The phase modulator could be converted to an intensity modulator by inserting another polarizer at the output [13],[19] (fig. 9a). As an alternative, a Mach-Zehnder interference scheme (fig. 9.b) can be used to achieve intensity modulation [19],[20]. Here, the input optical field is divided equally into the two arms of the modulator. An external field applied to the arms causes light in one arm to be phase shifted relative to the other. When recombined at the output, the light interferes and if the relative phase shift is 180^{o}, complete intensity modulation is observed. The Mach-Zehnder will be examined in more detail in the rest of this section.

A geometry in which the external field is applied to the modulator arms in opposite directions with a

Figure 9.

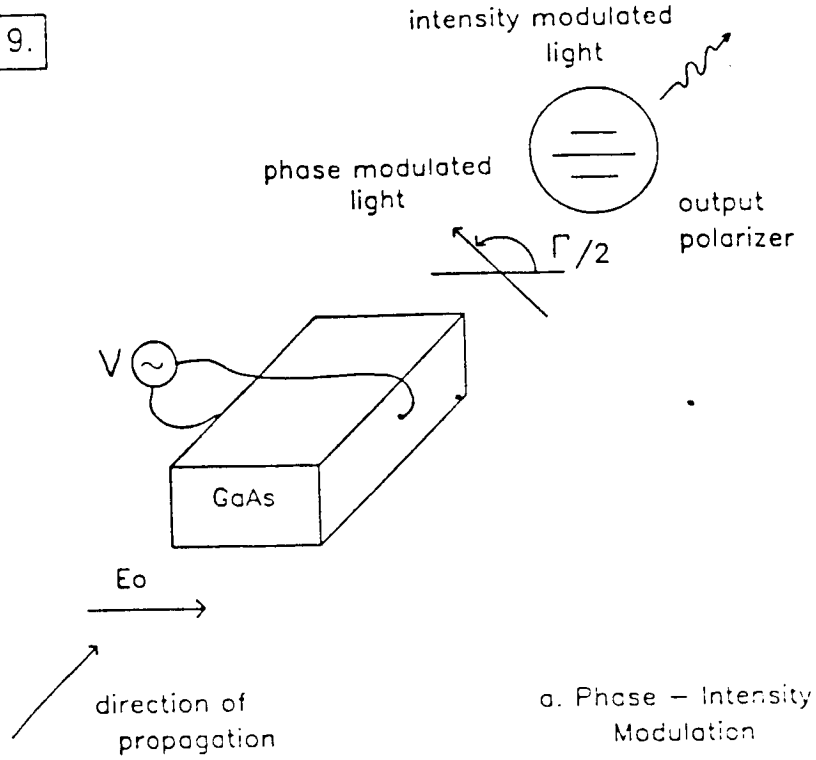

a. Phase – Intensity Modulation

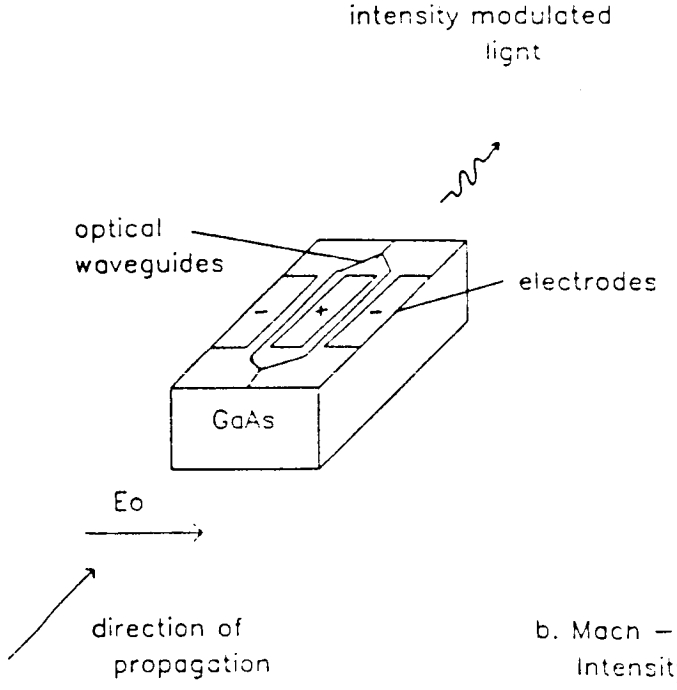

b. Mach – Zehnder Intensity Modulation

polarization parallel to the incident light polarization (fig 9.b) will produce the maximum relative phase shift available in GaAs. The externally applied fields are:

$$\underline{E}_1 = \frac{1}{\sqrt{2}} \left(\hat{a}_x + \hat{a}_y \right) E_m = -\underline{E}_2 \qquad (3.16.a)$$

where $\underline{E}_1$ is applied to one of the modulator arms and $\underline{E}_2$ is applied to the other. The incident optical field ($\underline{E}_o$) can be represented as it was in section 3.1.

$$\underline{E}_o = \frac{E_o}{\sqrt{2}} \left(\hat{a}_x + \hat{a}_y \right) \qquad (3.16.b)$$

The field at the output of each arm has been phase shifted to :

$$\underline{E}_{1out} = \frac{E_o}{\sqrt{2}} \left[a_x e^{-jk_x l} + a_y e^{-jk_y l} \right] \qquad (3.17.a)$$

$$= \frac{E_o}{\sqrt{2}} e^{-jk_o l} \left[\hat{a}_x e^{j\theta} + \hat{a}_y e^{-j\theta} \right] \qquad (3.17.b)$$

$$\underline{E}_{2out} = \frac{E_o}{\sqrt{2}} e^{-jk_o l} \left[\hat{a}_x e^{-j\theta} + \hat{a}_y e^{j\theta} \right] \qquad (3.17.c)$$

where $$\theta = \frac{\Gamma}{2} = \frac{\pi l}{\lambda} n_o^3 r_{41} E_m \qquad (3.18)$$

is the relative phase shift derived in section 3.1. When the phase shifted fields reach the output guide, they interfere and add vectorially to give:

$$\underline{E}_{out} = \frac{E_o}{\sqrt{2}} e^{-jk_o l} (\hat{a}_{x'} + \hat{a}_{y'}) \left[e^{j\theta} + e^{-j\theta}\right] \qquad (3.19)$$

$$= \frac{E_o}{\sqrt{2}} \cos\left[\frac{\Gamma}{2}\right] e^{-jk_o l} (\hat{a}_{x'} + \hat{a}_{y'})$$

The light at the output of the modulator is polarized in the same direction as the input light. The magnitude has been changed (due to the applied field) while the phase shift is equal to the propagation delay through the modulator. The intensity at the output is:

$$I = \frac{1}{2} \underline{E} \cdot \underline{E}^* = E_o^2 \cos^2\left[\frac{\Gamma}{2}\right] \qquad (3.20)$$

and intensity modulation is seen to be an inherent property of the device. Since the phase shift is proportional to E_m, the relation between the output intensity and the applied field is not linear (fig. 10). However, if the device is biased with a 90^o phase shift, small signal modulation that is approximately linear can be achieved.

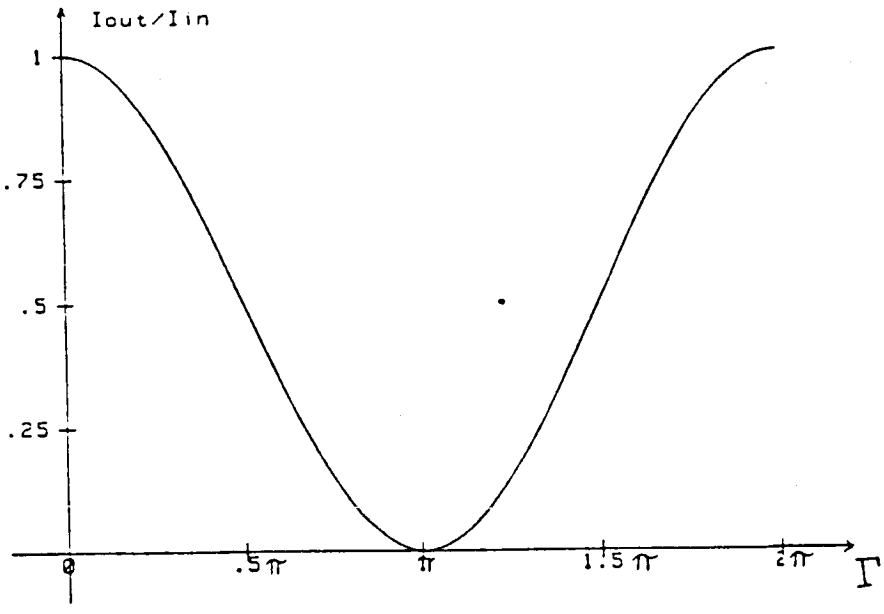

Figure 10. Output Intensity vs. Phase Shift
for the Mach–Zehnder Modulator

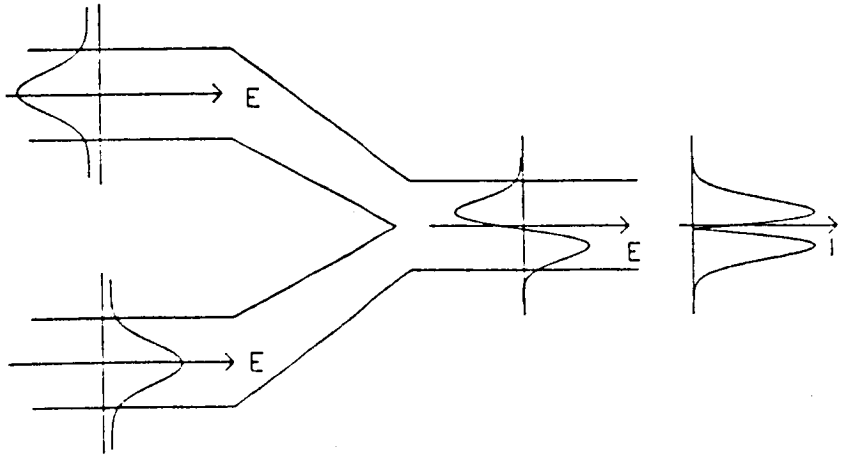

Figure 11. Exciting the first assymetric
optical waveguide mode

3.3 Waveguide Constraints

Some further insight into the nature of the modulation can be gained if the equations are derived in a slightly different way. The derivation is the same as the previous section up to equation (3.17). The exponentials can be converted using Euler's formula to give,

$$\underline{E}_{1out} = \frac{E_o}{\sqrt{2}} e^{-jk_o l} \left\{ (\hat{a}_x + \hat{a}_y)\cos(\Theta) + j\hat{a}_z \sin(\Theta)\sqrt{2} \right\} \quad (3.21.a)$$

$$\underline{E}_{2out} = \frac{E_o}{\sqrt{2}} e^{-jk_o l} \left\{ (\hat{a}_x + \hat{a}_y)\cos(\Theta) - j\hat{a}_z \sin(\Theta)\sqrt{2} \right\} \quad (3.21.b)$$

The modulation process is really a mode conversion in the modulator arms. Optical power is converted from its input polarization $(\underline{a}_x + \underline{a}_y)/2$, to the orthogonal component $\underline{a}_z$ through the electro-optic effect. The conversion is in opposite directions for the two arms and the $\underline{a}_z$ components will always interfere destructively.

In the previous analysis, a method of guiding the light through the modulator has not been discussed. It will be shown in Chapter 4, that it is possible for the optical waveguides to support multiple modes. If the

output waveguide supports a second mode, the above analysis breaks down. The opposite $\underline{a}_z$ fields can excite an assymetric mode in the output guide (fig 11). If supported, the light will propagate (with two intensity peaks) to the output of the modulator and no intensity modulation takes place. If the output guide is single mode, the energy which would excite the assymetric mode is simply radiated into the surrounding substrate and does not reach the modulator output. Therefore, the output guide must be single mode to prevent excitation of the assymetric mode and achieve intensity modulation. The problem of designing single mode optical waveguides will be addressed in the next chapter.

Chapter 4: Optical Waveguides

4.1 Waveguiding Structures

The Mach-Zehnder modulator requires some form of optical waveguiding which must meet two requirements. First, the optical guides must exhibit low propagation loss [20]. Otherwise, too much optical power is lost in the modulator even if no intensity modulation takes place. Inefficiency due to coupling and propagation is a disadvantage of external modulation that needs to be minimized. The second requirement of the optical waveguides is that they be single mode. As discussed in the previous section, this is necessary to achieve the intensity modulation in the Mach-Zehnder.

Four possible dielectric waveguiding structures are shown in figure 12 [7],[20],[21],[22]. In all optical waveguides, the light will concentrate in the area with the highest index of refraction and trail off exponentially in the areas of lower index. In all of the waveguides shown, the light is vertically confined to the layer with the highest index of refraction. However, each employs a somewhat different method of lateral confinement to form "channel" waveguides. In

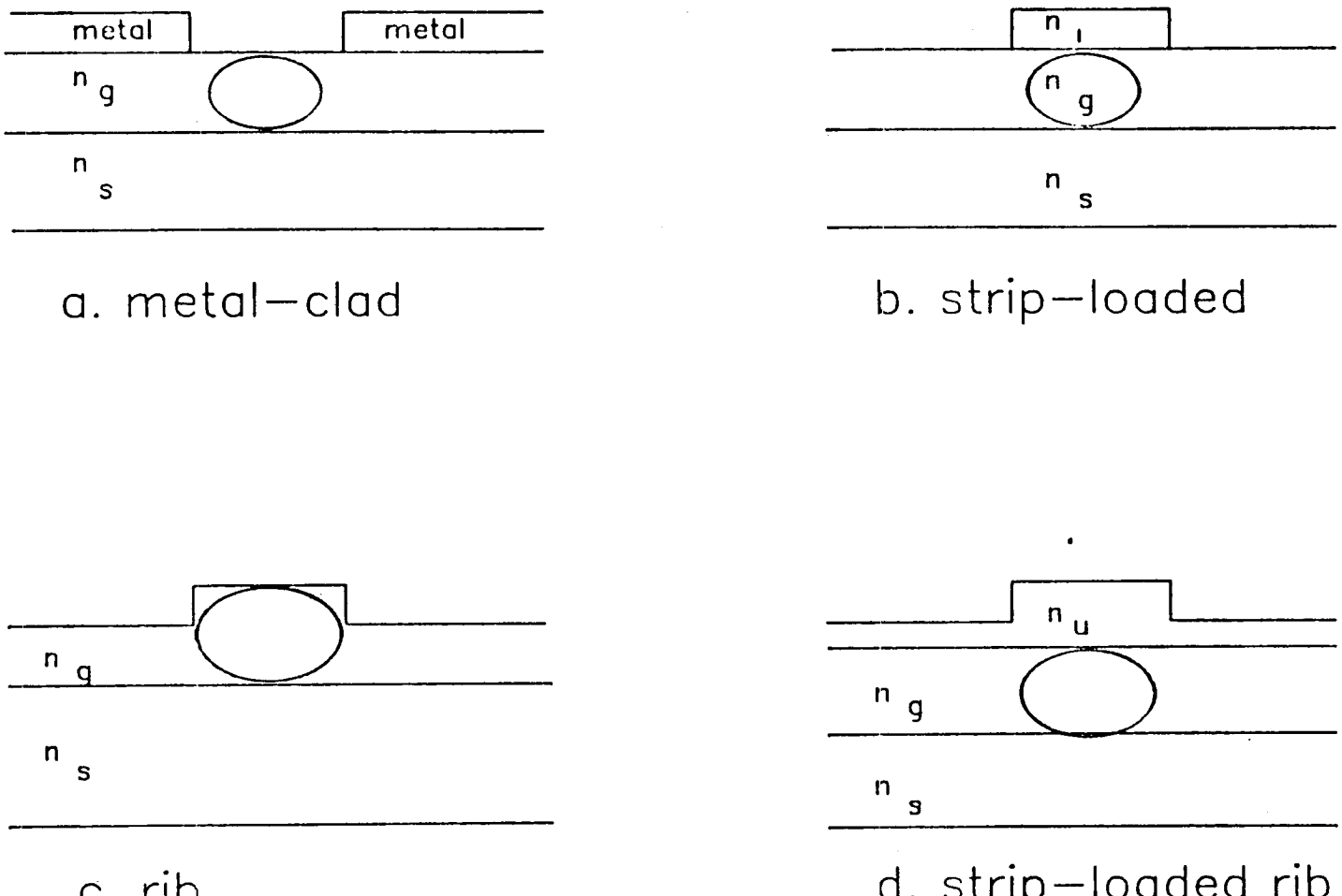

Figure 12. Optical Waveguiding Structures

the metal clad waveguide (fig. 12a), lateral guiding takes place because the metal reduces the effective index of the substrate below. This gives the center unmetalized strip a higher index than the surround and the light concentrates in the center. In the strip loaded and rib waveguide structures, the effective index of the center is again higher for guidance in this region. In the strip loaded rib waveguide, the ridge again increases the effective index of the center relative to the sides. But here, the guide layer is separated from the surface by an insulating layer.

A significant step toward reducing propagation losses can be taken with the proper choice of the waveguide structure. In the metal clad waveguide, losses result when fringes of the optical field are absorbed by the metal. In all optical waveguides, a major source of loss is scattering from imperfections in the guide. The lateral confinement is patterned by lithography and formed by etching or liftoff processes. These techniques yield sidewalls which are <u>not</u> perfectly vertical, <u>not</u> perfectly smooth and hence, scattering from these lithographically defined boundaries results in losses. In metal clad, strip loaded, and rib waveguides, the optical field is in close contact with these lithographically defined boundaries. However, the

strip loaded rib waveguide has an isolation layer between the lithographically defined loading rib and the guide layer. This means that the light intensity at the lithographically defined boundary is decreased, and less light is scattered [23]. For this reason, the strip-loaded rib waveguide was chosen to provide low loss optical waveguiding for the modulator.

4.2 The Effective Index Method

The optical fields can be calculated for the strip loaded rib waveguide by using an effective index method. This approximation is valid if the optical field is well confined and for modes not near cutoff [22]. It is assumed that the light passes through a polarizer before entering the waveguide and is polarized parallel to the film layers. Furthermore, the solution is separable and can be written as $E_y(x,y) = E_y(x)E_y(y)$. $E_y(x)$ is found by solving a 4-layer planar guide in regions I, II, and III as if each is infinite in the y direction (d/dy = 0) as shown in figure 13.b. The different guide layer thickness causes the effective propagation constant in the center guide to be different from the outer guides. An effective index in each of the three regions is then

Figure 13. The Effective Index Method

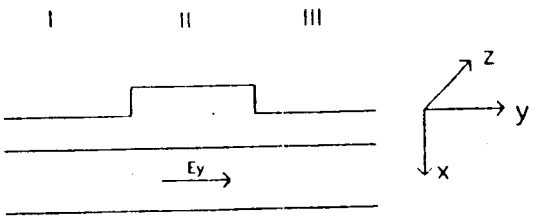

a. Ridge Waveguide showing regions for effective indices and direction of assumed light polarization

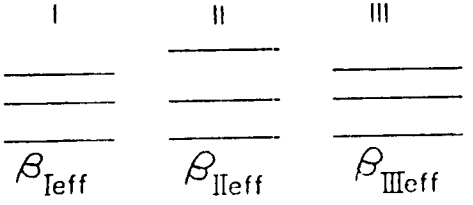

b. Treated as 3,4–Layer Planar Guides

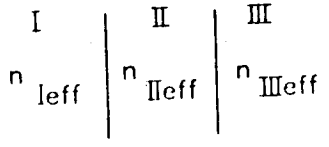

c. Transverse 3–Layer Guide

Figure 14. TE and TM mode definitions for optical waveguides.

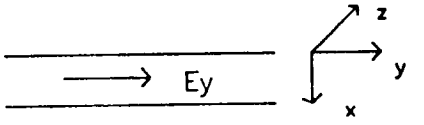

a. TE mode: Hx, Ey, Hz are nonzero

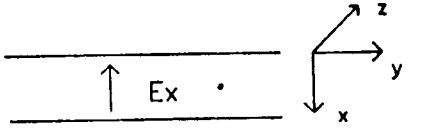

b. TM mode: Ex, Hy, Ez are nonzero

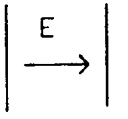

c. Lateral 3–layer guide is TM mode

obtained as $n_{eff} = \beta_{eff} / k_0$ and a 3-layer planar guide (fig. 13.c) is solved in the lateral direction to give $E_y(y)$ and the propagation constant for the total guide. The total optical field is then the product of the separated solutions.

The terms TE and TM when used in reference to optical waveguiding hold a somewhat different meaning than their use in microwaves. The microwave definition states that TE implies $E_z = 0$ while TM means $H_z = 0$ for propagation along the z axis. A more stringent definition is used when referring to optical waveguides because light can be polarized before it enters the guide. The only nonzero components of the TE mode are H_x, E_y, and H_z (fig. 14a) while the TM mode has only E_x, H_y, and E_z components (fig. 14b). Using these definitions, the solution for $E_y(x)$ is a TE mode while $E_y(y)$ represents a TM mode solution (fig. 14c). The total solution $E_y(x,y)$ is the product of a TE and a TM mode and thus has both E_z and H_z components.

4.2.1 The 4-Layer Planar Guide

The 4 layer planar waveguide is shown in figure 15 with the coordinate system defined. For confinement of

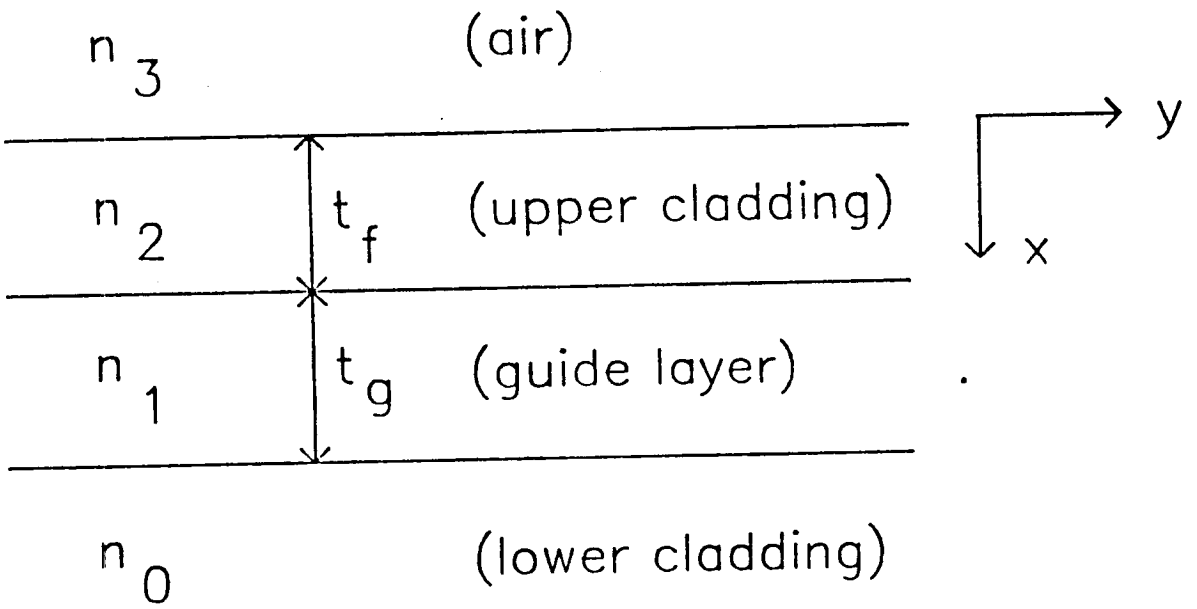

Figure 15. The 4—Layer Planar Waveguide

light in the guide layer, it must have the highest index of refraction ($n_1 > n_2 \geq n_0 > n_3$). In addition, the propagation constant must be restricted ($n_2 k_0 < \beta_{eff} < n_1 k_0$) to avoid propagation in the cladding layers.

To find a TE solution, assume a solution in each of the layers using trigonometric, hyperbolic, and exponential functions. Unspecified constants are left in the solutions and are used to satisfy the boundary conditions on the electric and magnetic fields. Appropriate functions capable of satisfying the boundary conditions are found to be: [22],[24]

$$E_y(x) = \begin{cases} A\ G\ \sinh(\Psi)\ \exp(q_3 x) & (4.1.a) \\ A\ G\ \sinh(q_2 x + \Psi) & (4.1.b) \\ A\ \cos[h1(x - t_f - t_g) + \phi)] & (4.1.c) \\ A\ \cos(\phi)\ \exp[q_0(t_g + t_f - x)] & (4.1.d) \end{cases}$$

where the $e^{j(wt - \beta z)}$ factor has been omitted for notational convenience. The constants G, psi, phi, q_0, h_1, q_2, and q_3 will be chosen to satisfy the boundary conditions. For equations (4.1), the film layers are specified by the suffix letter on the equation as defined in equations (4.2).

$$x \leq 0 \qquad (4.2.a)$$

$$0 \leq x \leq t_f \qquad (4.2.b)$$

$$t_f \leq x \leq (t_f + t_g) \qquad (4.2.c)$$

$$(t_f + t_g) \leq x \qquad (4.2.d)$$

This convention will be adhered to for the rest of this section.

The unspecified constants q_0, h_1, q_2, and q_3 are related to the propagation constant by:

$$q_3^2 = \beta_{eff}^2 - n_3^2 k_0^2 \qquad (4.3.a)$$

$$q_2^2 = \beta_{eff}^2 - n_2^2 k_0^2 \qquad (4.3.b)$$

$$h_1^2 = \beta_{eff}^2 + n_1^2 k_0^2 \qquad (4.3.c)$$

$$q_0^2 = \beta_{eff}^2 - n_0^2 k_0^2 \qquad (4.3.d)$$

A derivation of the required boundary conditions is supplied in Appendix B.1. Using the boundary condition requiring that E_y be continuous at the interface $x = t_f$ yields:

$$G \sinh(q_2 t_f + \Psi) = \cos[h_1(t_f - t_f - t_g) + \phi] \qquad (4.4.a)$$

$$G = \frac{\cos[\, h_1 t_g - \phi \,]}{\sinh[\, q_2 t_f + \Psi \,]} \qquad (4.4.b)$$

In addition, continutiy of dE_y / dx is required at all of the interfaces.

$$\frac{dE_y(x)}{dx} = \begin{cases} A\, G\, q_3 \sinh(\Psi) \exp(q_3 x) & (4.5.a) \\ A\, G\, q_2 \cosh(q_2 x + \Psi) & (4.5.b) \\ -A\, h_1 \sin[h_1(x - t_f - t_g) + \phi] & (4.5.c) \\ -A\, q_0 \cos(\phi) \exp[q_0(t_g + t_f - x)] & (4.5.d) \end{cases}$$

Equating at the boundaries yields:

1. $x = 0$

$$A\, G\, q_3 \sinh(\Psi) = A\, G\, q_2 \cosh(\Psi) \qquad (4.6.a)$$

$$\Psi = \tanh^{-1}\left\{\frac{q_2}{q_3}\right\} \qquad (4.6.b)$$

2. $x = t_f$

$$A\ G\ q_2 \cosh(q_2 t_f + \Psi) = - A\ h_1 \sin(h_1 t_g - \phi) \qquad (4.7.a)$$

$$q_2 \coth(q_2 t_f + \Psi) = h_1 \tan(h_1 t_g - \phi) \qquad (4.7.b)$$

3. $x = (t_f + t_g)$

$$- A\ h_1 \sin(\phi) = - A\ q_0 \cos(\phi) \qquad (4.8.a)$$

$$\phi = \tan^{-1}\left\{\frac{q_0}{h_1}\right\}. \qquad (4.8.b)$$

Substituting (4.6) and (4.8) into (4.7) gives a single equation to account for all three boundary conditions.

$$q_2 \coth\left\{q_2 t_f + \tan^{-1}\left[\frac{q_2}{q_3}\right]\right\} = h_1 \tan\left\{h_1 t_g - \tan^{-1}\left[\frac{q_0}{h_1}\right]\right\} \qquad (4.9)$$

Since the tangent function repeats every pi radians, the higher order modes can enter the solution here. After some rearranging, the total eigenvalue equation becomes:

$$\Delta = 0 = h_1 t_g - m\pi - \tan^{-1}\left[\frac{q_0}{h_1}\right] - \tan^{-1}\left\{\frac{q_2}{h_1}\coth\left\{q_2 t_f + \tanh^{-1}\left[\frac{q_0}{h_1}\right]\right\}\right\} \qquad (4.10)$$

where $m = 0, 1, 2, \ldots$ is the mode number.

Now, the propagation constant can be found using a computational bisection technique to find a root of eq. (4.10) [25]. The endpoints are $n_2 k_0 \leq \beta_{eff} \leq n_1 k_0$ and equations (4.3) and (4.10) are used until $|\Delta| \leq 10^{-6}$ in eq. (4.10). Then β_{eff} can be substituted into equations (4.4.b), (4.5), (4.7), and (4.1) to determine the actual field quantities. The subroutines for solving the

eigenvalue equation and determining the field intensity are included in Appendix C.

4.2.2 Lateral Solution

Once the 4-Layer planar guides have been solved in the three regions (fig. 13), an effective index for each region can be determined from the effective propagation constant in that region [21],[22].

$$n_{eff} = \frac{\beta_{eff}}{k_o} \tag{4.11}$$

The lateral 3-Layer planar guide is shown in figure 16 with the same absolute coordinate system that was used for the 4-Layer solution. Again, the notational convention of relating the regions with the letter suffix in each equation will be used.

$$|y| \leq \frac{t_{RW}}{2} \tag{4.12.a}$$

$$|y| \geq \frac{t_{RW}}{2} \tag{4.12.b}$$

The solution of the 3-Layer planar guide can be derived in the same way as the 4-Layer solutions. However, the equations are simplified by symmetry because the outer regions have the same effective index. Solutions of the form:

$$E_y(y) = \begin{cases} A \cos(h_2 y) & (4.13.a) \\ A\, G \exp(-q_1 |y|) & (4.13.b) \end{cases}$$

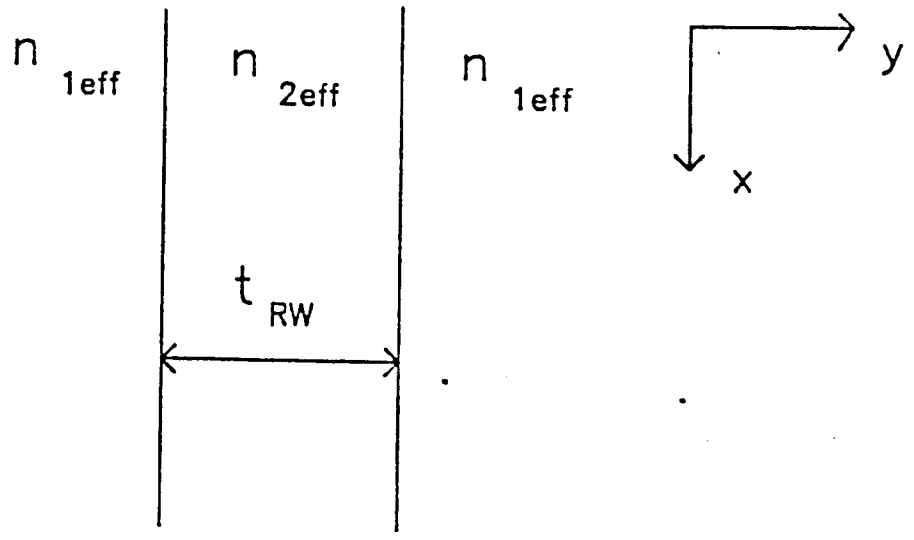

Figure 16. Lateral 3—Layer Planar Waveguide

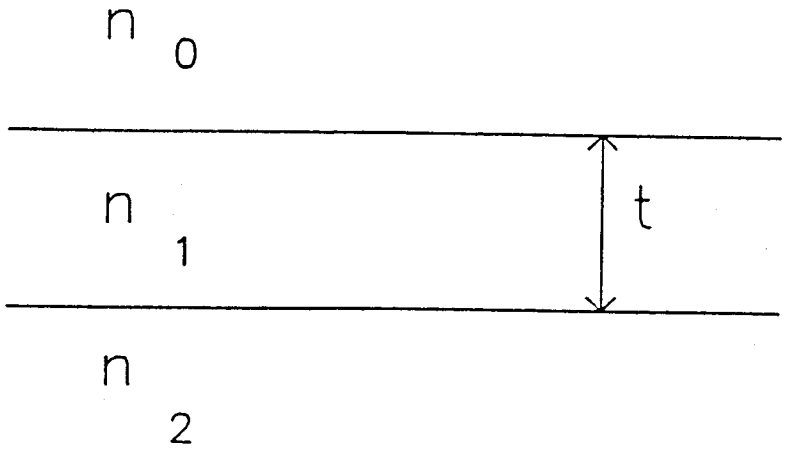

Figure 17. Assymetric planar waveguide

where the constants q_1 and h_2 are defined by

$$h_2^2 = \beta^2 + n_{2eff}^2 k_0^2 \qquad (4.14.a)$$

$$q_1^2 = \beta^2 - n_{1eff}^2 k_0^2 \qquad (4.14.b)$$

and are used to satisfy the boundary conditions. The required boundary conditions are derived in Appendix B.2. The constant G is determined by the boundary condition requiring continuity of E_y at $y = t_{RW}/2$.

$$A \cos (h_2 t_{RW} / 2) = A G \exp (-q_1 t_{RW} / 2) \qquad (4.15.a)$$

$$G = \cos (h_2 t_{RW} / 2) \exp (q_1 t_{RW} / 2) \qquad (4.15.b)$$

The boundary condition requiring dE_y / dy be continuous at $y = t_{RW} / 2$ is again used to determine an eigenvalue equation. Starting with dE_y / dy,

$$\frac{dE_y(y)}{dy} = \begin{cases} - A h_2 \sin (h_2 |y|) & (4.16.a) \\ - A G q_1 \exp (-q_1 |y|) & (4.16.b) \end{cases}$$

$$- A h_2 \sin(h_2 t_{RW}/2) = -A G q_1 \exp(-q_1 t_{RW}/2) \qquad (4.16.c)$$

substituting for G, and modifying the equation to account for higher order modes yields the final eigenvalue equation.

$$\Delta = 0 = h_2 t_{RW} - m\pi - 2\tan^{-1}\left[\frac{q_1}{h_2}\right] \qquad (4.17)$$

The propagation constant is again found as a root of eq. (4.17) by using a bisectional technique [25] with $n_{1eff} k_0 \leq \beta \leq n_{2eff} k_0$ in equations (4.14) and (4.17). It is not necessary to reprogram the eigenvalue equation

because equation (4.10) degenerates to eq. (4.17) when $t_g = 0$. Again, the subroutines for solving the eigenvalue equation and determining the field quantities are included in appendix C.

4.3 Single Mode Guidance

At the end of chapter 3, it was indicated that the output waveguide of the Mach-Zehnder must be single mode for intensity modulation. The modulator will be most efficient if all guides only support a single mode.

For a 3-layer assymetric planar guide (fig. 17), the cutoff conditions can be determined from the following equations [21],[26].

$$\nu = \frac{1}{2}\, t\, k_0\, (n_1^2 - n_2^2)^{1/2} \qquad (4.18.a)$$

$$\nu_c = \frac{1}{2} \tan^{-1} \left\{ \left[\frac{n_2^2 - n_0^2}{n_1^2 - n_2^2} \right]^{1/2} \right\} + \frac{M\pi}{2} \qquad (4.18.b)$$

where ν is the normalized frequency, ν_c is the cutoff normalized frequency for mode M, and k_0 is the freespace wave number. Equating (4.18.a) with (4.18.b) where $t = t_c$ gives:

$$t_c = \frac{M\pi + \tan^{-1} \left\{ \left[\frac{n_2^2 - n_0^2}{n_1^2 - n_2^2} \right]^{1/2} \right\}}{k_0 \, (n_1^2 - n_2^2)^{1/2}} \qquad (4.19)$$

as the cutoff condition for the thickness of the center layer. This condition requires that $t \geq t_c$ for mode M to propagate in the guide. Therefore, requiring $t < t_c$ prevents the second mode from propagating and ensures single mode guidance.

Since the final solution in the effective index approximation is the product of $E_y(x)$ and $E_y(y)$, the total number of propagating modes is the product of the number of vertical modes and the number of lateral modes. This means that single mode waveguiding is required in each of the 4-layer guides as well as in the 3-layer transverse guide. For the transverse 3-layer guide, equation (4.19) with M=1 gives the rib width at which the second lateral mode begins to propagate. This represents the assymetric mode to be eliminated for Mach-Zehnder intensity modulation. If the field intensity is negligible in one of the outer regions of the 4-layer guide, the cutoff condition can be approximated by equation (4.19). These conditions will be used to limit the thickness of the guide layer (in the 4-layer guide) and the rib width to ensure that a single mode is supported by the total guide.

4.4 Isolation from the Substrate

Before proceeding with the design of single mode waveguides, the theory must be made more complete to describe real waveguides. Due to the absorption problem discussed in section 2.4, the vertical guidance must be produced using varied concentrations of GaAlAs in the film layers. However, these layers will be grown on a pure GaAs substrate which has not been included in this analysis. The complete film layer structure is shown in figure 18. According to the Sellmier equation (Appendix A), the GaAs substrate has the highest index of refraction in the system. Therefore, light will tend to couple from the guide layer n_1, to the substrate through the lower cladding layer n_0. Since the substrate is not transparent at 0.82 um, this light is absorbed and represents additional propagation loss.

This coupling phenomenon has been analyzed by Boyd [23],[38] using the following analysis of a 3-layer guide on a substrate. If it is assumed that the field in the air is negligible, the 3-layer (n_2, n_1, n_0) guide on the GaAs substrate can be considered using this analysis. First, the 3-layer guide is solved neglecting the substrate. Then, the assymetric 3-layer planar guide can be solved by using an eigenvalue equation to

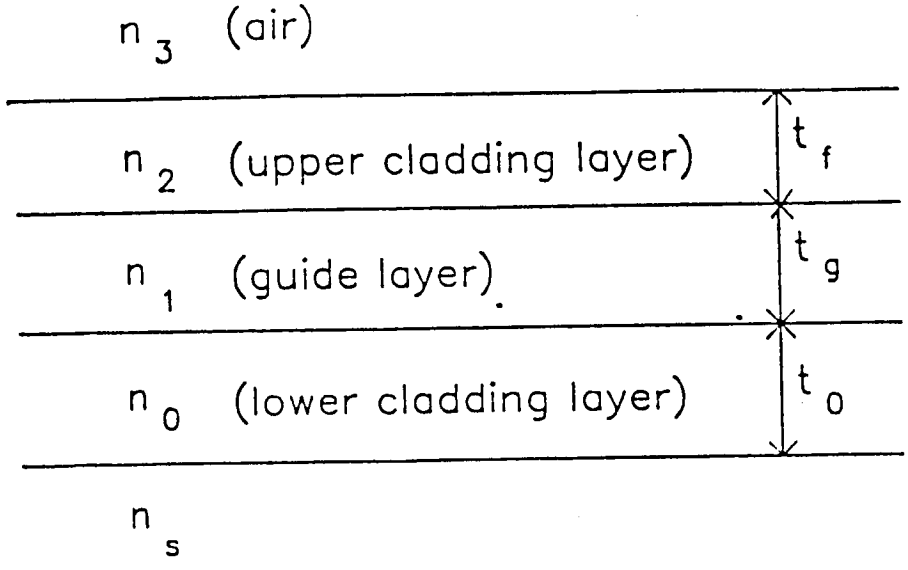

Figure 18. The 5—Layer Structure

give the effective propagation constant in an analysis similar to section 4.2. From the propagation constant, the following parameters are defined:

$$n_{eff} = \beta_{eff} / k_0 \qquad (4.20.a)$$

$$p = (\beta_{eff}^2 - (k_0 n_0)^2)^{1/2} \qquad (4.20.b)$$

$$q = (\beta_{eff}^2 - (k_0 n_2)^2)^{1/2} \qquad (4.20.c)$$

$$w_{eff} = t_g + \left[\frac{1}{p}\right] + \left[\frac{1}{q}\right] \qquad (4.20.d)$$

The attenuation constant representing coupling to the substrate is then given by:

$$\alpha = 4 \frac{(n_1^2 - n_{eff}^2)(n_{eff}^2 - n_0^2)(n_s^2 - n_{eff}^2)^{\frac{1}{2}}}{n_{eff} w_{eff} (n_1^2 - n_0^2)(n_s^2 - n_0^2)} e^{-2pt_0} \qquad (4.21)$$

If the light is propagating in the z direction with initial intensity I_0, the intensity at any point along the guide (neglecting scattering losses) is given by:

$$I = I_0 e^{-\alpha z} \qquad (4.22)$$

The design goal will be to ensure that the lower cladding layer is sufficiently thick to make radiation into the substrate negligible over the length of the modulator.

4.5 The Modulator Waveguides

With all of the necessary equations to characterize the strip loaded rib waveguide programmed (Appendix C), it is now possible to design optical waveguides for the modulator. As explained in section 2.4, the layers must be GaAlAs to shift the absorption edge and make the films transparent at 0.82 um wavelength. Data on the position of the absorption edge is scarce for low aluminum concentrations. The photon energy of the absorption edge vs aluminum concentration is plotted in figure 19 using the data of figure 6 [15]. The light wavelength is related to phototon energy (E) by

$$\lambda = \frac{1.2\ \mu m \cdot eV}{E\ (ev)} \qquad (4.23)$$

The photon energy corresponding to the design wavelength of 0.82 um is indicated in the figure. The absorption edge is at this wavelength for an aluminum mole fraction of about 0.7. Leaving a small safety margin, a minimum aluminum aluminum mole fraction of 0.1 was chosen for the film layers [23]. In order to avoid unnecessary absorption, it is necessary that all 4 of the film layers be transparent to the 0.82 um light.

The layer structure shown in figure 20 was designed based on several decisions. To minimize the chance of error in fabrication, it is possible to ensure a single

Absorption Edge For GaAlAs

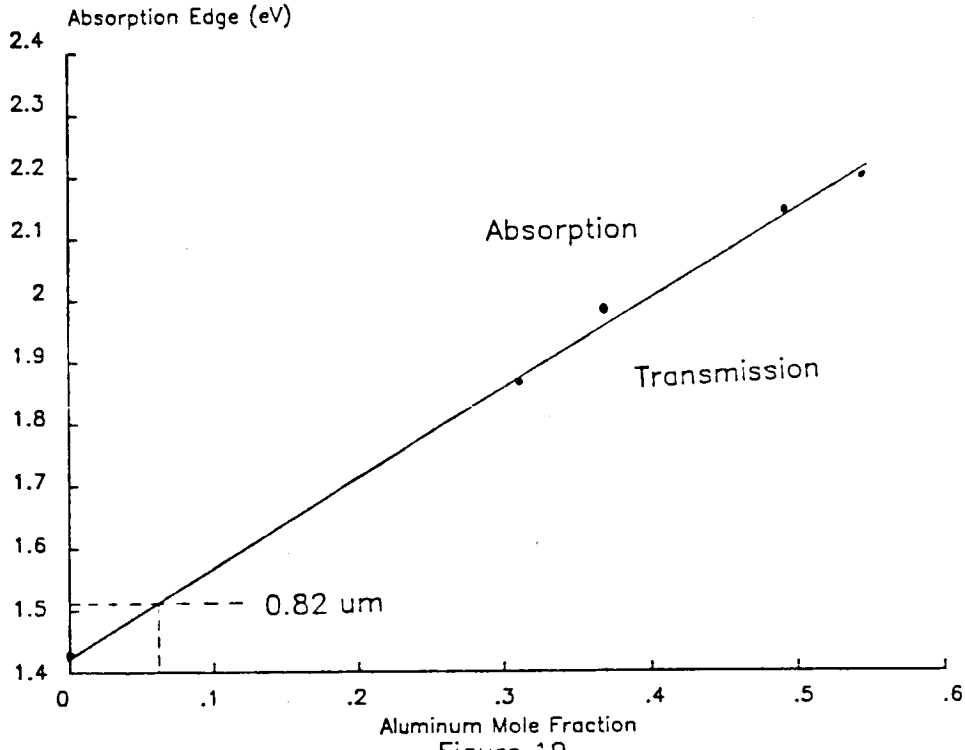

Figure 19.

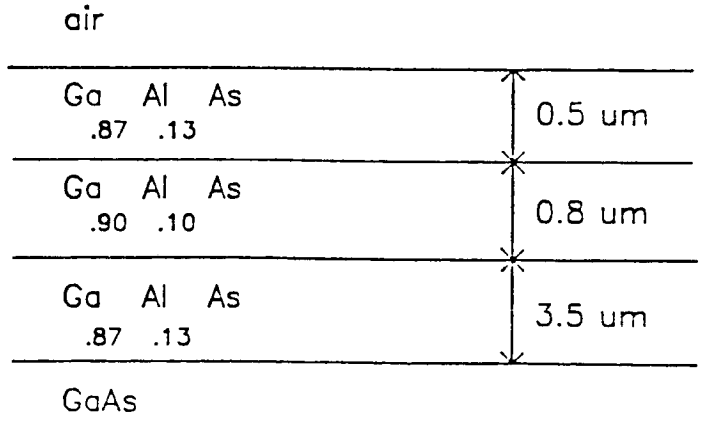

Figure 20. The Waveguide Layer Structure for the Initial Modulator Design

vertical mode independent of the thickness of the top layer. This is the layer which will be etched and subjected to any surface damage effects. Plots of the guide layer cutoff thickness vs. aluminum mole fraction are shown in figure 21 for an infinite upper cladding layer and for none at all. For the 0.8 um guide layer thickness, an aluminum mole fraction of 0.1 ensures single mode propagation independent of the upper cladding thickness.

Next, the thickness of the lower cladding layer was determined to isolate the guide from the substrate. For the 0.8 um guide layer, the 3-layer planar structure has an effective index, $n_{eff} = 3.5542$. For the lower cladding thickness of 3.5 um, an attenuation constant of 0.0018 m^{-1} is calculated. Attenuation is usually referred to in dB / length. This can be converted using:

$$\alpha \left[\frac{dB}{cm}\right] = -20 \log \left[e^{-\alpha(cm^{-1})}\right] \qquad (4.24.a)$$

$$= 1.6 \times 10^{-4} \ \frac{dB}{cm} \qquad (4.24.b)$$

This means that over a 2 cm device length, the power lost to the substrate is negligible. This is essential to meet the goal of low loss optical waveguides.

With single mode propagation insured in the vertical direction, the rib width can be chosen to ensure that a single mode is supported in the lateral

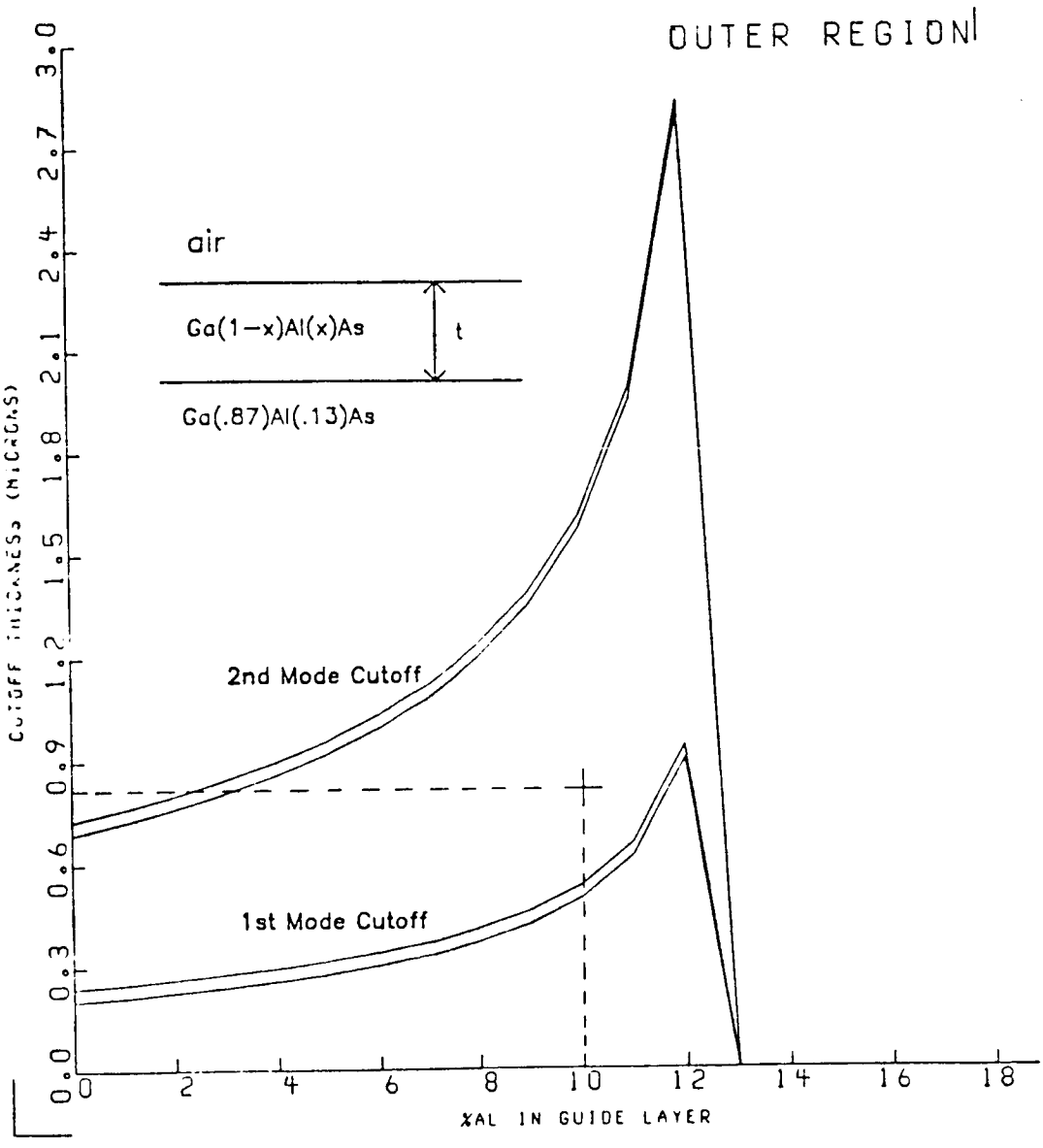

Figure 21a. Vertical Cutoffs without an Upper Cladding Layer

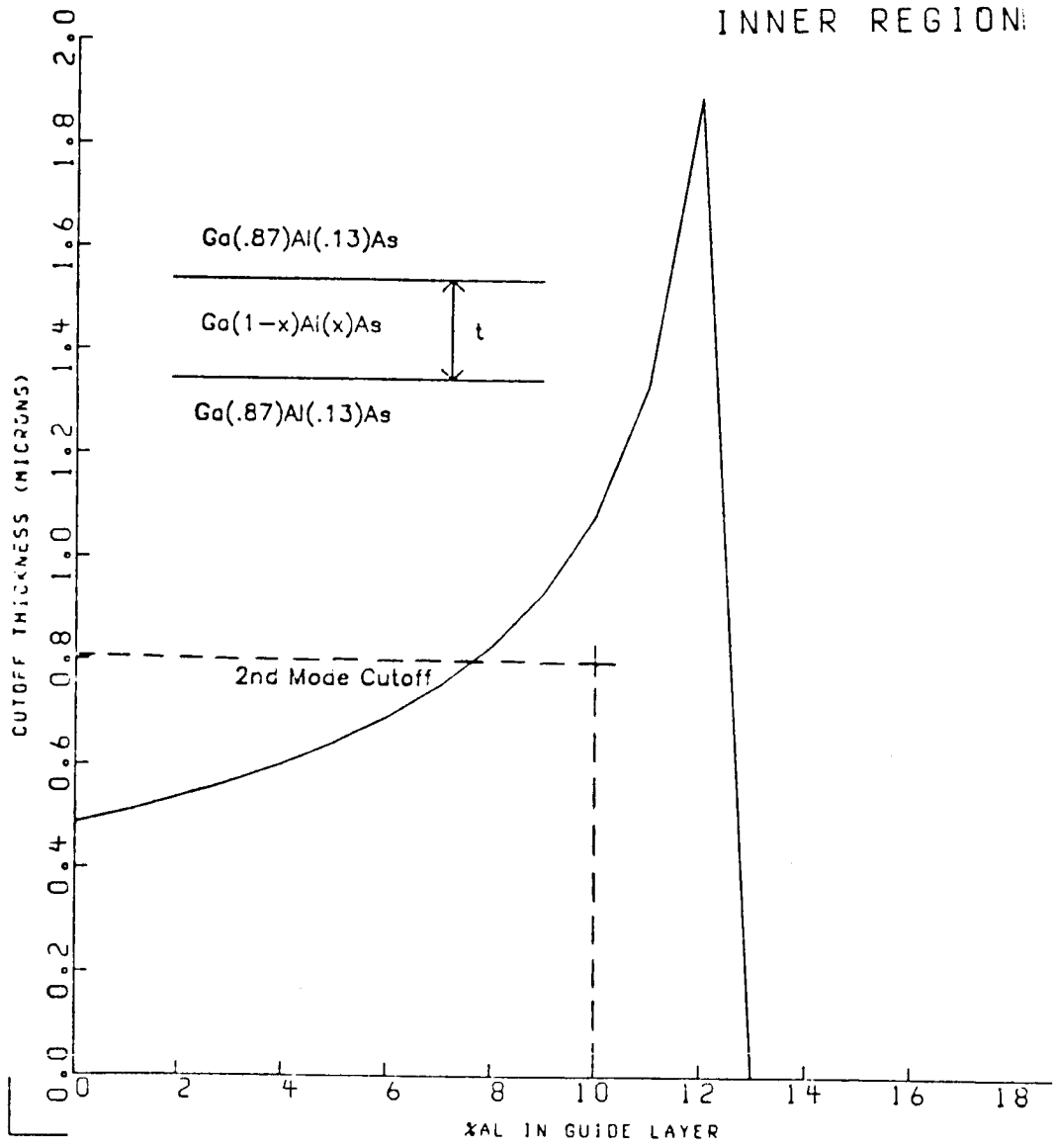

Figure 21b. Vertical Cutoffs with an Infinite Upper Cladding Layer

direction as well. Since the indices of refraction are effective indices resulting from the solution of the 4-Layer guides, an analytical expression of t_c as a function of rib height is not easily determined. Therefore, the cutoff rib width was determined as a function of rib height by running the analysis program for a series of rib heights. The results are plotted in figure 22. Since the lateral guide is symmetrical, there is no cutoff for the 1^{st} mode and any rib width below the 2^{nd} mode cutoff ensures single mode guidance.

For fabrication reasons, a rib height of 0.065 um and a rib width of 10 um was chosen. The analysis results produced by the program (including effective indices, and vertical and lateral field intensity plots) are shown in figures 23, 24, and 25. The vertical 3-layer approximations appear valid for the 0.5 um upper cladding layer thickness because the field intensity is nearly zero at the air interface. In addition, the separation of $E_y(x,y) = E_y(x)\ E_y(y)$ should be valid for the lateral confinement shown in figure 25 [22]. It should be pointed out that in order to get better confinement under the ridge, the rib width must be increased. This is impossible if the single mode condition is to be satisfied.

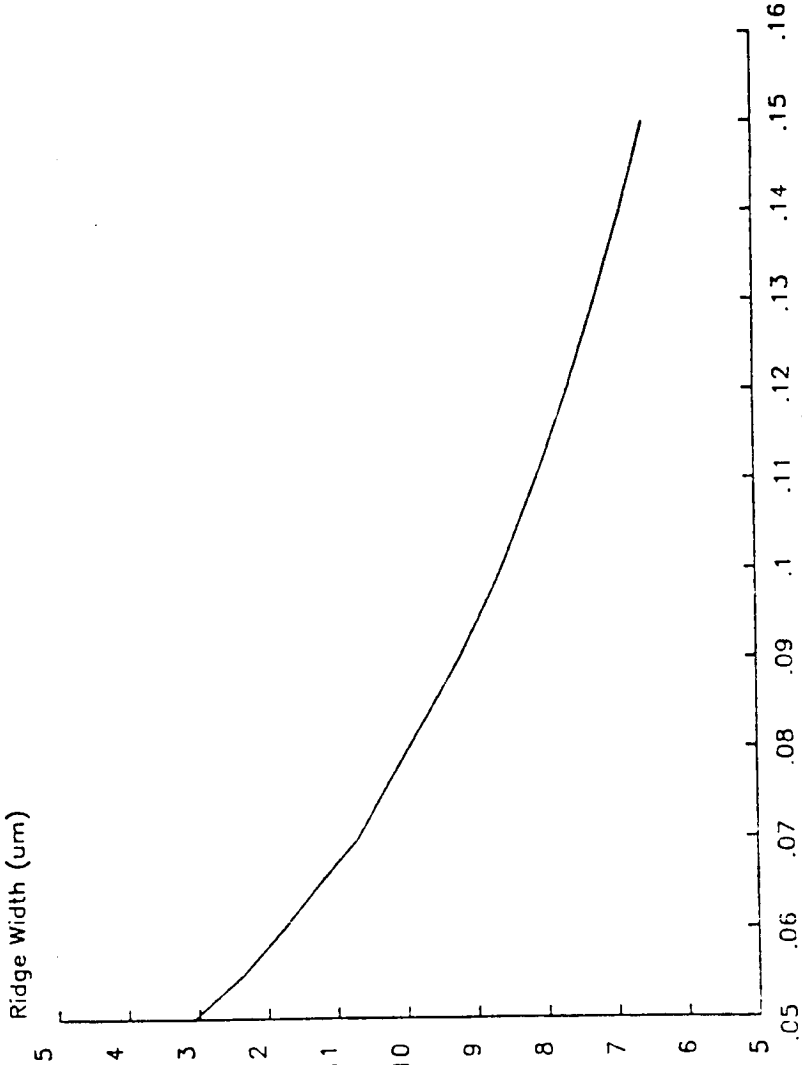
Ridge Width for 2nd Mode Cutoff
Ridge Width (um)
15
14
13
12
11
10
9
8
7
6
5
.05
.06
.07
.08
.09
.1
.11
.12
.13
.14
.15
.16
Ridge Height (um)

Figure 22.

Figure 23. Results of the Ridge Waveguide Analysis Program

```
OUTER REGION (VERTICAL MODE)
TE NUMBER OF MODES =  1
TM NUMBER OF MODES =  1
PROPAGATION CONST =  27220896.0000000000
EFFECTIVE INDEX =    3.55353

RIDGE REGION (VERTICAL MODE)
TE NUMBER OF MODES =  1
TM NUMBER OF MODES =  1
PROPAGATION CONST =  27230036.0000000000
EFFECTIVE INDEX =    3.55375

LATERAL GUIDING
TE NUMBER OF MODES =  1
TM NUMBER OF MODES =  1
PROPAGATION CONST =  27229712.0000000000

FOR THE FINAL GUIDE
EFFECTIVE INDEX =  3.5540
PROPAGATION CONST =  27229712.0000000000
WAVELENGTH = 1.00 MICRONS

ENTER 1 TO RUN OR QUIT (0)  ?

                GA-AL-AS WAVEGUIDE
```

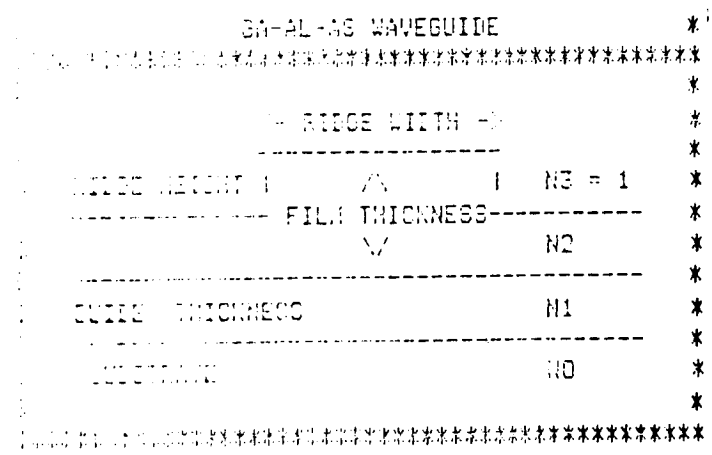


```
     ENTER RIDGE WIDTH (MICRONS)      10.0000
     ENTER RIDGE HEIGHT (MICRONS)     0.65000E-01
     ENTER FILM THICKNESS (MICRONS)   0.50000
     ENTER SUBSTRATE THICKNESS (MICRONS) 0.80000
     ENTER WAVELENGTH (MICRONS)       0.82000
     ENTER EFFECTIVE INDEX N3         1.0000
     ENTER % AL IN N2                 13.000          N2 =    3.5407
     ENTER % AL IN N1                 10.0000         N1 =    3.5649
     ENTER % AL IN N0                 13.000          N0 =    3.5407
     ENTER 1                          0.00000
```

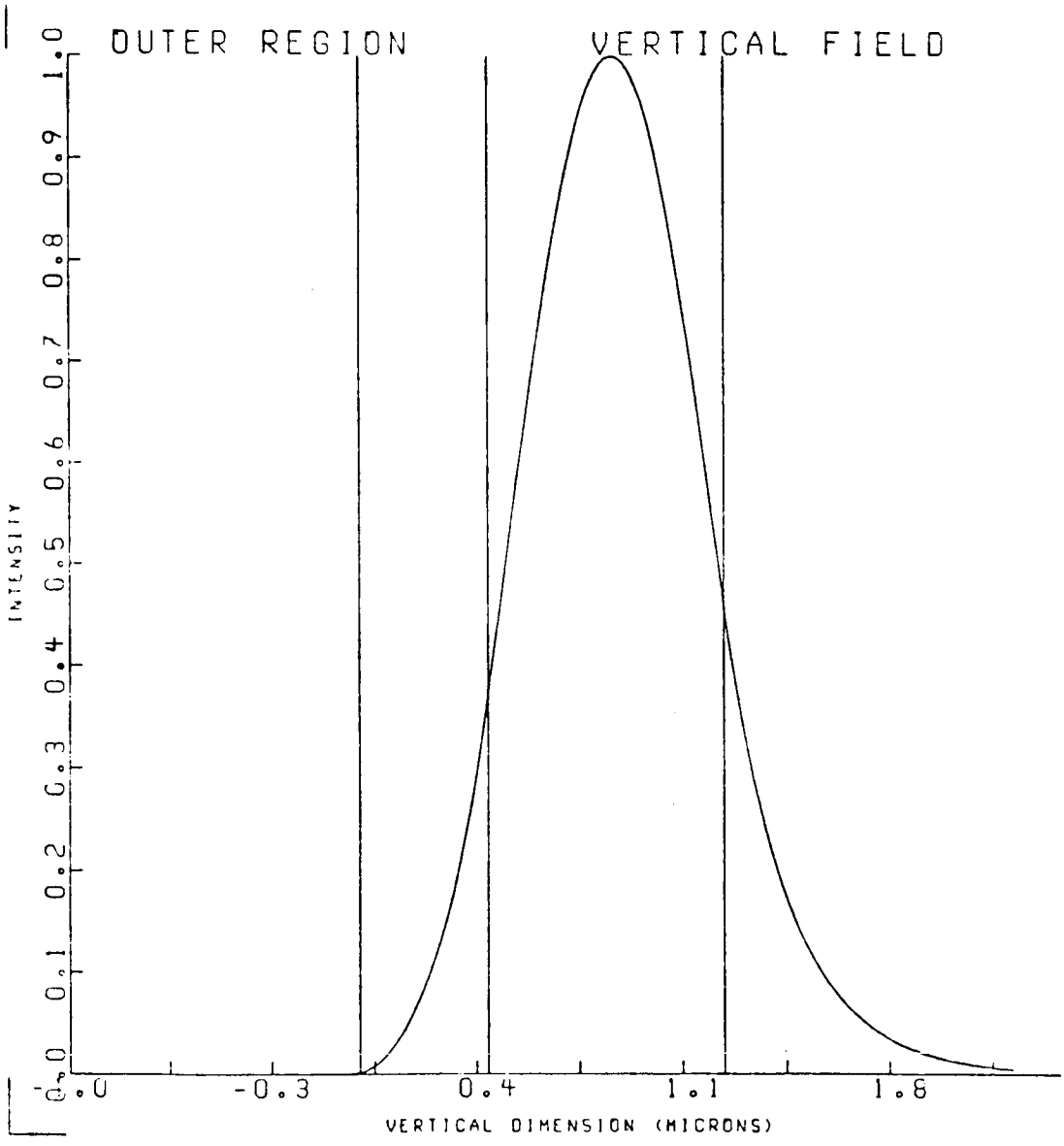

Figure 24a. Vertical Field Intensity
in the Region Outside of the Ridge

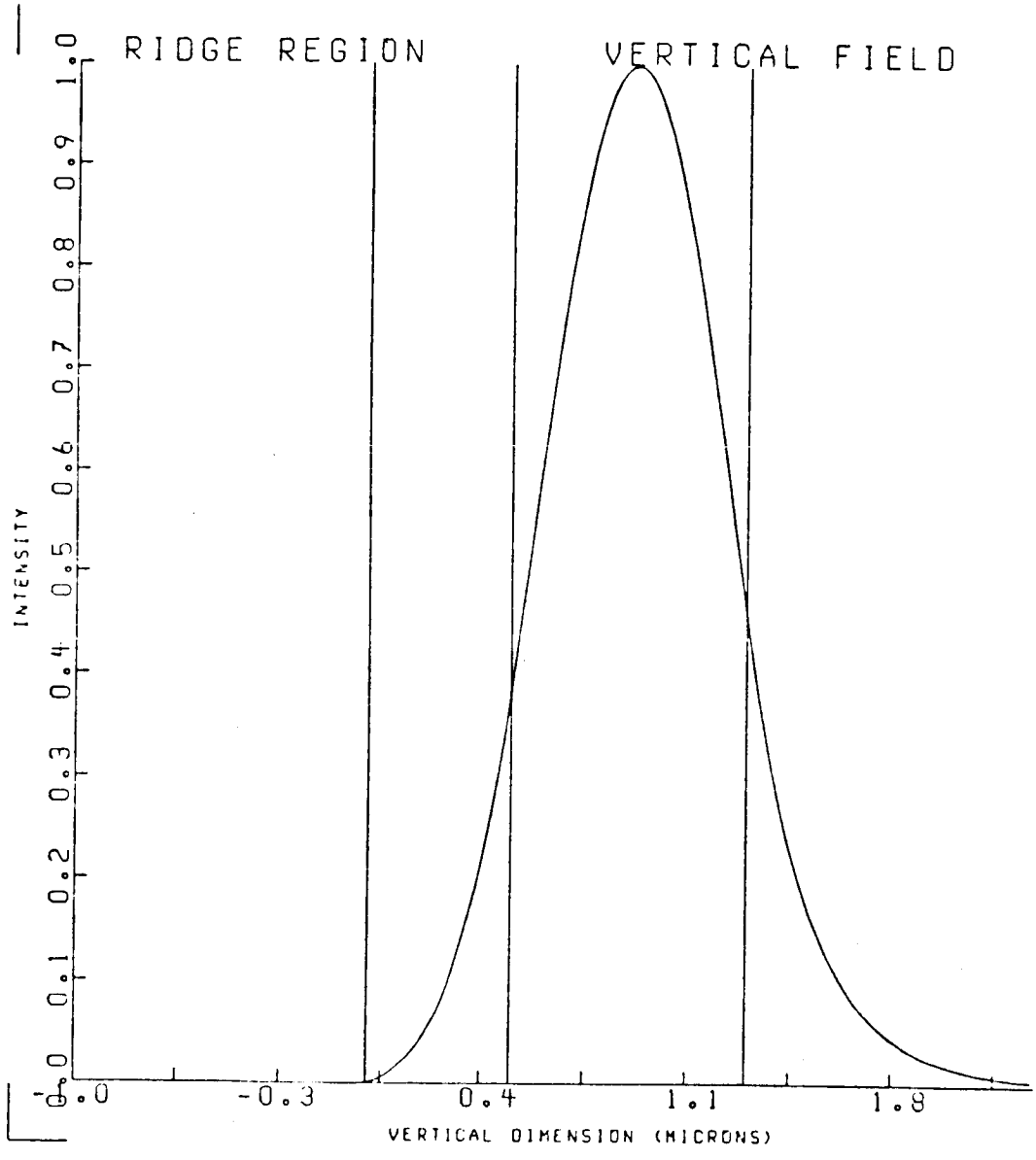

Figure 24b. Vertical Field Intensity
in the Region Under the Ridge

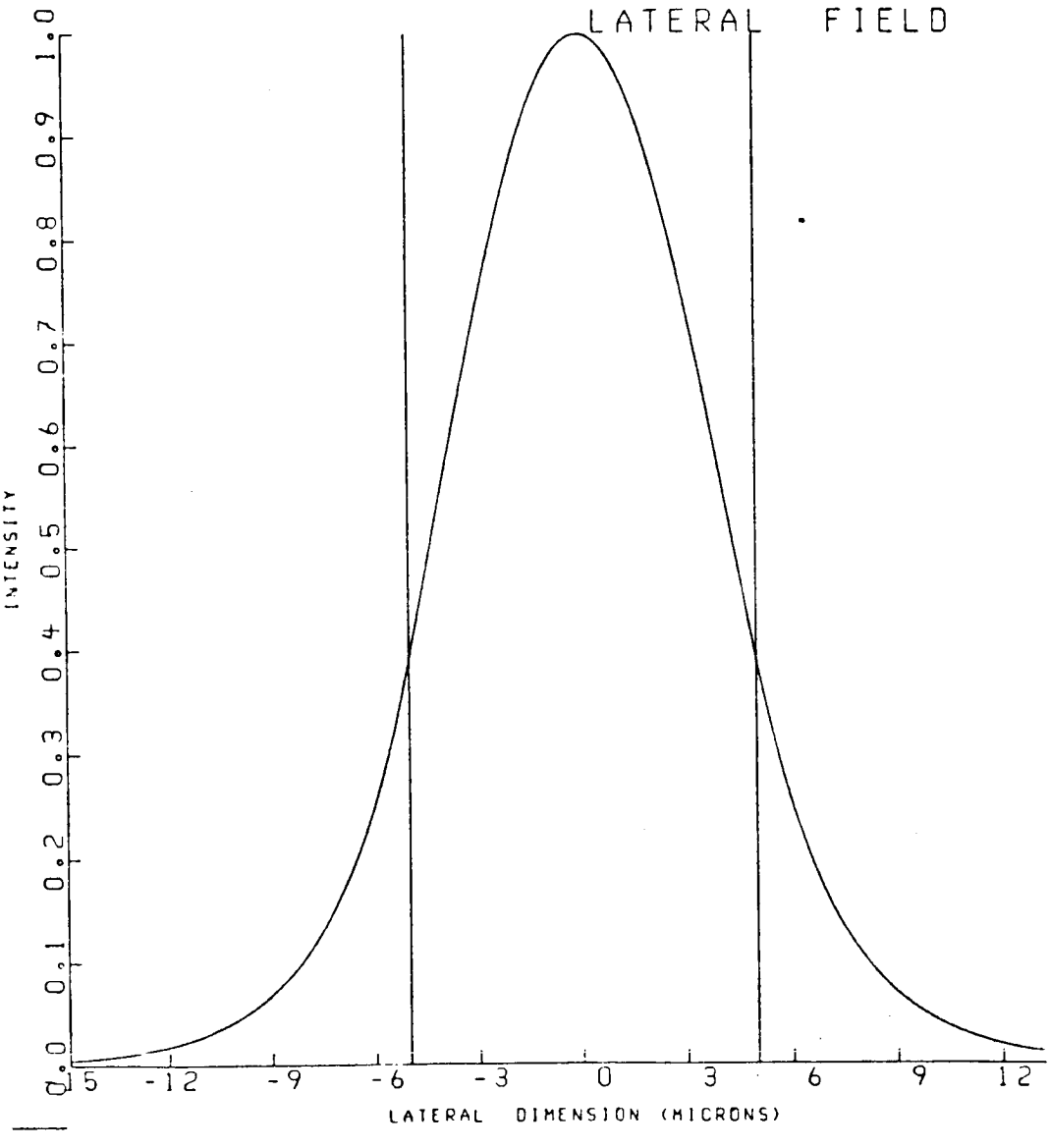

Figure 25. Lateral Field Intensity Profile

4.6 The Y-Branch

Another factor in the design of optical waveguides for the Mach-Zehnder modulator is the design of efficient Y-branches for optical power dividing and recombination. It has been documented [5] that if the angle of the Y separation is too large, significant power is reflected back into the input guide. On the other hand, a small angle requires a long device for adequate separation of the modulator arms. Sasaki and Mikosniba provided an excellent model for the power transfer through a Y junction [30]. Figure 26.a shows the Y junction and the dimensional notation used in this model. The waveguide analysis program is used to calculate $n_0(n_{1eff})$, $n_1(n_{2eff})$, and the propagation constant for the rib widths d and 2d. The parameter V_i is then calculated from the definition

$$V_i = 2\, k_0\, d\, \sqrt{n_1^2 - n_0^2} \qquad (4.25)$$

Using the corresponding graph in figure 26.b, a normalized branching angle for the desired power transmission ratio (P_t/P_i) can be determined. The actual branching angle is then related to the normalized angle by:

$$\theta_1 = \theta\, \beta\, d \qquad (4.26)$$

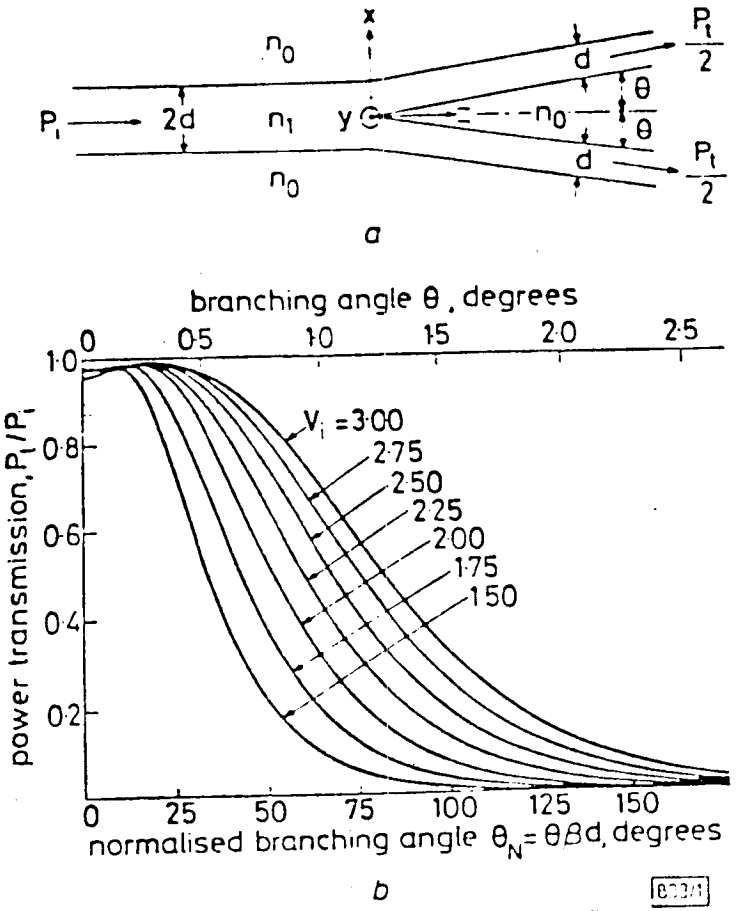

Figure 26.

a. Dimensioned Y–Branch

b. Power Transmission Ratio

Table 1

θ	θ_N	Pt/Pi
0.1	13.615	0.98
0.3	40.845	0.92
0.5	68.075	0.65
1.0	136.15	0.15

where β is the propagation constant for a waveguide of rib width of either d or 2d because the propagation constant's are approximately equal anyway.

For the waveguide structures chosen in section 5.5, a branching angle of 0.3^{o} was chosen in the following way. The power transmission ratio was calculated for a series of possible branching angles. From the waveguide analysis program using the configuration designed in the previous section,

$n_0 = 3.55356$

$n_1 = 3.55375$

$d = 5$ um

$\beta = 27229712\ m^{-1}$

lambda = 0.82 um

Substituting into equation (4.24), V_i is calculated as 2.82 indicating a high power transmission ratio is available. The transmission ratio for the series of branching angles (using the graph in fig. 26.b) is shown in table 1. It can be somewhat arbitrarily required that 90% of the incident power be transmitted to the modulator arms. A branching angle of 0.3^{o} meets this goal with some margin for error. For higher branching angles, the power transmission ratio begins to fall off rapidly.

Chapter 5: Electrodes & Modulator Response Analysis

5.1 Electrode Geometry

With the optical waveguides designed, the next step is to determine an electrode geometry which will take advantage of the maximum electro-optic effect. It was discussed in Chapter 2 that transmission line (travelling wave) electrodes offer the potential for higher bandwidth. With this motivation and realizing that little work has been reported on travelling wave modulators fabricated on semiconductor substrates [7], this thesis will deal exclusively with this type of electrode configuration.

Two electrode geometries which could be used as 50 ohm transmission line structures on semi-insulating GaAs are shown in figure 27. This chapter will show that the coplanar structure meets all the requirements set up by the foregoing analysis. The microwave field under the electrode gap is essentially parallel to the film layers. This will take advantage of the maximum electro-optic effect for the E_y optical waveguide mode. In addition, these electrodes can be driven so that the microwave fields are in opposite directions in the

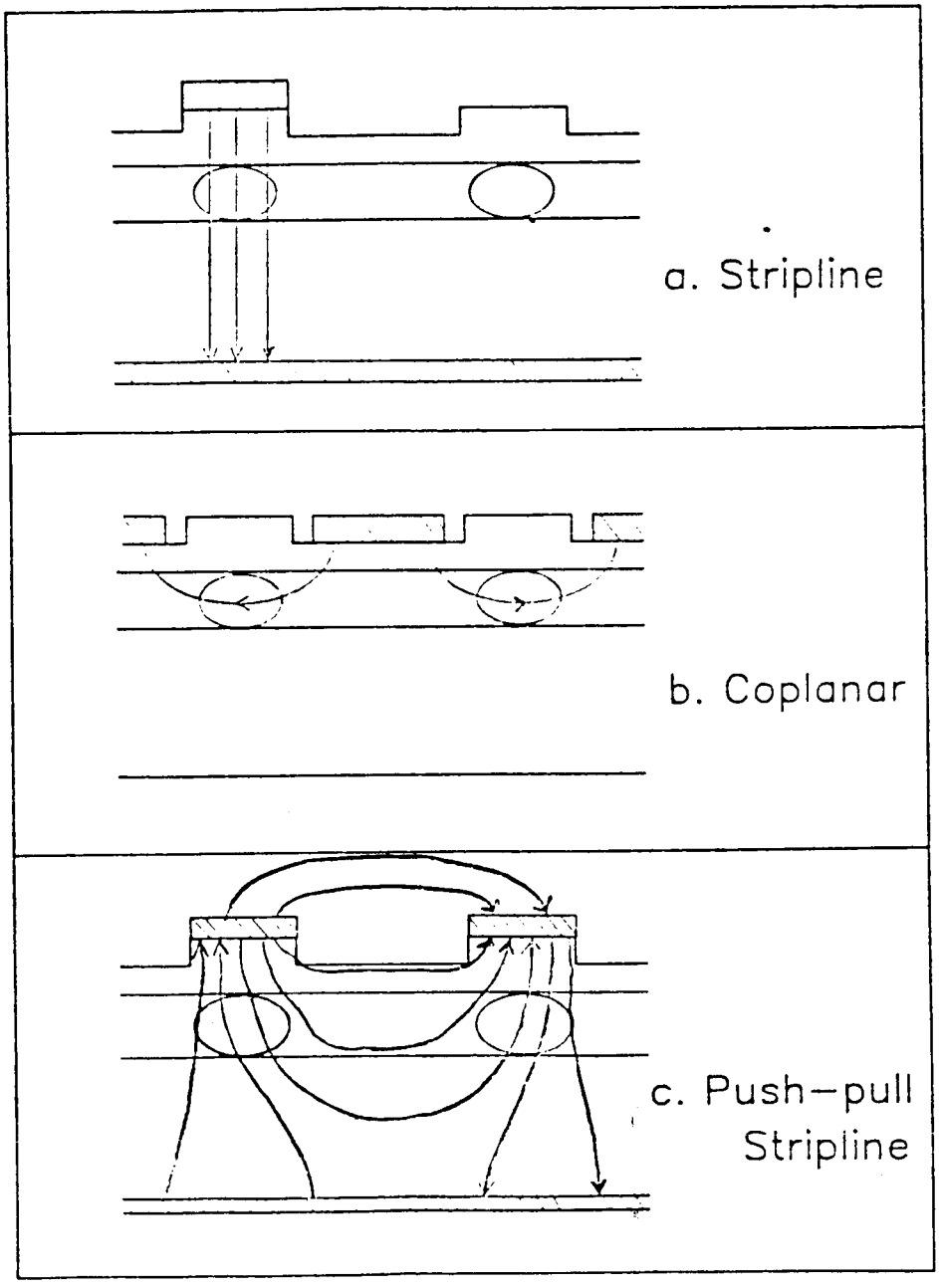

Figure 27. Potential Electrode Geometries

modulator arms. This corresponds to the more efficient push-pull configuration which was assumed in the Mach-Zehnder analysis of Chapter 3.

In contrast, the stripline of figure 27.a creates a vertical external field for a maximum electro-optic effect on the E_x optical waveguide mode. While this mode has not been analyzed, this alternative geometry is certainly possible. One disadvantage of the stripline is that the field interaction is only in one arm of the modulator. This is less efficient than the push-pull and results in a longer interaction region to achieve the same phase shift. If a second strip is added, the field lines are severely distorted and the field in the waveguide region may no longer be vertical.

A less obvious effect of the electrode geometry is its effect on the optical waveguiding properties of the modulator. The metal overlayer contributes negatively to the effective index of the region beneath it [21]. This means that the optical waveguiding properties of the ridge are reduced by the stripline. The optical guidance is enhanced by the coplanar electrodes. In addition, the coplanar electrodes are geometrically farther from the optical field, implying less light will be absorbed, and the propagation losses will be lower than for the stripline. For all of the above reasons,

the analysis will proceed with the coplanar waveguide structure as the modulator electrode.

5.2 Electrode Impedance

The dimensioned coplanar electrode geometry is shown in figure 28. No attempt was made to rederive the theoretical analysis of this structure because programs to compute the impedance of this structure had already been developed at NASA by Dr. Rainee Simons [29],[30]. However, an understanding of the limitations of his analysis is essential to ensure that it is correctly applied to the modulator problem. The first assumption is that the thickness of the electrodes is zero (t = 0). Since the electrodes only need to be 2 or 3 skin depths thick (2 - 3 um at 5 GHz), this should have little effect on the impedance calculation. Second, the substrate is treated as a dielectric. For semi-insulating GaAs, the intrinsic conductivity is 10^{-6} mho/m [15] and indicates the relative magnitude of the conduction current. At 5 GHz, the relative magnitude of the displacement current is given by $w\epsilon$ and is on the order of 10^{11} mho/m. These numbers indicate that the displacement current dominates and the intrinsic GaAs can be treated as a dielectric (ϵ_r = 13.1). In

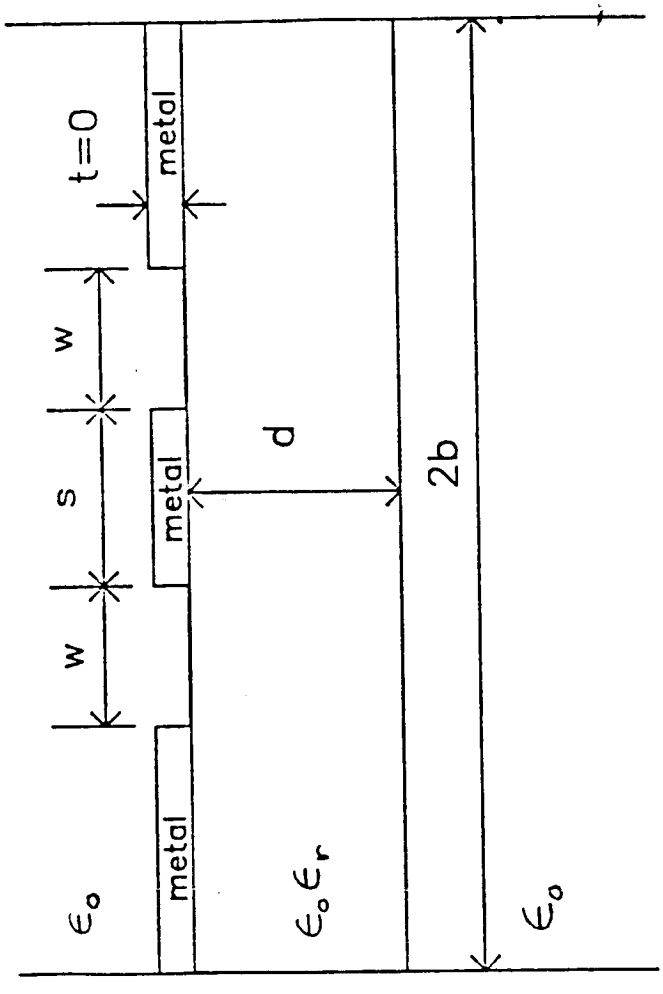

Figure 28. Coplanar Waveguide

addition, the analysis does not account for the GaAlAs film layers grown on the substrate for optical waveguiding. However, the film thicknesses (~5 um) are much less than the substrate thickness (~250 um) and the film layers with small aluminum mole fractions will have nearly the dielectric constant of GaAs.

The program used is a full wave calculation of the coplanar waveguide impedance. This technique is valid for higher frequencies (up to 26 GHz [29]) than a quasi-static approximation. The design is for a center frequency of 5 GHz (highest reported GaAs modulator) though the coplanar structure has a very large bandwidth. If b, d, s, f, & ϵ_r are specified, the program can be used to find a slot width (w) which gives a Z_0 of 50 $\pm$ 0.5 ohms. Using this method, the data shown in table 2 was generated. A plot of s vs. w to give Z_0 = 50 ohms is shown in figure 29. The analysis begins to break down for w > d and the s vs. w curve begins to level out in this region. This means that a small fabrication error in s or w could result in a large variation of Z_0 from 50 ohm. This data will be used to design 50 ohm transmission lines for the modulator as well as efficient tapering from the small modulator dimensions to the larger dimensions required for microwave connections.

Table 2

Er = 13

d = 250 um

t = 0 um

2b = 10 um

f = 5 GHz

Zo = 50 + 0.5 Ohms

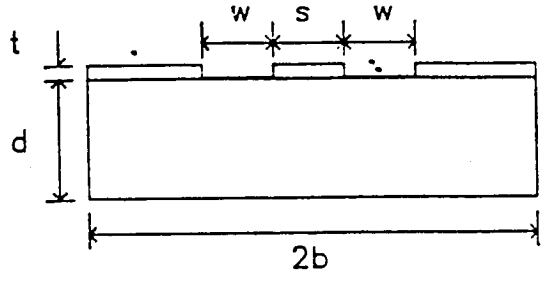

s (um)	w (um)	$K = \lambda_o / \lambda$	Zo(Ω)
10	8.75	0.3780	49.862
25	21.25	0.3784	49.557
50	43.75	0.3799	50.110
100	82.50	0.3848	50.062
200	137.5	0.3981	49.573
300	185.	0.4134	50.148
400	210.	0.4258	49.644
500	237.5	0.4382	49.870
600	262.5	0.4499	50.226

Coplanar Waveguide Electrode
Dimensions for 50 ohm Impedance

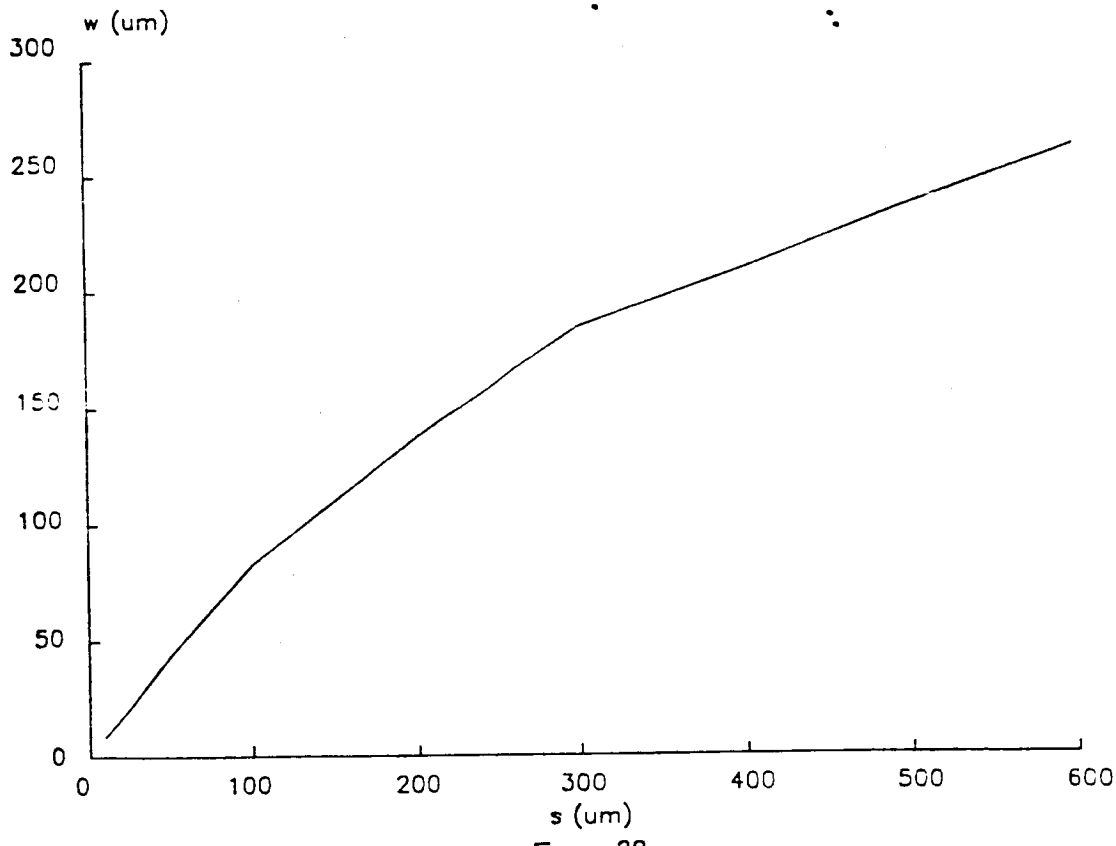

Figure 29.

5.3 Electrode Design

In addition to the 50 ohm impedance constraint, several factors from the modulator standpoint need to be considered in the electrode design. First, the branching angle limits the amount of space available between the optical waveguide branches. With a branching half-angle of 0.3^{o}, the distance along the propagation direction will be very long when compared to the lateral spacing between the waveguides. With this constraint, the electrode dimensions were chosen as:

$$s = 22.4 \text{ um} \qquad w = 20.0 \text{ um}$$

To center the 10 um wide optical ridges in the slot gaps requires a length (along the propagation direction) of 3.1 mm. For a more detailed dimensional description see the full device design in figure 30. For this choice of s and w, the calculated waveguide parameters are:

$$Z_{0} = 50.099 \text{ ohm}$$

$$K = 0.37837$$

where K is the ratio of the guide wavelength and the free space wavelength of the 5 GHz signal.

From the required dimensions, it is apparent that some form of tapering is necessary before external connections can be made to feed and terminate the transmission line. Since the design is already a 50 ohm

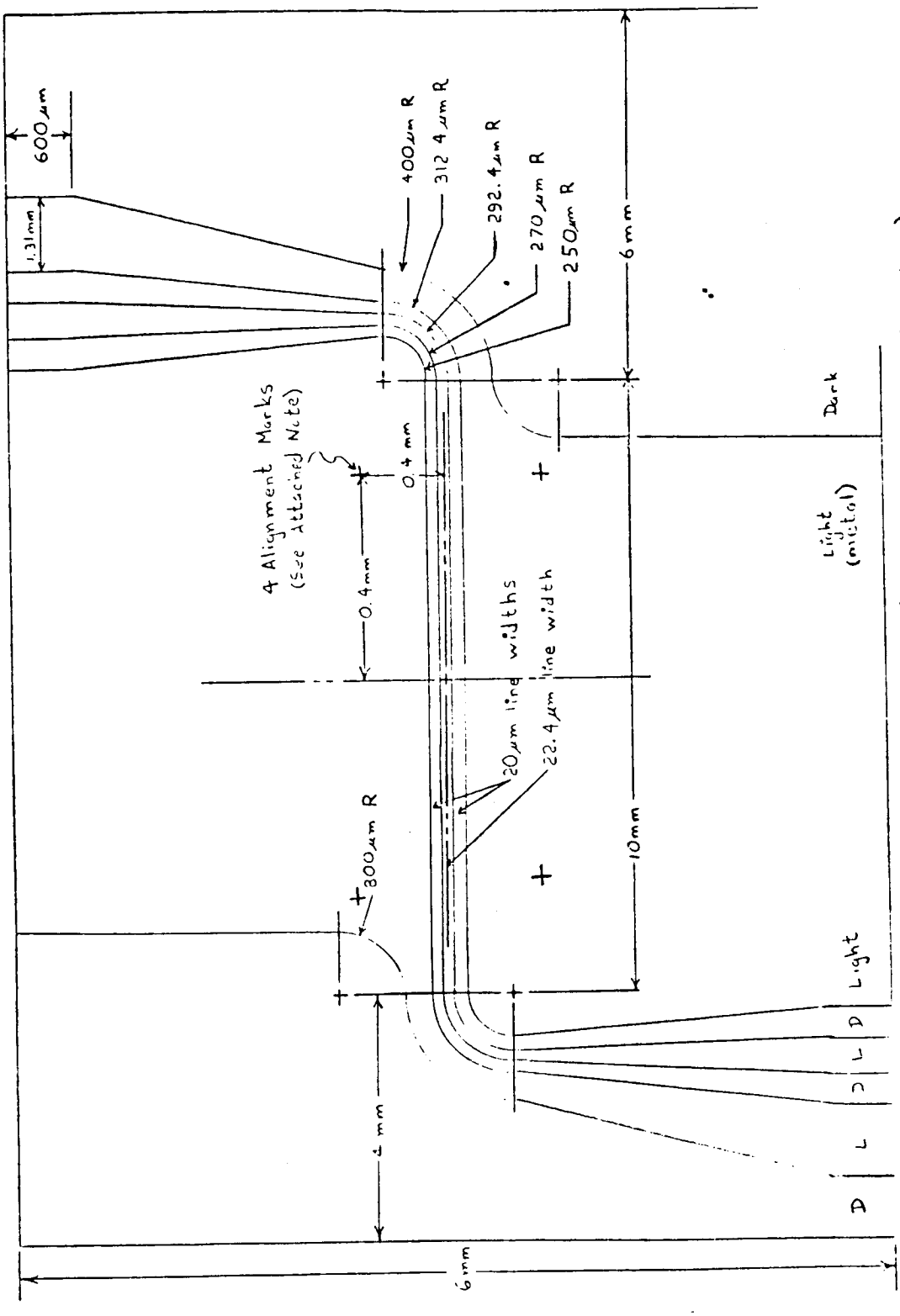

Figure 30. Initial Modulator Design (Microwave Electrodes)

line, no matching network is required if the s and w can be maintained for 50 ohms in the taper. A 6 point linear interpolation using the data in table 2 was used to taper from s = 22.4 um to s = 600 um and from w = 20.0 um to w = 262.5 um over a distance of about 2 mm. This taper is also shown in figure 30.

The final point to be resolved is how to connect to the center electrode without interfering with the optical waveguides. The only way to get this electrode to an external connection is for it to pass over one of the optical waveguides. This will affect the optical waveguiding properties as well as increasing the propagation loss (due to absorption in the metal). Since the light connects to the modulator at the ends, it is most convenient to bring the microwave signal in through the sides. This implies that one of the outer electrodes must also pass over the optical wavegudes. To minimize this interference, the outer electrode must be narrowed. Calculations of Z_0 as a function of b (table 3) show that b should be greater than 0.1 mm to maintain the 50 ohm impedance. Specification of the electrodes also completes the optical waveguide design. The full modulator dimensions are shown in figures 30 and 31.

Table 3

Er = 13
d = 250 um
t = 0 um
s = 22.5 um
w = 20 um
f = 5 GHz
Zo = 50 + 0.5 Ohms

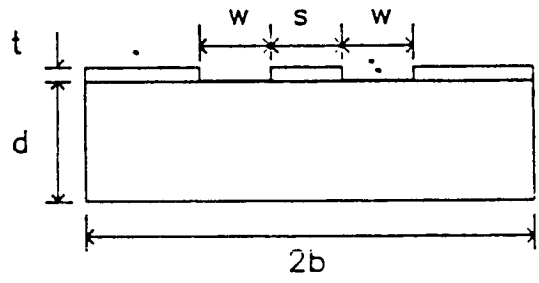

b	Zo(Ω)
5 mm	50.100
1 mm	50.095
500 um	50.076
250 um	49.963
100 um	49.228
50 um	46.924

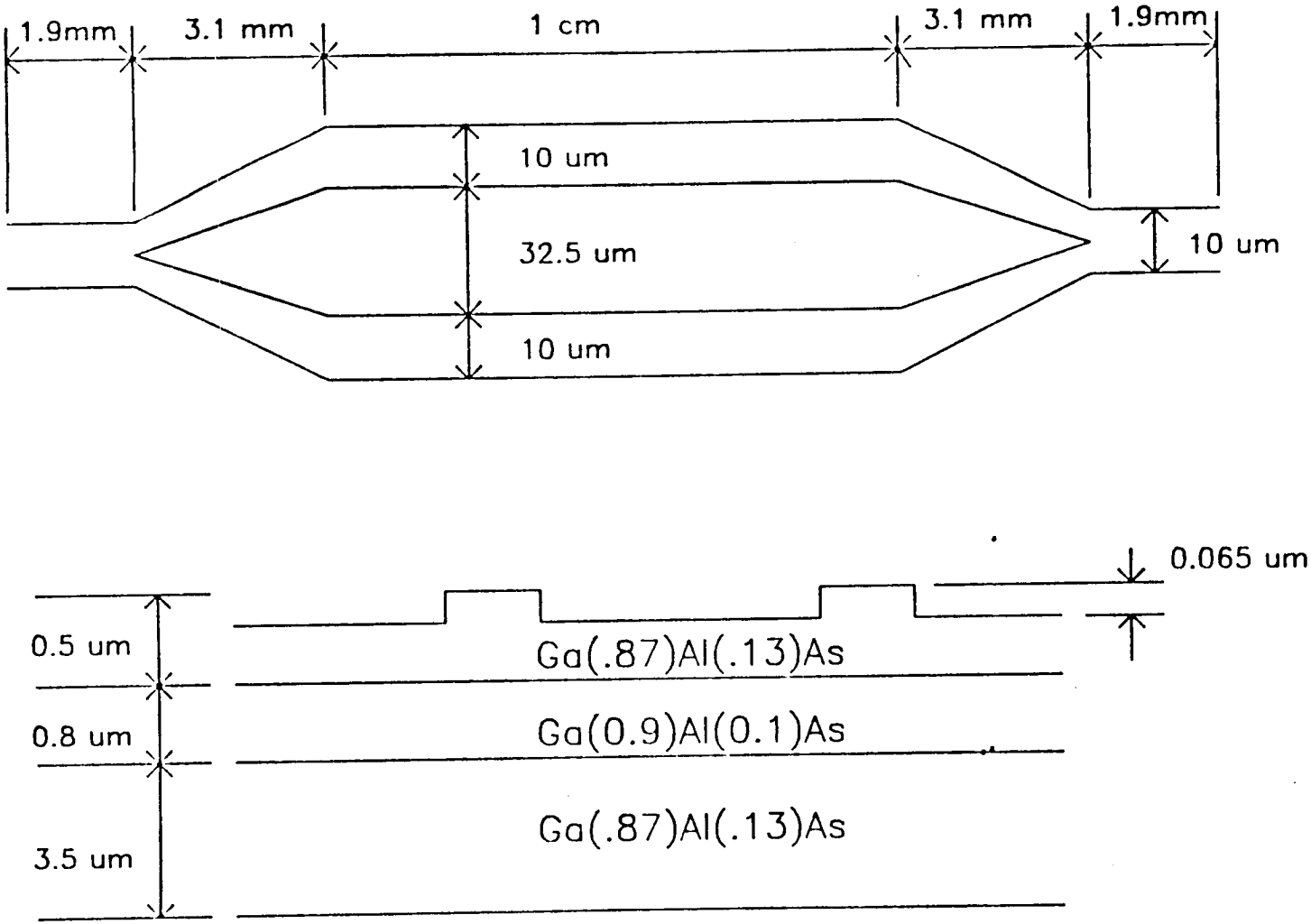

Figure 31. Modulator Design (optical waveguides)

5.4 Bandwidth

It has been mentioned on several occasions that a modulator with travelling wave electrodes has the potential to achieve higher bandwidths. This is because the travelling wave electrodes can overcome the transit time limitation of bulk electrodes [13].

This can be seen by considering a modulator with bulk electrodes. In the derivation of the electro-optic phase shift, it was assumed that an external field (E_m) was applied to the crystal. When the applied field is modulated at high frequencies, the applied field changes during the time it takes the light to propagate through the modulator. This reduces the electro-optic phase shift. The bandwidth is limited by the transit time of the light passing through the modulator. Yariv provides a simple (though somewhat arbitrarily defined) expression for the usable bandwidth of a transit time limited modulator [13]

$$f_{max} = \frac{c}{4\, n\, l} \qquad (5.1)$$

where f_{max} is the maximum usable frequency (bandwidth), n is the index of refraction of the electro-optic crystal, and l is the interaction length. For a 1 cm long modulator using GaAlAs layers (n~3.55), the maximum usable bandwidth is $f_{max} \sim 2.1$ GHz. It will be shown

that this can be significantly improved by using travelling wave electrodes.

Another possible limitation for the bulk electrode modulator is its loading effect on the external driving circuitry. That is, the RC time constant of the electrode geometry may limit the modulation bandwidth to a frequency even lower than the transit time limitation. The GaAs modulators reported by Donelly et. al. [6] and Buchmann et. al. [5] claimed RC time constants as the bandwidth limitation.

Both transit-time and RC limitations can be overcome if transmission line electrodes are used. With a transmission line electrode, the microwave signal propagates through the modulator along with the light. An infinite bandwidth is theoretically possible if the microwave field propagates along the electrodes at the same speed as the light propagates. In reality, the microwave field propagates slower than the light and the bandwidth is limited by the "walkoff" as the fields propagate through the device. In the following analysis, the subscript "o" refers to the optical field (light) while the microwave field quantities are indicated with an "m" subscript. Following Yariv's analysis [13], light enters the modulator arms at $z = 0$ and is at position $z(t') = (t'-t)c/n_o$ at some later time

(t'). The optical phase velocity is determined by the effective index (n_o) of the waveguide as:

$$v_o = \frac{c}{n_o} \tag{5.2}$$

At higher frequencies, the electro-optic phase shift must be considered time dependent as the fields propagate. The rigorous expression for the phase shift over a modulator arm of length l is:

$$\Gamma(t) = \frac{2\pi}{\lambda} n_o^3 r_{41} \int_0^l e_m(z)\, dz \tag{5.3.a}$$

$$= a \frac{c}{n_o} \int_t^{t+\tau_d} e_m(t', z(t'))\, dt' \tag{5.3.b}$$

where the parameters a, and T_d have been defined as

$$a = \frac{2\pi}{\lambda} n_o^3 r_{41} \tag{5.4.a}$$

$$\tau_d = \frac{n_o}{c} l = \text{optical transit time} \tag{5.4.b}$$

Taking the modulation field to be single frequency, it can be expressed as

$$e_m(t', z(t')) = E_m e^{j(w_m t' - k_m z)} \tag{5.5.a}$$

$$= E_m e^{j(w_m t' - k_m \frac{c}{n}(t'-t))} \tag{5.5.b}$$

where z has been replaced with its optical time dependence. This expression can be inserted into equation (5.3.b) to determine the phase shift. Performing the integration yields:

$$\Gamma(t) = r \Gamma_o e^{jw_m t} \tag{5.6}$$

where $\Gamma_o = alE_m$ is the d.c. phase shift, $e^{jw_m t}$ is the high frequency modulation signal, and r is the reduction factor caused by the "walkoff"

$$r = \frac{e^{jw_m\left(1 - \frac{v_o}{v_m}\right)\tau_d} - 1}{jw_m\tau_d\left(1 - \frac{v_o}{v_m}\right)} \qquad (5.7)$$

Following Yariv's analysis has given an expression for the electro-optic phase shift at the end of the modulator arms for high frequencies.

For the Mach-Zehnder modulator, the maximum bandwidth of the intensity modulation at the output is desired. From Chapter 3,

$$I_{out} = I_{in}\cos^2\left(\frac{\Gamma_o}{2}\right) \qquad (5.8.a)$$

is the output intensity when the "walkoff" is not accounted for. With the "walkoff" accounted for,

$$I_{out} = I_{in}\cos^2\left(\frac{|\Gamma(t)|}{2}\right) \qquad (5.8.b)$$

To evaluate the 3 dB bandwidth, the Mach-Zehnder is biased at $I_{out} = 0.5I_{in}$ by applying a DC voltage across the electrodes. Since this is a DC bias, the bias intensity is given by (5.8.a). Now, the AC modulation is really the change in intensity from the bias point and the reduction factor must be accounted for as shown in figure 32. The figure shows an analysis similar to

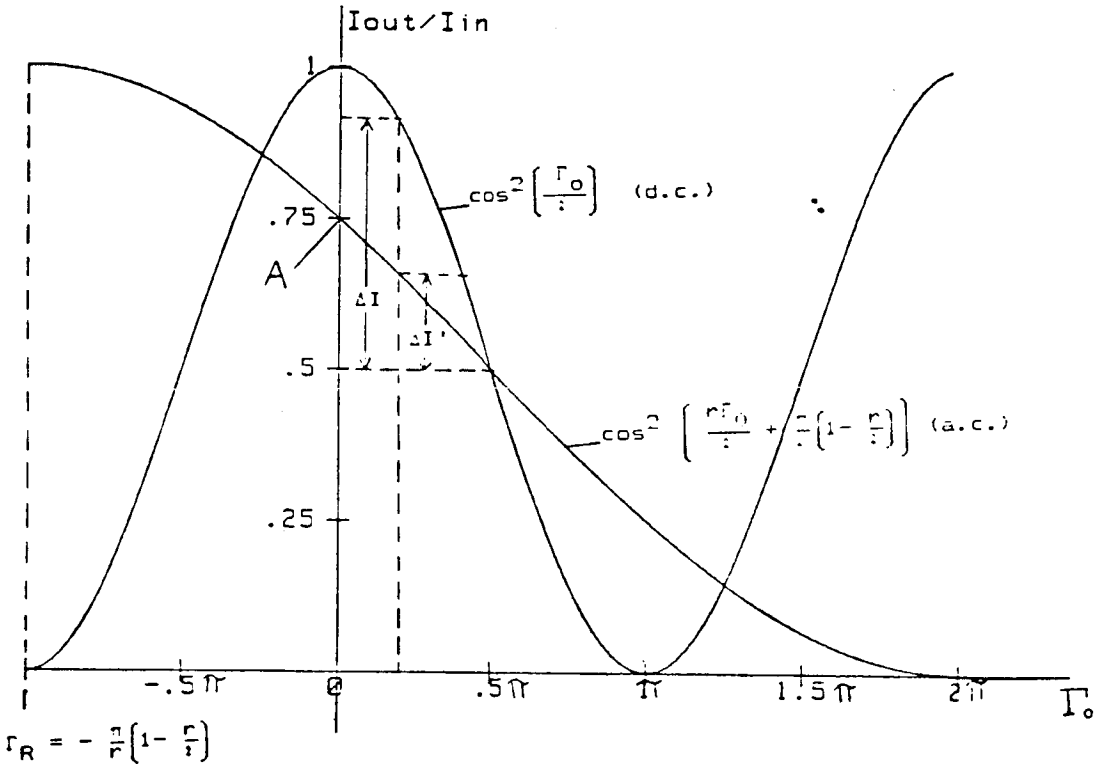

Figure 32. Mach–Zehnder Intensity Output for Low and High Frequency Modulation

methods used in large signal power amplifier design. The DC plot is used to establish the bias point at $I_{out} = I_{in}/2$ and the modulation is described by changes along the AC curve. For low frequencies, $|r| \sim 1$ and the AC curve closely follows the bias curve. As the frequency increases, $|r| < 1$ and the AC curve is elongated along the Γ_o axis. To determine a 3 dB bandwidth, consider the ratio $\delta I'/\delta I$ indicated in the figure. This ratio is a function both of the reduction factor and the phase shift.

Consider the case of complete intensity modulation. For low frequencies (where $r \sim 1$) the intensity change is $\delta I = 0.5\ \delta I_{in}$ for $\delta\Gamma = \pi / 2$. The 3 dB bandwidth is determined by finding the reduction factor for which $\delta I' = 0.25\ \delta I_{in}$ when $\delta\Gamma = \pi / 2$. Mathematically, this is the point at which (point A on the figure)

$$\frac{I_{out}}{I_{in}} = 0.75 = \cos^2 \left\{ \frac{\pi}{2} \left[1 - \frac{r}{2} \right] \right\} \qquad (5.9.a)$$

$$r = \left[1 - \frac{4}{\pi} \cos^{-1} \left(\sqrt{0.75} \right) \right] = \frac{1}{3} \qquad (5.9.b)$$

The modulation frequency at which this reduction is achieved can be determined from the definition of the reduction factor. Phi can be defined as

$$\phi = w_m\ \tau_d \left[1 - \frac{v_o}{v_m} \right] \qquad (5.10)$$

to simplify the reduction factor to:

$$r = \frac{e^{j\phi} - 1}{j\phi} = \frac{(\cos\phi - 1) + j\sin\phi}{j\phi} \qquad (5.11)$$

It is really the magnitude of the reduction factor which effects the intensity modulation (5.8.b). Taking the magnitude gives after some trigonometric substitutions:

$$|r| = \frac{\sin\left(\frac{\phi}{2}\right)}{\frac{\phi}{2}} \qquad (5.12)$$

Equating (5.12) with (5.9.b) gives the angle as :

$$\phi = 0.7254\ \pi \qquad (5.13)$$

Before substituting into (5.10) to find the bandwidth, the velocity of propagation can be converted to index of refraction by,

$$\frac{v_o}{v_m} = \frac{c}{n_o} \cdot \frac{n_m}{c} = \frac{n_m}{n_o} \qquad (5.14)$$

where n_m is the effective index seen by the microwave field and is related to the guide wavelength (lambda prime) by,

$$n_m = \frac{1}{\bar{\kappa}} = \frac{\lambda}{\lambda'} \qquad (5.15)$$

Using (5.14), (5.15), (5.4.b), and (5.13) in (5.10) gives the desired bandwidth limit:

$$w_m\, l_m \left[\frac{n_o}{c}\right]\left[1 - \frac{n_m}{n_o}\right] = \phi \qquad (5.16.a)$$

$$f_m\, l_m = \frac{\phi\left[\frac{c}{n_o}\right]}{\left[2\pi\left[\frac{n_m}{n_o}\right]\right]} \qquad (5.16.b)$$

Substituting the previous results

$$n_o = 3.55367 \qquad (5.17.a)$$

$$n_m = 2.6429 \qquad (5.17.b)$$

yields

$$f_m \, l_m = \frac{0.7254 \, \pi \, (3 \times 10^8 \text{ m/s})}{3.55367 \left[2\pi \left(1 - \frac{2.6429}{3.55367}\right)\right]} \qquad (5.18.a)$$

$$= 11.95 \text{ GHz} \cdot \text{cm} \qquad (5.18.b)$$

as the bandwidth length product of the designed modulator. It is observed that the 11.95 GHz theoretical bandwidth of a 1 cm long modulator is significantly greater than the transit time limited bandwidth.

Before leaving the discussion of modulator bandwidth, there are two important points to consider. First, the bandwidth is intimately tied to the length of the interaction region. For increased bandwidth, the device can be shortened. It will be seen in the next section that this requires additional drive power. Second, the result (5.18) is for full intensity modulation over the nonlinear intensity function. Therefore, it represents a minimum theoretical bandwidth of the modulator. If the drive signal is smaller, requiring a smaller phase shift, the modulation will be more linear. It follows that the reduced distortion will allow a higher bandwidth for small signals and the

above analysis could be rederived using a small signal analysis.

5.5 Modulator Power Requirements

To determine the drive power required by the modulator, the field created by the coplanar electrodes must be determined. The full wave analysis used to determine the impedance was also used by Simons to calculate the electric fields [31]. The equations are provided in Appendix D along with a listing of the program used to calculate the fields. Before presenting the results, there are several limitations of using this analysis. The electrodes are again assumed to have zero thickness. In reality, the electrodes must be several skin depths thick to reduce thin film resistivity losses. At 5 GHz, using gold electrodes ($\sigma = 4.1 \times 10^7$ mhos/m), the skin depth is:

$$\delta = \sqrt{\frac{2}{\omega\mu\sigma}} = 1.1\ \mu m \qquad (5.19)$$

$$= \sqrt{\frac{2}{2\pi(5\times10^9)(4\pi\times10^{-7})(4.1\times10^7)}}$$

So, the electrode thickness should be at least 3 um. The optical guide region is the region from 0.5 um to 1.3 um below the surface. However, the guide region is

below the electrode gap where the fringes (not rigorously accounted for due to zero thickness assumption) will have minimal effect on the solution. The other potential problem is that the GaAlAs layers are not accounted for in the analysis. While the dielectric constant of the films is nearly that of the GaAs substrate (as in impedance calculations), the film boundaries may be important is determining the fields. At the dielectric interfaces, some charge can collect and shield the fields. Therefore, the actual field in the guide layer will be slightly smaller than the calculated result.

Using the field program, the field for z = 0 um to z = 1.5 um (fig. 33) was calculated using a small grid (z = 0.1 um , y = 0.5 um) and was found to be approximately parallel to the film layers. At the four edges of the optical guide region (fig. 33) the fields are found to be:

$$E_{\pi}\ (a) = 48314.4\ V_o \quad (V/m) \qquad (5.20.a)$$

$$E_{\pi}\ (b) = 45610.95\ V_o \quad (V/m) \qquad (5.20.b)$$

$$E_{\pi}\ (c) = 45859.3\ V_o \quad (V/m) \qquad (5.20.c)$$

$$E_{\pi}\ (d) = 46193.8\ V_o \quad (V/m) \qquad (5.20.d)$$

where V_o is the voltage applied across the coplanar electrodes. The average field in the region of the guided light is:

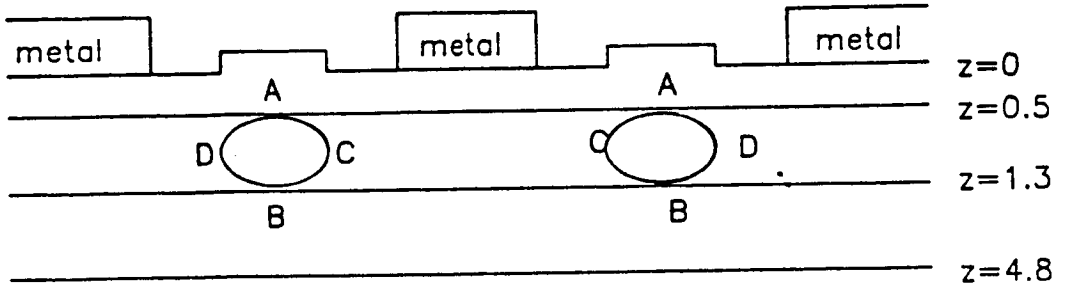

Figure 33. Modulator Cross Section

$$E_\pi = 46500 \; V_o \qquad (V/m) \qquad (5.20.e)$$

Remembering the phase shift equation of chapter 3,

$$\Gamma = \frac{2\pi}{\lambda} n_o^3 \, r_{41} \, l \, E_m \qquad (5.21)$$

full intensity modulation requires $\Gamma = \pi$ and a field of:

$$E_\pi = \frac{(\Gamma=\pi)\ \lambda}{2\pi \, n_o^3 \, r_{41} \, l} = 831000 \quad \frac{V}{m} \qquad (5.22)$$

Substituting into equation (5.20.e) gives the required voltage as $V_{pi} = 17.9$ V for a 1 cm interaction region. This is for full intensity modulation with no DC bias. The modulator can be operated in the push-pull configuration by applying a DC voltage to bias the modulator at $I_{out} = 0.5 \; I_{in}$. The required AC voltage is reduced by a factor of 2 and is: $V_{pi} = 8.9$ V. An important point is that E_{pi} is inversely proportional to l. The required field intensity can be reduced with a longer interaction region. In designing a modulator, there is a tradeoff between bandwidth and drive power through the device length. A short modulator gives a higher bandwidth at the expense of higher drive power and vice versa.

The mimimum power required by the modulator can be estimated from the time average power flow down the transmission line electrodes. This is given by:

$$P = \frac{1}{2Z_o} \int (\underline{E} \cdot \underline{E}^*) \, dS \qquad (5.23.a)$$

$$P = \frac{1}{2Z_o} \sum_{\substack{\text{cross} \\ \text{sectional} \\ \text{area}}} (E_y^2 + E_z^2) \Delta A \qquad (5.23.b)$$

The field along the direction of propagation is purely imaginary (Appendix D) and so does not carry any time average power flow. This summation was carried out by a computer using a tight grid near the electrodes (where the field intensity is not uniform) and a wider grid far from the electrodes (where the field changes more slowly). The summation was terminated when the field intensity had reached 10% of its maximum value. The result is that

$$\Sigma (E_y^2 + E_z^2) = 2.92734 \; V_o^2$$

giving a total power of

$$P = .5 \; (2.92374) \; V_o^2 \; / \; Z_o$$

$$P = 2.335 \text{ Watts}$$

for a modulator operated in push-pull configuration with an impedance of 50 ohms.

This is a high drive power requirement and raises concerns about the substrate's ability to handle this power. But, this power is not consumed by the modulator. Instead, the power just propagates down the transmission line and is dissipated in the 50 ohm termination. There is only a small amount of power (~4uW) dissipated through resistivity of the GaAs. Another concern is that the required field intensity not exceed the dielectric breakdown point of the GaAs

substrate. The highest field intensity created by the coplanar electrodes is 4.96×10^4 V/m (at the center of the electrode gap on the wafer surface) while dielectric strength of GaAs is 4×10^7 V/m [15]. These two results insure that no physical damage to the modulator will result from the required field intensity and power.

Chapter 6: Fabrication

6.1 The Fabrication Process

With the design of a GaAs modulator completed, the next step is to begin characterizing a fabrication process. The steps required to fabricate the modulator are outlined in section 6.1.1. The procedure can be broken down into 4 major steps. The first step, the epitaxial growth process, was contracted outside NASA and will be described below. The rest of the fabrication process will be described in more detail in the rest of this chapter. In addition, the drawings of the specially designed test fixture are included in Appendix E.

The modulator is fabricated on a (100) semi-insulating GaAs substrate. The (100) specification is the orientation of the crystal lattice as was chosen in chapter 3 to utilize the maximum electro-optic phase shift in GaAs. The semi-insulating substrate acts as a dielectric for the coplanar transmission line electrodes. The GaAlAs film layers can be grown by molecular Beam Epitaxy (MBE) to produce low loss optical waveguides [32]. The epitaxial growth process means that the lattice of the grown layers copies the

C-2

orientation of the substrate. Since the GaAlAs lattice spacing is closely matched to that of GaAs [33], a crystal film which is almost identical to GaAs results. The MBE process produces very high quality films with layer defect densities on the order of 2000 defects/cm^2. Taking the lattice spacing of 5.6533A [14] into account gives a volume defect density of 3.5×10^{10} defects/cm^3. Since the molecular density of the GaAs crystal is 2.21×10^{21} molecules/cm^3, only about 1 in 6×10^{10} molecules is a defect.

The growth of the films was contracted by NASA to Perkin-Elmer's Physical Electronics Division in Eden Prairie, Minnesota. The growth process placed some limitations on the design of the optical waveguides. The MBE process can control the film thickness very accurately (on the order of an atomic diameter). However, the aluminum mole fraction of the film layers has not been well characterized. The relative difference of 0.1 to 0.13 (aluminum mole fraction) was designed based on the tolerances Perkin-Elmer determined feasible. To prevent oxidation of the top GaAlAs layer, a 100 A GaAs overlayer was specified in the growth process. This overlayer will protect the GaAlAs from the time it is first exposed to air after growth at Perkin-Elmer, until stage II processing begins at NASA.

6.1.1 Outline of Modulator Fabrication Process

I. Epitaxial growth of GaAlAs films

- A. Start with (100) semi-insulating GaAs wafer
- B. Grow 3.5 um $Ga_{.87}Al_{.13}As$ by MBE
- C. Grow 0.8 um $Ga_{.90}Al_{.10}As$ by MBE
- D. Grow 0.5 um $Ga_{.87}Al_{.13}As$ by MBE
- E. Grow 100 A GaAs by MBE

II. Etching of Optical Waveguides

- A. Clean wafer
- B. Remove GaAs overlayer
- C. Pattern waveguides using photoresist
  1. Apply photoresist
  2. Expose through waveguide mask
  3. Develop
  4. Pattern leaves photoresist over areas not to be etched
- D. Etch 650 A of $Ga_{.87}Al_{.13}As$ layer
- E. Remove photoresist

III. Metallization of microwave electrodes

- A. Clean wafer
- B. Pattern waveguides using photoresist
  1. Apply photoresist

2. Expose through waveguide mask
3. Soak in chlorobenzene
4. Develop
5. Pattern leaves photoresist over areas not to be metallized

C. Evaporate 2-3 um of gold

D. Soak in acetone to liftoff metal deposited on photoresist

IV. Packaging

A. Cut device to final size (2cm x 6mm)

B. Cleave ends of optical waveguides

C. Insert into specially designed fixture

D. Bond connectors

6.2 Lithography

Lithography is the process of transferring geometric shapes onto the semiconductor substrate [34]. The lithographic process to be used for the modulator fabrication is shown in figure 34. The geometric pattern is transferred from the mask to the photoresist by exposing the photoresist to ultraviolet light through the mask. The mask is in contact with the photoresist during exposure for exact 1:1 printing of the pattern

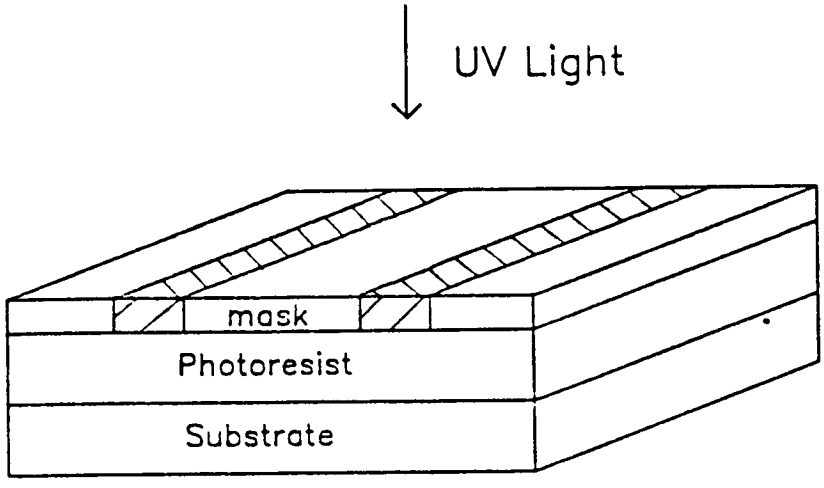

a. Exposure

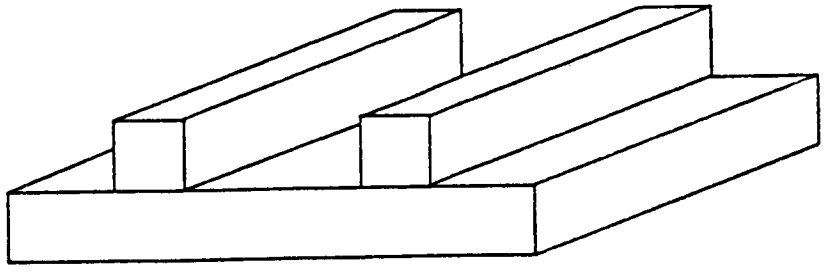

b. After Developing

Figure 34. Pattern Transfer by Photolithography

and to avoid diffraction of the light around small device features. Positive photoresists are normally used because negative resists can swell when developed. This swelling is negligible until device features are smaller than about 5 um [34]. After exposure, the resist is developed and removed everywhere that it was exposed to light. The result is a mask on the device surface which can be used in further processing.

The process of making a mask for the Mach-Zehnder optical waveguides presents some unique problems. Usually, a mask is made to scale many times the desired size and photographically reduced to the desired size. The original, large scale mask is made by cutting the pattern out of a thin sheet of rubylith. The minimum feature size which can be cut on the rublith is about 10 mil (250 um). The final device can be reduced until the feature size reaches about 1 um and is limited by diffraction through the optics of the photoreduction system.* In the case of the Mach-Zehnder, the feature size is limited by the aspect ratio of the device. That is, the ratio of the minimum feature size to the overall device length. The largest original that can be

---

*For even smaller feature sizes, electron beam lithography can be used.

photoreduced is 1 meter. To produce a modulator that is 2 cm long requires a reduction of 50:1 from the 1 meter original. This means that the minimum feature size is d = 250um/50 = 5 um. In the Mach-Zehnder, the minimum feature is at the point of the Y-Branch split (fig 26.a). To achieve this limit, the minimum optical waveguide ridge width is 2d = 10 um. This was the ridge width chosen in chapter 4 "for fabrication reasons".

Unfortunately, the available photoreduction facilities are not equipped to handle the required 50:1 reduction. With some effort, the photoreduction was manipulated to achieve the 50:1 reduction with limited success. Figure 35 shows the two modulator arms after a 50:1 reduction. The lines are fuzzy because the final reducing lens is f#=9 and is nearing its resolving power for the 10 um line width. Also, the reduction camera is not vibration isolated. Small vibrations can be significant when attempting to produce 10 um lines.

The sidewalls of the optical waveguide ridge must be smooth to reduce scattering of light from the edges. Although the strip loaded ridge waveguide is less susceptible to this scattering than other structures, it is still a significant concern. Therefore, a better mask is presently being contracted out by NASA. The facilities available at the mask contractor should be

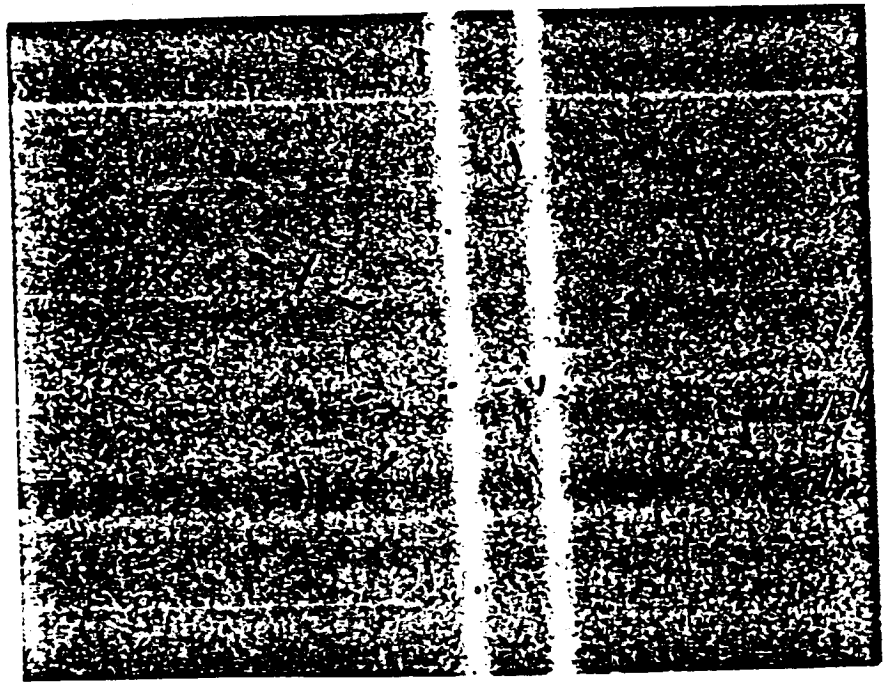

Figure 35. Parallel Modulator Arms on Waveguide Mask (line width = 10 um)

able to produce a straight waveguide edge to a tolerance of about 0.1 um. This will be a great improvement over the mask shown in figure 35.

6.3 Etching

The loading ridge of the optical waveguides is formed by an etching process. Once the photoresist has been patterned, the surface of the wafer is etched chemically or by a dry etching technique. The resist is not effected by the etching process, and protects the film layers below. After etching, the photoresist can be removed by an acetone rinse and the mask geometry has been transferred onto the device.

There are basically two methods of etching; wet etching and dry etching. Wet etching is a chemical etchant (usually an acid solution) which attacks the GaAs or GaAlAs layers. Wet etching leaves a smooth surface in the etched region but etches in all directions. This leads to the undercutting shown in figure 36. Dry etching techniques such as Plasma Etching or Reactive Ion Etching (RIE) use chemical reactions between the top film layer aided by high energy ion bombardment to etch the surface [34]. The result of RIE is a vertical sidewall (no lateral

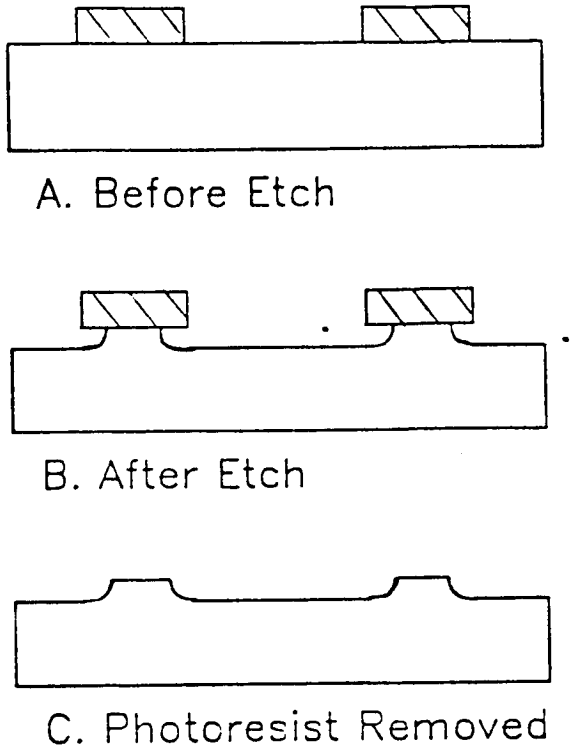

Figure 36. The Etching Process

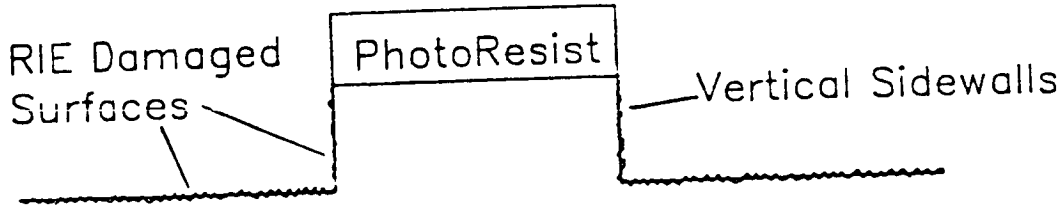

Figure 37. Surface damage caused by
Reactive Ion Etching

etching) but, the etched surface is damaged by the high energy ion bombardment (fig 37).

For the 10 um wide waveguides, a 650 A etch is required by the design of Chapter 4. For this small etch depth, the lateral etch distance of a wet chemical etch is also small. Therefore, it will not significantly effect the 10 um ridge width. The smooth surface remaining after a wet chemical etch is desirable to reduce scattering losses in the optical waveguides. Therefore, a wet chemical etch was chosen for the modulator fabrication process. If a narrowar ridge is fabricated in future designs, the etch depth will be larger (fig. 22). Reactive Ion Etching may be required at that point if lateral etching becomes significant. RIE is also the method used by Buchmann et. al. [5] in fabricating the sharp tip of the Y-Branch to reduce scattering and reflection losses at the junction.

A very slow wet chemical etch is required to form the 650 A step. Inoue and Sakaki [35] reported thinning of $Ga_{.87}Al_{.13}As$ film layers by 200A using weak acid solution of $3H_3PO_4 : 1H_2O_2 : 75H_2O$ at 0^oC. This etch was characterized at NASA for GaAs and two mole fractions of $Ga_{1-x}Al_xAs$. The etch was found to be highly temperature sensitive so temperature was carefully monitored and maintained using an ice bath. Prior to etching, the

solution was always at $3^{o}C$ with a rise during etching to $4-5^{o}C$. The results are tabulated in table 4 for the available aluminum mole fractions. Since the top layer of the modulator is $Ga_{.87}Al_{.13}As$, it is important that this etch be characterized accurately. Table 5 shows the results of this etch on 4 separate occasions. The deviation between these trials is 15.9 Å/min (9.3%). For the 3 minutes 42 seconds required to etch the ridge, a final result of 650 $\pm$ 25.6 A is obtained.

6.4 Metallization

The microwave electrodes are added to the modulator by the process of metallization. The metallization process is shown in figure 38. The process begins with exposure of the photoresist through the mask to transfer the electrode geometry to the resist. Before development, the wafer is soaked in chlorobenzene to harden a thin layer near the top of the photoresist. The resist is then developed for a period longer than normal to produce the undercutting shown in the figure. A thin layer of titanium (200A) followed by the gold electrode layer is then deposited by an evaporation process [35]. The thin layer of titanium is used because it adheres to the GaAs better than gold. The

Table 4

Material	Etch Rate (A/min)
GaAs	147.29
Ga(.87)Al(.13)As	170.33
Ga(.4)Al(.6)As	184.51

Table 5

Trial	Etch Rate (A/min)
1	167.9
2	170.33
3	179.5
4	163.6

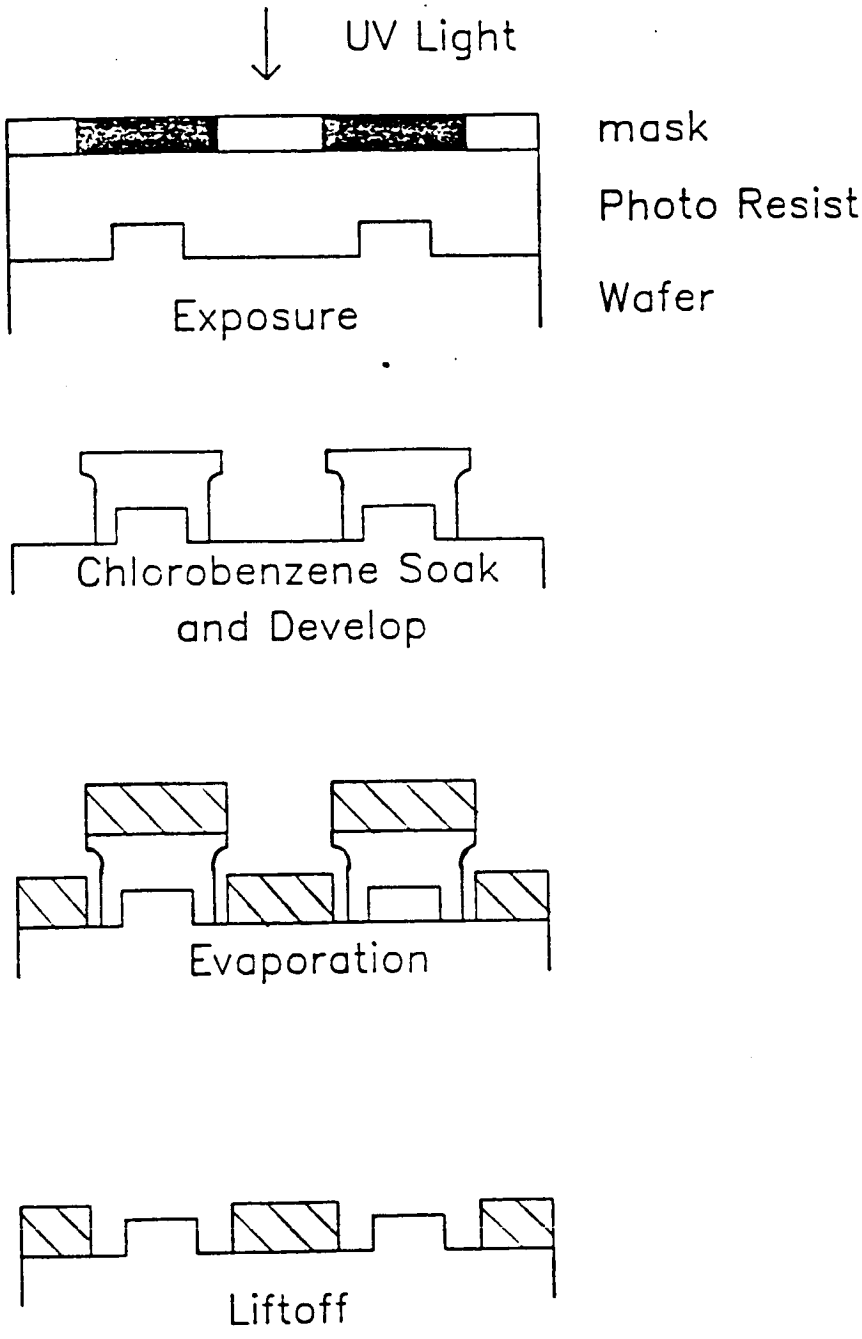

Figure 38. The metallization process

gold will then readily adhere to the titanium layer. When the wafer is soaked in acetone, the remaining photoresist is removed along with any metal deposited on the resist layer. The undercut achieved using the chlorobenzene soak leaves gaps in the metal layer through which the acetone can attack the photoresist.

The available processing facilities limit the metal thickness to about 1 um. This is because as the metal particles deposit on the substrate, their energy is transferred to the substrate through inelastic collisions [36]. This energy transfer results in heating of the substrate. Since the evaporation process takes place in a vacuum, the substrate cannot radiate this heat energy to a surrounding atmosphere. For thicknesses above 1 um, thermal expansion of the substrate destroys the film adhesion. That is, the GaAs substrate expands at a different rate than the metallic film layer. The resulting shear stresses pull the metallic layer away from the substrate.

In order to achieve a metal thickness of 2 or 3 skin depths, this metallization process will have to be improved. One option is the addition of a water cooled substrate holder. The cooling could be used to control the substrate temperature and reduce the thermal stresses for thicker films. Another alternative is to

evaporate only a thin (<500A) metal seed layer. Then the electrodes can be built up to several microns by an electroplating process.

6.5 GaAs Dry Run

To evaluate the processing, a dry run of the process was performed on a semi-insulating GaAs substrate (without the MBE film layers). The developed photoresist for the optical waveguides is shown in figure 39a and figure 39b shows the etched rib after the photoresist was removed. The poor quality of the mask is manifested in the ragged edges of the waveguides. The tip of the Y-Branch is shown in figure 40. This structure is difficult to fabricate because the region between the ridges is becoming infinitescimally narrow. The diffraction limitations in the photoreduction process used to make the mask are again the cause of the ragged edges of the Y-Branch. These problems should all be solved by the new mask.

The alignment of the electrode layer photoresist is shown in figure 41. The lines of resist used to protect the optical waveguide ridges can be aligned well and cover the edges completely. The picture shows the short

Figure 39.

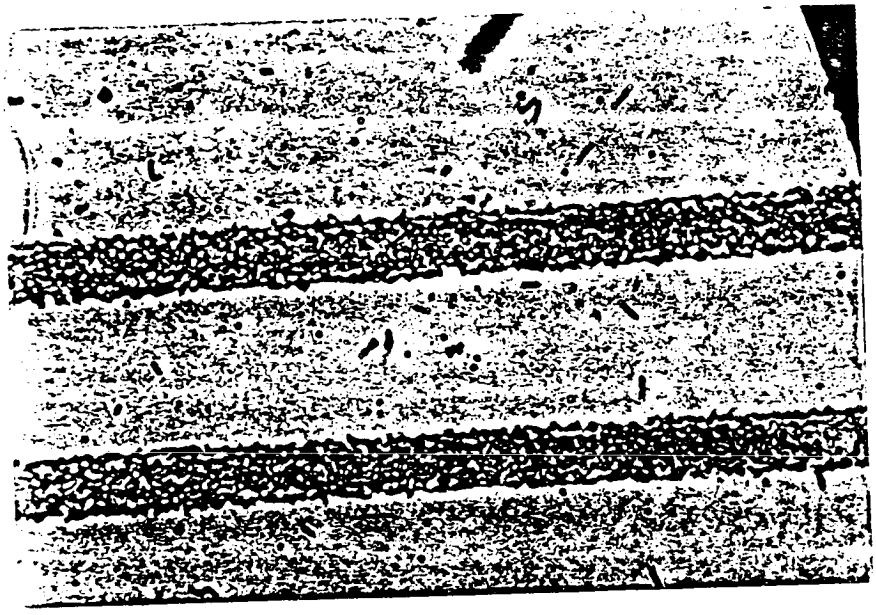

a. Photoresist pattern of optical waveguides

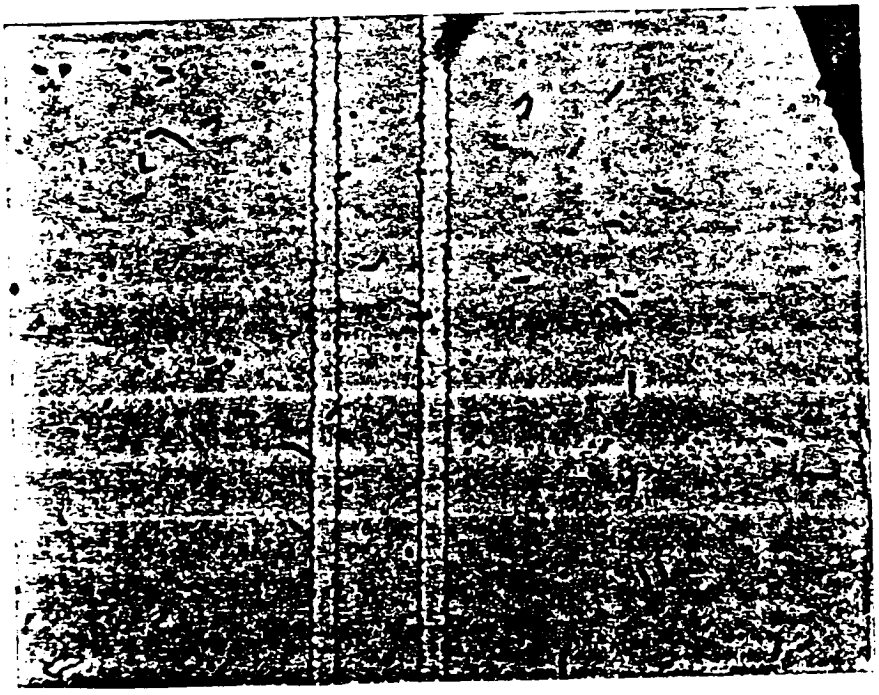

b. Etched ridges of optical waveguides

Figure 40. 650Å Etched Y-Branch on GaAs

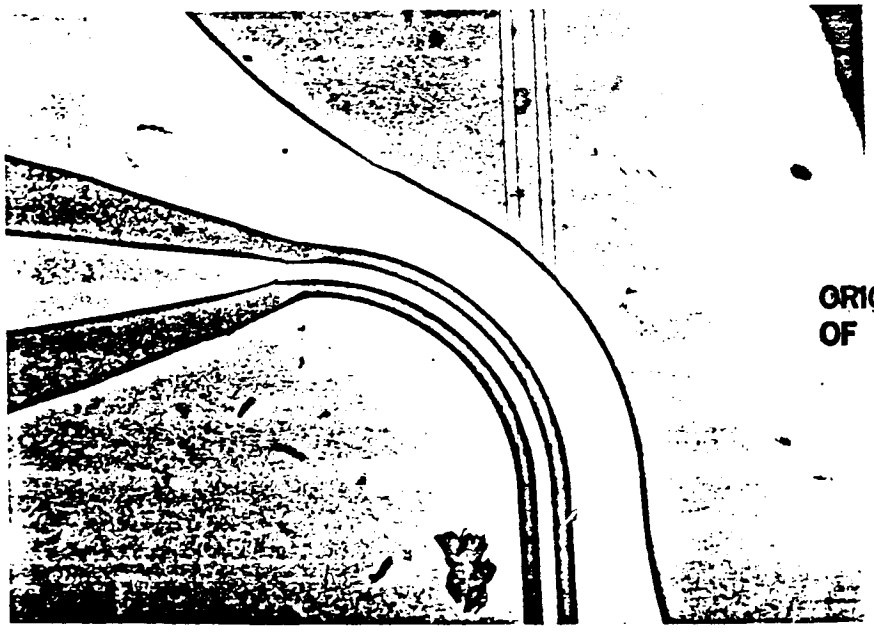

Figure 41. electrode photoresist over optical waveguides on GaAs

length of the optical waveguide ridges which will be covered by metal so that the electrodes can connect to the outside world. Unfortunately, the liftoff procedure was not successful on this dry run. This was most likely due an error in the chlorobenzene soak. However, this procedure has been successfully demonstrated at NASA on numerous other devices.

The results of the dry run show that a somewhat crude first modulator can be fabricated. The lithography limits imposed by the mask photoreduction process will result in a modulator with higher propagation loss than desired. However, upon delivery of the MBE grown films, an initial modulator can be fabricated for testing.

Chapter 7: Conclusion and Paths for Future Work

A Mach-Zehnder modulator operating at 0.82 um wavelength, using the electro-optic effect of GaAs, and utilizing transmission line electrodes has been investigated for the first time. A modulator fabricated on GaAs and operating at this wavelength can potentially be integrated with a GaAs laser or other microwave components on an MMIC. The electro-optically induced phase shift has been rigorously derived for the geometry in which it is maximized. The electro-optically induced phase shift is converted to intensity modulation of light using the Mach-Zehnder interference scheme. The optical waveguiding properties of the strip-loaded ridge waveguide have also been examined. GaAlAs film layers were used to provide a transparent medium in which the light can travel. The optical waveguide was analyzed using the effective index method to determine the field intensity profiles and mode cutoff conditions in the case where the light is polarized parallel to the film layers. An optical waveguide analysis program was written and used as a tool to design single mode optical waveguides for the modulator.

To take advantage of the maximum electro-optic phase shift in GaAs, a coplanar waveguide structure was

used for the microwave electrodes. Electrodes with a 50 ohm impedance at the design frequency of 5 GHz were designed using available programs. The theoretical bandwidth of the modulator was calculated at 11.95 GHz and is limited by the walkoff between the microwave signal and the light propagating through the modulator. This is higher than any GaAs modulator yet reported. The electric field was calculated to determine the required microwave power for full intensity modulation (2.335 W).

Some preliminary experiments to characterize a fabrication process for the modulator were carried out. An initial mask was made using photoreduced photolithography. A weak acid solution of ($3H_3PO_4$: $1H_2O_2$: $75H_2O$) was characterized with an etch rate of 170.33 A/min on the $Ga_{.87}Al_{.13}As$ top layer of the modulator. A dry run of the modulator fabrication process was also demonstrated on semi-insulating GaAs. Also, a modulator test fixture was designed, machined, and is described in an appendix.

The immediate goal of future work on this project should be the fabrication and testing of the initial modulator design. The purchasing process to acquire an improved mask has been initiated to improve the fabrication quality of this initial design. Also, some

effort has been made to set up optics for modulator testing. The optics were set up with the help of a summer intern a NASA. Coupling of 633 nm light into a planar (Si-Nitride-Air) waveguide was demonstrated. Some experiments to characterize the propagation loss and single mode guidance of the strip-loaded ridge waveguides would also be useful.

Once the initial modulator is demonstrated, the most urgent improvement required is to reduce the microwave drive power. This could possibly be accomplished by p-n doping of the substrate in a way which will concentrate the microwave field in the region of the optical waveguides. Optimizing the overlap of the optical and microwave fields can dramatically improve the modulator's efficiency. Finally, the long range goal of the project could be to integrate the laser with a GaAs/GaAlAs heterostructure laser or some microwave circuitry in a GaAs MMIC.

Appendix A : Properties of GaAlAs

A.1 Electro-optic Effect

In the design equations for the modulator, the electro-optic coefficient of GaAlAs is required. Unfortunately, no data on the electro-optic effect in GaAlAs is available in the literature. The electro-optic effect is primarily a geometrical effect of the material lattice. A nice property of GaAlAs (which makes GaAlAs epitaxial layers easy to grow) is that the AlAs lattice is closely matched to the GaAs lattice [33]. Both are cubic lattices with a lattice spacing of about 5.65A. Therefore, the electro-optic coefficient for GaAlAs can be approximated by the electro-optic coefficient of GaAs.

GaAs has the zincblende structure. Its only nonzero electro-optic coefficients are $r_{41}=r_{52}=r_{63}$. Table 6 summarizes data on the r_{41} electro-optic coeffient available in the literature. No data is available for wavelengths below the absorption edge of GaAs. For a "worst case" analysis, the coefficient can be taken as its smallest value:

$$r_{41} = 1.1 \times 10^{-12} \quad m/V$$

Table 6

wavelength (um)	r_{41} (m/V)	source
0.88	-1.5×10^{-12}	[16]
0.90	1.1×10^{-12}	[13]
1.06	1.5×10^{-12}	[37]
1.15	1.43×10^{-12}	[13]
3.39	1.24×10^{-12}	[13]
10.60	1.51×10^{-12}	[13]

A.2 Index of Refraction

In order to design the optical waveguide structures required for the Mach-Zehnder modulator, it is necessary to know the index of refraction of the film layers. The index of refraction is a function both of wavelength and aluminum concentration. The index of refraction is given by an experimentally determined equation known as the Sellmier Equation [27].

$$n^2(w,x) = A + \frac{B \cdot}{w^2 - C} - D * w^2$$

where,

$A = 10.906 - 2.92x$

$B = 0.97501$

$C = (0.52886 - 0.735x)^2$ if $x \leq 0.36$

$\quad\;\; (0.30386 - 0.105x)^2$ if $x \geq 0.36$

$D = 0.002476(1.41x + 1)$

w = wavelength of light

x = aluminum mole fraction

This equation was programmed as a subroutine in the optical waveguide program (see listing of SUBROUTINE ALTON$ in Appendix C). A graph of the index of refraction as a function of aluminum concentration is shown in figure 42. Over the region of interest, the index of refraction is monotonically decreasing with increasing aluminum concentration.

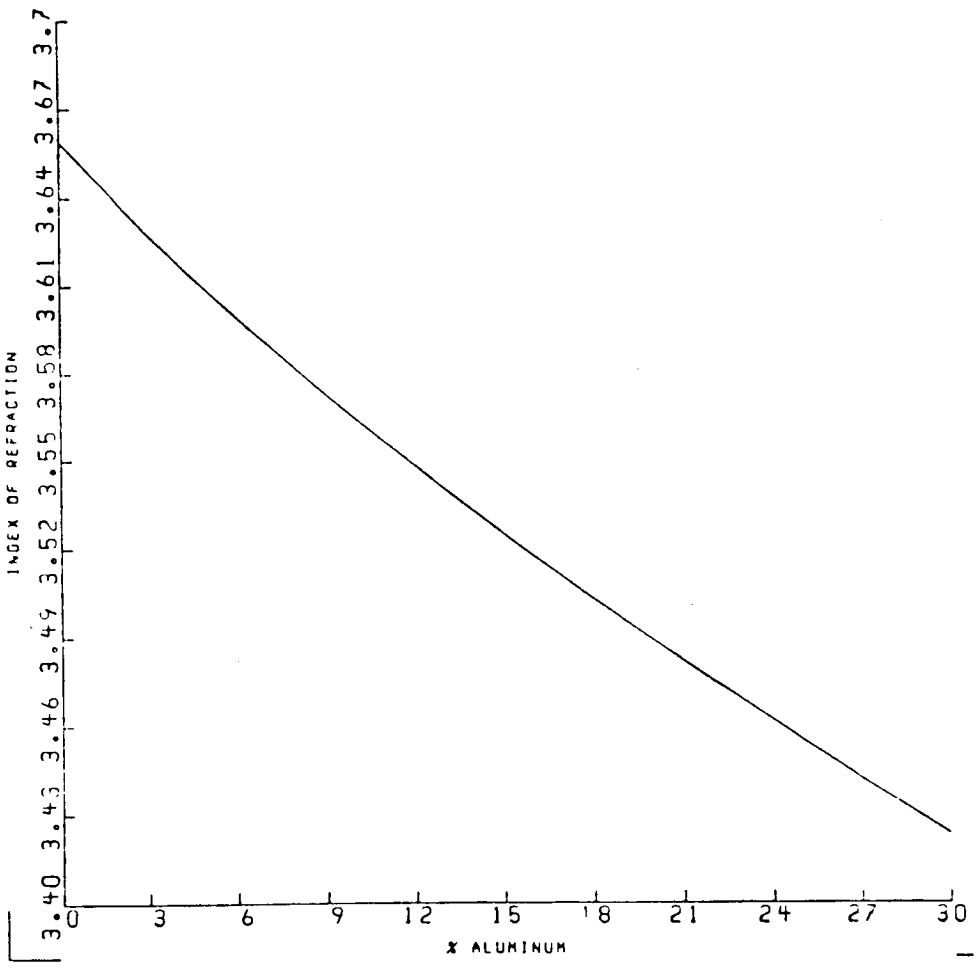

Figure 42. Index of refraction of Ga(1−x)Al(x)As

Appendix B: Derivation of Boundary Conditions for Optical Waveguides

The standard boundary conditions are,

$$\hat{n} \cdot (\underline{H}_2 - \underline{H}_1) = 0 \qquad \text{(B.1.a)}$$

$$\hat{n} \times (\underline{E}_2 - \underline{E}_1) = 0 \qquad \text{(B.1.b)}$$

$$\hat{n} \cdot (\underline{D}_2 - \underline{D}_1) = \rho_s \qquad \text{(B.1.c)}$$

$$\hat{n} \times (\underline{H}_2 - \underline{H}_1) = \underline{J}_s \qquad \text{(B.1.d)}$$

B.1. 4-Layer Planar Guide

TE mode: H_z, H_x, $E_y(x)$

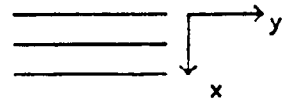

Maxwells Equations for TE waves are [39],

$$\nabla_t \times \underline{e}_t = - j\omega\mu\underline{h}_z \qquad \text{(B.2.a)}$$

$$\beta\hat{a}_z \times \underline{e}_t = \omega\mu\underline{h}_t \qquad \text{(B.2.b)}$$

$$\nabla_t \times \underline{h}_t = 0 \qquad \text{(B.2.c)}$$

$$\hat{a}_z \times \nabla_t\underline{h}_z + j\beta\hat{a}_z \times \underline{h}_t = -j\omega\varepsilon\underline{e}_t \qquad \text{(B.2.d)}$$

$$\nabla_t \cdot \underline{h}_t = j\beta\underline{h}_z \qquad \text{(B.2.e)}$$

$$\nabla_t \cdot \underline{e}_t = 0 \qquad \text{(B.2.f)}$$

1.) Boundary Condition #1:

$$\beta\hat{a}_z \times \underline{E}_y = \omega\mu\underline{H}_x \qquad \text{from (B.2.b)}$$

$$- \beta E_y = \omega\mu H_x \qquad \text{(B.3.a)}$$

$$H_x = \frac{-\beta}{\omega\mu} E_y \qquad \text{(B.3.b)}$$

The first two standard boundary conditions are conditions on:

$$\hat{n} \cdot \underline{H} = \underline{a}_x \cdot \underline{H} = H_x \qquad \text{(B.4.a)}$$

$$\hat{n} \times \underline{E} = \hat{a}_x \times \underline{E} = E_y \hat{a}_z \qquad \text{(B.4.b)}$$

Since H_x and E_y are related by (B.3.c), the first two standard boundary conditions are the same. (B.1.b) is chosen as the boundary condition and requires that the transverse component of $\underline{E}$ be continuous over the interfaces.

That is:

$$E_{y2} = E_{y1} \qquad \text{(B.5)}$$

2.) Boundary Condition #2:

The third standard boundary condition (B.1.c) is not useful because the normal component of $\underline{E}$ (E_x) is zero everywhere. With no free surface current density on the waveguides, the fourth standard boundary condition degenerates to:

$$\hat{a}_x \times (\underline{H}_2 - \underline{H}_1) = 0 \qquad \text{(B.6.a)}$$

$$H_{2z} = H_{1z} \qquad \text{(B.6.b)}$$

Equation (B.2.a) can be used to relate E_y and H_z.

$$-j\omega\mu\underline{H}_z = \nabla_t \times \underline{E}_y = -\hat{a}_y \frac{dE_y}{dx} \qquad \text{(B.7.a)}$$

$$H_z = \frac{1}{j\omega\mu} \cdot \frac{dE_y}{dx} \qquad \text{(B.7.b)}$$

The second waveguide boundary condition can be expressed as:

$$\frac{dE_{y2}}{dx} = \frac{dE_{y1}}{dx} \qquad (B.8)$$

B.2. Transverse 3-Layer Planar Guide

TM mode: E_z, H_x, $E_y(y)$

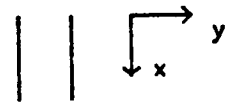

Maxwells Equations for TM waves are,

$$\nabla_t \times \underline{e}_z - j\beta\hat{a}_z \times \underline{e}_t = -jw\mu\underline{h}_t \qquad (B.9.a)$$

$$\nabla_t \cdot \underline{e}_t = 0 \qquad (B.9.b)$$

$$\nabla_t \times \underline{h}_t = jw\epsilon\underline{e}_z \qquad (B.9.c)$$

$$-\beta\hat{a}_z \times \underline{h}_t = w\epsilon\underline{e}_t \qquad (B.9.d)$$

$$\nabla_t \cdot \underline{h}_t = 0 \qquad (B.9.e)$$

$$\nabla_t \times \underline{e}_t = -j\beta\underline{e}_z \qquad (B.9.f)$$

1.) Boundary Condition #1:

$$-\beta\hat{a}_z \times \underline{H}_x = w\epsilon\underline{E}_y\hat{a}_y \qquad \text{from (B.9.d)}$$

$$\hat{a}_y\beta H_x = w\epsilon E_y\hat{a}_y \qquad (B.10.a)$$

$$H_x = \frac{w\epsilon}{\beta}E_y \qquad (B.10.b)$$

The last two standard boundary conditions are conditions on:

$$\hat{n} \cdot \underline{E} = \hat{a}_y \cdot \underline{E} = E_y \qquad (B.11.a)$$

$$\hat{n} \times \underline{H} = \hat{a}_y \times \underline{H} = H_x\hat{a}_y \qquad (B.11.b)$$

Since H_x and E_y are related by (B.10.c), the last two standard boundary conditions are the same. (B.1.c) is chosen as the boundary condition. Continuity of $\underline{D}$ can be approximated by continuity of $\underline{E}$ if the change in index of refraction across the film boundaries is small. With no free charge on the boundaries, this requires that the normal component of $\underline{E}$ be continuous over the interfaces.

That is: $$E_{y2} = E_{y1} \qquad (B.12)$$

2.) Boundary Condition #2:

The first standard boundary condition (B.1.a) is not useful because the normal component of $\underline{H}$ (H_y) is zero everywhere.

The second standard boundary condition (B.1.b) is on E_z and can be related to E_y by:

$$jw\,\underline{E}_z = \nabla_t \times \underline{H}_y = \frac{dH_y}{dy} = \frac{w\varepsilon}{\beta} \cdot \frac{dE_y}{dy} \qquad (B.13.a)$$

$$E_z = \frac{1}{j\beta} \cdot \frac{dE_y}{dy} \qquad (B.13.b)$$

The second waveguide boundary condition can be expressed as:

$$\frac{dE_{y2}}{dx} = \frac{dE_{y1}}{dx} \qquad (B.14)$$

APPENDIX C: WAVEGUIDE ANALYSIS PROGRAM

```
C*************************************************************************
C
C       WAVEGUIDE ANALYSIS PROGRAM
C
C       BY D. M. MATERNA    1986
C
C       THIS PROGRAM WAS CREATED ON THE IBM 370 TIME SHARING SYSTEM
C            TO ANALYZE A STRIP LOADED RIDGE WAVEGUIDE USING AN
C            EFFECTIVE INDEX METHOD.
C
C       REFERENCES:  S. LIN, "OPTIMIZATION OF OPTICAL CHARACTERISTI
C                         TRAVELLING WAVE MODULATORS", MIT THESIS, M.S.
C                         IN ELECTRICAL ENGINEERING,  JAN. 1985.
C
C                    M. J. ADAMS, "AN INTRODUCTION TO OPTICAL
C                         WAVEGUIDES", JOHN WILEY & SONS, 1981,
C                         CHAPTERS 2 & 6.
C
C
C      SUBROUTINES CALLED :
C          1. CHANGE : GETS THE WAVEGUIDE DIMENSIONS
C               A. DRAWIT : DRAWS THE STRIP-LOADED RIDGE WAVEGUIDE
C               B. ALTON : CALCULATES REFRACTIVE INDEX OF GAALAS LAYERS
C          2. EIGEN4 : SOLVES 4-LAYER EIGENVALUE EQUATION FOR BETA
C               A. ERPLOT : PLOTS ERROR VS. BETA
C               B. ERROR4 : CALCULATES ERROR FOR A SPECIFIC BETA
C          3. LFIELD : PLOTS LATERAL FIELD PROFILES
C               A. XYPLOT : PLOTTING ROUTINE
C          4. VFIELD : PLOTS THE VERTICAL FIELD PROFILES
C               A. XYPLOT : PLOTTING ROUTINE
C          5. CUTPLT : CALCULATES GUIDE LAYER CUTOFF THICKNESS
C               A. ALTON : CALCULATES REFRACTIVE INDEX OF GAALAS LAYERS
C          6. NMODES : CALCULATES NUMBER OF MODES SUPPORTED
C                      BY A GUIDE
C
C
C*************************************************************************
C
C     VARIABLE LIST
C
      REAL BETA1,BETA2,NEFF1,NEFF2,Q0,H1,Q2,Q3
      REAL PHI1,PHI2,PSI1,PSI2,G1,G2,GLAT,BETAFF
      REAL PI,NAIR,NFILM,NGUIDE,NSUB,WAVLEN
C
C
      INTEGER MODE,MVTE1,MVTE2,MLTE,FLAG
      INTEGER TMODES,MVTM1,MVTM2,MLTM
C
      DIMENSION TITLE1(3),TITLE2(3)
C
```

```
      DATA YANS/'Y   '/
C
C*************************************************************************
C
C     LOAD THE WAVEGUIDE PARAMETERS
C
C        FLAG: (1 = NEW PARAMETERS, 2 = CHANGE IN PARAMETERS)
C        RW = RIDGE WIDTH
C        RH = RIDGE HEIGHT
C        FT = UPPER CLADDING THICKNESS BEFORE RIDGE IS ETCHED
C        GT = GUIDE LAYER THICKNESS
C        WAVLEN = WAVELENGTH OF LIGHT
C        NAIR = INDEX OF REFRACTION OF TOP LAYER (AIR)
C        NFILM = INDEX OF REFRACTION OF UPPER CLADDING
C        NGUIDE = INDEX OF REFRACTION OF GUIDE LAYER
C        NSUB = INDEX OF REFRACTION OF LOWER CALDDING
C
C
      FLAG = 1
10    CALL CHANGE(FLAG,RW,RH,FT,GT,WAVLEN,NAIR,NFILM,NGUIDE,NSUB)
C
C*************************************************************************
C
      MODE = 0
      PI = 2 * ARSIN(1.0)
C
      WRITE(43,500) MODE
500   FORMAT(1X,'FOR VERTICAL MODE NUMBER ',I2)
      WRITE(43,510)
510   FORMAT(1X,'==============================')
C
C*************************************************************************
C
C       BEGIN BY SOLVING THE EIGENVALUE EQUATION TO
C           TO DETERMINE THE PROPAGATION CONSTANT
C
C     SOLVE IN THE VERTICAL DIRECTION - FOR BOTH REGIONS
C
      WRITE (43,505)
505   FORMAT(1X)
      WRITE (43,507)
507   FORMAT(1X,'=====  RIDGE REGION  =====')
      WRITE (43,505)
      CALL EIGEN4(FT,GT,NAIR,NFILM,NGUIDE,NSUB,MODE,WAVLEN,BETA2)
      IF(MODE.EQ.-1) GOTO 10
      NEFF2 = BETA2 *  WAVLEN / (2*PI)
C
      WRITE(43,505)
515   FORMAT(1X,'===== OUTER REGION  =====')
      WRITE (43,515)
      WRITE (43,505)
      IF(FT.GT.RH) CALL EIGEN4(FT-RH,GT.NAIR,NFILM,NGUIDE,NSUB,MODE,    -
     1      WAVLEN,BETA1)
      IF (FT.LE.RH) CALL EIGEN4(0.,GT+FT-RH,NAIR,NAIR,NGUIDE,NSUB,MODE,-
```

```
     1      WAVLEN,BETA1)
       IF(MODES.EQ.-1) GOTO 10
       WRITE (43,505)
       NEFF1 = BETA1 * WAVLEN / (2*PI)
C
       WRITE(43,520) NEFF1,NEFF2
520    FORMAT(1X,'NEFF1 = ',F10.5,10X,'NEFF2 = ',F10.5)
C
C*************************************************************************
C
C      SOLVE IN THE LATERAL DIRECTION
C
       IF (NEFF1 .NE. NEFF2) GOTO 15
           WRITE (43,505)
12         FORMAT(1X,'EFF INDEX 1 = EFF INDEX 2 -->NO LATERAL GUIDING!!')
           WRITE (43,12)
           GOTO 10
15         WRITE (43,505)
210        FORMAT (1X,'===== LATERAL SOLUTION =====')
            WRITE (43,210)
            WRITE (43,505)
           CALL EIGEN4(0.,RW,NEFF1,NEFF1,NEFF2,NEFF1,MODE,WAVLEN,BETAFF)
           IF(MODE.EQ.-1) GOTO 10
C
C*************************************************************************
C
C      PLOT THE VERTICAL FIELD INTENITY PROFILES IF DESIRED
C
       WRITE (43,505)
215    FORMAT (1X,'SEE THE VERTICAL FIELD PROFILE (Y/N) ? ')
       WRITE (43,215)
       READ (42,220)CHOICE
220    FORMAT(A1)
       WRITE (43,505)
       IF (CHOICE .NE. YANS) GOTO 20
       WRITE (43,505)
225    FORMAT (1X,'==== VERTICAL FIELD (OUTER REGION) =====')
       WRITE (43,225)
       WRITE (43,505)
       CALL VFIELD(BETA1,PI,NSUB,NGUIDE,NFILM,NAIR,WAVLEN,PHI1,PSI1,     -
      1    G1,GT,FT-RH,1)
       WRITE (43,505)
230    FORMAT(1X,'==== VERTICAL FIELD (RIDGE REGION) =====')
       WRITE (43,230)
       WRITE (43,505)
       CALL VFIELD(BETA2,PI,NSUB,NGUIDE,NFILM,NAIR,WAVLEN,PHI2,PSI2,     -
      1    G2,GT,FT,2)
C
C*************************************************************************
C
C       PLOT THE LATERAL FIELD INTENSITY PROFILE IF DESIRED
C
20      WRITE (43,505)
235    FORMAT(1X,'SEE THE LATERAL FIELD PROFILE (Y/N) ? ')
```

```
      WRITE (43,235)
      READ (42,220) CHOICE
      WRITE (43,505)
      IF (CHOICE .NE. YANS) GOTO 25
      WRITE (43,505)
240   FORMAT(1X,'==== LATERAL  FIELD  =====')
      WRITE (43,240)
      WRITE (43,505)
      CALL LFIELD(BETAFF,PI,NEFF1,NEFF2,WAVLEN,GLAT,RW)
C
C*************************************************************************
C
C      PLOT CUTOFF THICKNESS VS. %AL IF DESIRED
C
25    WRITE (43,505)
      WRITE (43,242)
242   FORMAT(1X,'CALCULATE VERTICAL 3-LAYER CUTOFFS (Y/N) ? ')
      READ(42,220) CHOICE
      IF (CHOICE .NE. YANS) GOTO 30
      IF (RH .LT. FT) GOTO 28
C
       DATA TITLE1/'OUTE','R RE','GION'/
       DATA TITLE2/'INNE','R RE','GION'/
C
          CALL TITLE3(2,12,22,TITLE1,0.,1.,0.)
          CALL CUTPLT(NAIR,NGUIDE,NSUB,WAVLEN)
          CALL TITLE3(2,12,22,TITLE2,0.,1.,0.)
28        CALL CUTPLT (NFILM,NGUIDE,NSUB,WAVLEN)
C
C*************************************************************************
C
C     CALCULATE THE NUMBER OF PROPAGATING MODES
C           USING 3-LAYER APPROXIMATION
C
30    MVTE1 = NMODES(NFILM,NGUIDE,NSUB,FT-RH,WAVLEN,PI,0)
      MVTM1 = NMODES(NFILM,NGUIDE,NSUB,FT-RH,WAVLEN,PI,1)
      MVTE2 = NMODES(NFILM,NGUIDE,NSUB,FT,WAVLEN,PI,0)
      MVTM2 = NMODES(NFILM,NGUIDE,NSUB,FT,WAVLEN,PI,1)
      MLTE = NMODES(NEFF1,NEFF2,NEFF1,RW,WAVLEN,PI,0)
      MLTM = NMODES(NEFF1,NEFF2,NEFF1,RW,WAVLEN,PI,1)
      RWMAX = NMODES(NEFF1,NEFF2,NEFF1,0.,WAVLEN,PI,2) / 10000.
C
C*************************************************************************
C
C        SUMARRIZE THE RESULTS OF THE PRESENT CONFIGURATION
C
         WRITE (43,505)
245   FORMAT (1X,'SUMMARY OF RESULTS:')
      WRITE(43,245)
246   FORMAT(1X,'-------------------')
      WRITE (43,246)
      WRITE (43,505)
100   FORMAT (1X,'TE NUMBER OF MODES = ',I2)
102   FORMAT (1X,'TM NUMBER OF MODES = ',I2)
```

```
104   FORMAT (1X,'TOTAL NUMBER OF MODES = ',I2)
105   FORMAT (1X,'PROPAGATION CONST = ',F20.10)
106   FORMAT (1X,'2ND MODE @ RW = ',F10.5,' MICRONS')
110   FORMAT (1X,'EFFECTIVE INDEX = ',F10.5)
250   FORMAT (1X,'OUTER REGION (VERTICAL MODE) :')
      WRITE (43,250)
      WRITE (43,505)
      WRITE (43,100) MVTE1
      WRITE (43,102) MVTM1
      WRITE (43,105) BETA1
      WRITE (43,110) NEFF1
      WRITE (43,505)
255   FORMAT (1X,'RIDGE REGION (VERTICAL MODE) :')
      WRITE (43,255)
      WRITE (43,505)
      WRITE (43,100) MVTE2
      WRITE (43,102) MVTM2
      WRITE (43,105) BETA2
      WRITE (43,110) NEFF2
      WRITE (43,505)
260   FORMAT (1X,'LATERAL GUIDING : ')
      WRITE (43,260)
      WRITE(43,505)
      WRITE (43,100) MLTE
      WRITE (43,102) MLTM
      WRITE (43,105) BETAFF
      TMODES = (MLTE * MIN0(MVTE1,MVTE2)) + (MLTM * MIN0(MVTM1,MVTM2))
      WRITE (43,505)
265   FORMAT (1X,'FOR THE TOTAL GUIDE : ')
      WRITE (43,265)
     WRITE(43,505)
      WRITE (43,104) TMODES
      WRITE (43,105) BETAFF
      WRITE (43,106) RWMAX
C
C*****************************************************************
C
      WRITE (43,505)
270   FORMAT (1X,'CHANGE PARAMETERS (Y) OR QUIT (N)  ? ')
      WRITE (43,270)
      READ  (42,220) CHOICE
      IF (CHOICE .EQ. YANS) GOTO 10
C
C     PRESENTLY ANALYZES ONLY 1 MODE
C
C     TERMINATE GRAPHICS TASK (CLEAN UP)
      CALL TERM
C
      STOP
      END
C
C*****************************************************************
```

```
C
C*****************************************************************
C
C        THIS SUBROUTINE IS USED TO INPUT THE WAVEGUIDE
C             PARAMETERS AT THE START OF THE PROGRAM &
C             CHANGE THEM FOR OTHER SOLUTIONS
C
C
C     SUBROUTINES CALLED :
C
C               DRAWIT:  DRAWS THE OPTICAL WAVEGUIDE
C                        WITH PARAMETERS LABELLED
C               ALTON:   CALCULATES INDEX OF REFRACTION FOR
C                        %AL IN GAALAS LAYERS.
C
C
C      PARAMETERS :
C
C               V(1) = A1 = RIDGE WIDTH
C               V(2) = A2 = RIDGE HEIGHT
C               V(3) = A3 = UPPER CLADDING LAYER THICKNESS
C               V(4) = A4 = GUIDE LAYER THICKNESS
C               V(5) = A5 = WAVELENGTH
C               V(6) = A6 = 1 = INDEX OF REFRACTION OF AIR
C               V(7) =  %AL IN UPPER CLADDING LAYER
C               V(8) =  %AL IN GUIDE LAYER
C               V(9) =  %AL IN LOWER CLADDING LAYER
C               V(12) =  A7 = INDEX OF REFRAC IN LOWER CLADDING LAYER
C               V(13) =  A8 = INDEX OF REFRAC IN GUIDE LAYER
C               V(14) =  A9 = INDEX OF REFRAC IN LOWER CLADDING LAYER
C
C*****************************************************************
C
      SUBROUTINE CHANGE(FLAG,A1,A2,A3,A4,A5,A6,A7,A8,A9)
C
      REAL V(15)
      INTEGER FLAG,CH
      DIMENSION M(15,9)
C
C*****************************************************************
C
C     LOAD VALUES INTO AN ARRAY FOR EASY MANIPULATION
C     THE ARRAY SUBSCRIPTS CORRESPOND TO MENU NUMBERS
C
      V(1) = A1
      V(2) = A2
      V(3) = A3
      V(4) = A4
      V(5) = A5
      V(6) = A6
      V(12) = A7
      V(13) = A8
      V(14) = A9
C
```

```
C*************************************************************************
C
C    DRAW THE WAVEGUIDE CONFIGURATION ON THE SCREEN
C
5      CALL DRAWIT
C
      WRITE (43,75)
C
C*************************************************************************
C
C     READ SCREEN MESSAGES FROM A FILE
C          DEVICE 98 = DATA.MENU
C
      REWIND 98
10    FORMAT (9A4)
      DO 30 I = 1,14
           READ (98,10) (M(I,J) ,J=1,9)
30    CONTINUE
C
C*************************************************************************
C
C     RESCALE FROM METERS TO MICRONS
C
      SCALE = 1000000
C
      DO 50 I = 1,5
      V(I) = V(I) * SCALE
50      CONTINUE
C
75    FORMAT (1X)
C
C*************************************************************************
C
      GOTO (100,200), FLAG
C
C    FLAG = 1 INDICATES INITIAL READING OF VALUES
C    FLAG = 2 INDICATES CHANGING A VALUE
C
C*************************************************************************
C
C      READ IN ALL VALUES FOR STARTING CONFIGURATION
C
100   FLAG = 2
      DO 110 I = 1,9
           WRITE (43,10) (M(I,J) , J=1,9)
           READ (97,105)V(I)
105        FORMAT (G11.5)
110   CONTINUE
C
C          CONVERT FROM %AL TO REFRACTIVE INDEX
C
      DO 150 I = 7,9
          V(I+5) = ALTON (V(I),V(5))
150   CONTINUE
```

```
C
C*****************************************************************
C
C     GIVE OPTION TO CHANGE  SINGLE VALUES  —
C
200   DO 210 I = 1,6
          WRITE (43,205) I,(M(I,J),J=1,8), V(I)
205       FORMAT (1X,I2,'.  ',8A4,G11.5)
210   CONTINUE
C
      DO 220 I = 7,9
          WRITE (43,225) I,(M(I,J),J=1,8),V(I),(M(I+5,J),J=1,3),V(I+5)
225       FORMAT (1X,I2,'.  ',8A4,G11.5,3A4,G11.5)
220    CONTINUE
C
      I = 10
      WRITE (43,205) I,(M(10,J),J=1,8),V(10)
C
C     SELECT OPTION BY ENTERING 01 TO 10
C
      WRITE(43,75)
      WRITE (43,250)
250   FORMAT(1X,'PARAMETER TO CHANGE (01-10) ? ')
      READ (42,255)CH
255   FORMAT (I2)
      IF (CH.EQ.10) GOTO 500
      WRITE (43,75)
      WRITE (43,10) (M(CH,J), J=1,9)
      READ (43,105) V(CH)
      WRITE (43,75)
      IF ((CH.LT.10).AND.(CH.GT.6)) V(CH+5) = ALTON(V(CH),V(5))
      GOTO 200
C
C*****************************************************************
C
C      CHECK THAT N1>N2>=N0>N3
C            FOR VALID OPTICAL WAVEGUIDING
C
500   IF ( V(6) .GT. V(13) ) GOTO 550
      IF ( V(12).GT. V(13) ) GOTO 550
      IF ( V(14).GT. V(13) ) GOTO 550
      GOTO 600
550   WRITE (43,75)
      WRITE (43,560)
      WRITE (43,75)
      GOTO 200
560   FORMAT (1X,'*** N1 MUST BE HIGHEST INDEX!!! ***')
C
C*****************************************************************
C
C     RESCALE FROM MICRONS TO METERS
C
600   DO 610 I = 1,5
      V(I) = V(I) / SCALE
```

```
610   CONTINUE
C
C*****************************************************************
C
C      RELOAD VALUES INTO PARAMETERS FOR PASSING TO MAIN PROGRAM
C
      A1 = V(1)
      A2 = V(2)
      A3 = V(3)
      A4 = V(4)
      A5 = V(5)
      A6 = V(6)
      A7 = V(12)
      A8 = V(13)
      A9 = V(14)
C
      RETURN
      END
C
C*****************************************************************
```

```
C*****************************************************************
C
C     THIS SUBROUTINE DRAWS THE WAVEGUIDE PICTURE
C          FOR THE USER TO REFERENCE ON VARIABLE ENTRY
C
C
C*****************************************************************
C
      SUBROUTINE  DRAWIT
C
      INTEGER I,J
      DIMENSION A(14,12)
C
C
10    FORMAT (12A4)
25    FORMAT (1X,12A4)
C
      REWIND 99
C
      DO 100 I = 1,14
      READ (99,10)  (A(I,J),J=1,12)
      WRITE (43,25) (A(I,J),J=1,12)
100   CONTINUE
C
      RETURN
      END
C
C*****************************************************************
```

```
C*****************************************************************
C
C     CONVERSION FROM %AL TO REFRACTIVE INDEX
C
C*****************************************************************
C
      FUNCTION ALTON (XAL,WAVLEN)
C
      XAL = XAL / 100.
C
      A = 10.906 - (2.92 * XAL )
      B = 0.97501
      IF (XAL.GE.(0.36)) C = (0.30386 - 0.105*XAL)**2
      IF (XAL.LT.(0.36)) C = (0.52886 - 0.735*XAL)**2
      D = 0.002467 * (1.41*XAL + 1)
C
      TEMP = B / (WAVLEN**2 - C)
      ALTON = SQRT( A + TEMP - (D * WAVLEN**2) )
C
      XAL = XAL * 100.
C
      RETURN
      END
C
C*****************************************************************
```

```
C*********************************************************************
C
C      THIS SUBROUTINE SOLVES THE EIGENVALUE EQUATION FOR
C               A 4-LAYER PLANAR WAVEGUIDE
C
C
C      SUBROUTINES CALLED :
C          1. ERPLOT : PLOTS THE ERROR IN THE EIGEN VALUE EQUATION
C                      VS. BETA TO FOR USER TO INSURE ONE ZERO
C          2. ERROR4 : RETURNS ERROR FOR A GIVEN BETA
C
C*********************************************************************
C
      SUBROUTINE EIGEN4(FT,GT,N3,N2,N1,N0,MODE,WAVLEN,BETAT)
C
C*********************************************************************
C
C
C      VABIABLE LIST
C
      REAL FT,GT,N0,N1,N2,N3,PI,BETAT
      REAL *8 ERRLO,ERRHI,ERR,OLDERR,FINERR
      REAL *8 BETAF,BETA,BETAHI,BETALO
      INTEGER MODE
C
      PI = 4*ATAN(1.0)
      BETA = BETAT
C
      WRITE (43,1111) PI
1111  FORMAT (1X,'PI =',G20.16)
C*********************************************************************
C
C      USE BISECTION TECHNIQUE TO SOLVE FOR PROPAGATION CONST
C
C
      BETAHI= 2*PI* N1/WAVLEN  - 1.
      IF (N2 .GT. N0) BETALO = 2*PI*N2/WAVLEN + 2.
      IF (N2 .LE. N0) BETALO = 2*PI*N0/WAVLEN + 2.
      WRITE(43,5) BETAHI,BETALO
5     FORMAT(1X,'HIGH BETA = ',F25.15,5X,'LOW BETA = ',F25.15)
C
      WRITE(43,505)
      WRITE(43,503)
503   FORMAT (1X,'SEE ERROR FUNCTION (Y/N) ? ')
      READ (42,504) QUES
504   FORMAT (A1)
DATA Y/'Y   '/
      IF(QUES .EQ. Y) CALL ERPLOT(BETALO,BETAHI,FT,GT,N0,N1,N2,N3,MODE,-
     1 PI,WAVLEN)
C
C
C*********************************************************************
C
C     CALCULATE ERRORS DUE TO HIGH AND LOW LIMITING VALUES
```

```
C          OF THE PROPAGATION CONSTANT
C
      ERRHI = ERROR4(BETAHI,FT,GT,N0,N1,N2,N3,MODE,PI,WAVLEN)
      ERRLO = ERROR4(BETALO,FT,GT,N0,N1,N2,N3,MODE,PI,WAVLEN)
      WRITE(43,10) ERRHI,ERRLO
10    FORMAT(1X,'LOW ERROR = ',F25.15,5X,'HIGH ERROR = ',F25.15)
      IF(ERRHI.LT.ERRLO) GOTO 100
      WRITE (43,505)
505   FORMAT (1X)
510   FORMAT('*****  NO VALID SOLUTION IN THIS DIRECTION *****')
      WRITE (43,510)
      WRITE (43,505)
      MODE = -1
      GOTO 200
C
C*************************************************************************
C
C     SOLVE FOR BETA BY BISECTION OF THE ERROR IN THE TRANCENDENTAL
C          EIGENVALUE EQN.   STOP WHEN ERROR4 < 0.000001
C
100   BETA = (BETAHI+BETALO)/2
      OLDERR = ERR
      ERR = ERROR4(BETA,FT,GT,N0,N1,N2,N3,MODE,PI,WAVLEN)
C
      IF (.00000000001 .LT. DABS(OLDERR-ERR)) GOTO 110
C
      IHI = IDINT(BETAHI - BETALO) + 1
      FINERR = 1.0
      DO 250 J = 1,IHI
          I = J - 1
      WRITE (43,241) I
241   FORMAT (1X,I3)
           BETA = BETALO + I
          ERR = ERROR4(BETA,FT,GT,N0,N1,N2,N3,MODE,PI,WAVLEN)
          IF (FINERR .LT. DABS(ERR) ) GOTO 240
               FINERR = DABS(ERR)
               BETAF = BETA
240       WRITE (43,245) BETA, ERR
245       FORMAT (1X,'BETA = ',G25.15,'ERR = ',G25.15)
250   CONTINUE
C
      ERR = FINERR
      BETA = BETAF
      IF (.000001 .GT. ERR) GOTO 150
C
C*************************************************************************
C
500   ERR = DABS( DMIN1( DABS(ERRHI),DABS(ERRLO) ))
      WRITE (43,505)
      WRITE (43,520)
520   FORMAT(1X,'*****  WARNING  *****')
      WRITE (43,505)
      WRITE(43,20) ERR
20    FORMAT(1X,'EIGENVALUE ERROR IN SOLUTION = ',F25.15)
```

```
      WRITE (43,505)
      GOTO 150
C
110   IF ( ERR  .LT. 0.0) GOTO 115
          BETALO = BETA
          ERRLO = ERR
          GOTO 120
115       BETAHI = BETA
          ERRHI = ERR
120   CONTINUE
C
C*****************************************************************
C
C      PRINT RESULTS ON SCREEN
C
      WRITE(43,25) ERRHI,ERRLO
25    FORMAT(1X,'LOW ERROR = ',F25.15,5X,'HIGH ERROR = ',F25.15)
C
      IF (0.000001 .LE. DABS(ERR)) GOTO 100
150   WRITE(43,30) ERR,BETA
30    FORMAT(1X,'FINAL ERR = ',F25.15,5X,'FINAL BETA = ',F25.15)
C
C
200   BETAT = BETA
      RETURN
      END
C*****************************************************************
```

```
C*****************************************************************
C
C      THIS SUBROUTINE WILL GIVE A QUICK PLOT OF BETA VS. ERROR
C                  AND ACEPT NEW END POINTS FOR BISECTION
C
C*****************************************************************
C
      SUBROUTINE ERPLOT(BETALO,BETAHI,FT,GT,N0,N1,N2,N3,MODE,PI,WAVLEN)
C
      REAL ERROR(101),X(101),BETA(101)
      INTEGER PLEFT,PRIGHT
C
      DATA Y/'Y   '/
C
5     SCALE = (BETAHI - BETALO) / 100
      BETA(1) = BETALO
      ERROR(1) = ERROR4(BETALO,FT,GT,N0,N1,N2,N3,MODE,PI,WAVLEN)
      DO 10 I = 2 , 101
            BETA(I) = BETA(I-1) + SCALE
            ERROR(I) = ERROR4(BETA(I),FT,GT,N0,N1,N2,N3,MODE,PI,WAVLEN)
10    CONTINUE
C
      CALL XYPLOT(BETALO,BETALO,BETALO,1,1.,101,X,ERROR)
      CALL XHAIRS(1)
      CALL GRCPF(0.,0.,0.,'U',0,XC,YC,ZC)
      CALL UPLOT(100.,0.,0.,'U','A',0,'Y',15)
      CALL DISPLA(1)
C
100   FORMAT(1X,'LEFT X-POINT (000-100) : ')
105   FORMAT(1X,'RIGHT X-POINT (000-100): ')
110   FORMAT(1X)
115   FORMAT(I3)
C
200   WRITE (43,110)
      WRITE (43,100)
      READ (42,115) PLEFT
      WRITE (43,105)
      READ (42,115) PRIGHT
C
      BETALO = BETA(PLEFT+1)
      BETAHI = BETA(PRIGHT+1)
C
      IF ( (BETAHI - BETALO) .LT. 100) GOTO 1000
C
      WRITE (43,300)
300   FORMAT (1X,'EXPAND SCALE (Y/N) ? ')
      READ (42,310) QUES
310   FORMAT (A1)
      IF (QUES .EQ. Y) GOTO 5
C
1000  RETURN
      END
C
C*****************************************************************
```

```
C*****************************************************************
C
 REAL FUNCTION ERROR4 *8(BETA,FT,GT,N0,N1,N2,N3,M,PI,WAVLEN)
C
C          FUNCTION WHICH RETURNS THE SIGNED ERROR IN THE EIGENVALUE
C          EQUATION DUE TO THE GIVEN BETA
C
C*****************************************************************
C
      REAL N0,N1,N2,N3,PI
      REAL *8 Q0,H1,Q2,Q3,X,BETA,AHTAN
C
C
      H1=( (2*PI*N1/WAVLEN)**2 -BETA**2 )**0.5
      Q3=( BETA**2 - (2*PI*N3/WAVLEN)**2 )**0.5
      Q0=( BETA**2 - (2*PI*N0/WAVLEN)**2 )**0.5
       Q2=( BETA**2 -(2*PI*N2/WAVLEN)**2 )**0.5
      IF (FT .LE. 0.0)   GOTO 50
C
C      4 LAYER SOLUTION
C
      X=Q2/Q3
      IF ( DABS(X) .LT. 1.0 ) GOTO 10
20    FORMAT (1X, '***** INVALID ARCTANH !!!! *****')
      WRITE (43,20)
10    AHTAN=0.5*DLOG( (1+X)/(1-X) )
      X=DATAN( Q2/(H1*DTANH(Q2*FT+AHTAN)) )
      GOTO 100
C
C     3 LAYER SOLUTION
C
50    X = DATAN (Q3/H1)
C
100   ERROR4=H1*GT - M*PI - DATAN(Q0/H1) - X
C
      RETURN
      END
C
C*****************************************************************
```

```
C*****************************************************************
C
      SUBROUTINE LFIELD(BETA,PI,NEFF1,NEFF2,WAVLEN,G,RW)
C
C     THIS SUBROUTINE CALCULATES THE LATERAL FIELD QUANTITIES
C
C*****************************************************************
C
      REAL X(1501),Y(1501),EFIELD(750),NEFF1,NEFF2
      INTEGER IVARS(9)
      DIMENSION YTITLE(3),XTITLE(7),PTITLE(6)
C
      SCALE = 50000000
      V = PI*RW* SQRT( NEFF2**2 - NEFF1**2 ) /WAVLEN
      H1=SQRT( (2*PI*NEFF2/WAVLEN)**2 - BETA**2)
      Q0=SQRT( BETA**2 - (2*PI*NEFF1/WAVLEN)**2)
      G = COS(H1*RW/2)/EXP(-Q0*RW/2)
C
      I1 = INT((RW*SCALE/2) +.5)
      I2 = INT( (RW*SCALE*2) + .5)
      IF (I2 .GT. 750) I2 = 750
      I3 = I2 + 1
C
      DO 100 I = 1 , I2
          IF (I .LE. I1) EFIELD(I) = COS(H1*I/SCALE)
          IF (I .GT. I1) EFIELD(I) = G * EXP(-Q0*I/SCALE)
          EFIELD(I) = EFIELD(I)**2
          X(I) = I * .02
100       CONTINUE
C
      DO 160 I = 1,I2
           Y(I) = EFIELD ( I3 - I )
160   CONTINUE
C
      Y(I3) = 1.
C
      DO 170 I = 1,I2
          Y(I+I3) = EFIELD(I)
170   CONTINUE
C
      X1 = I1 * .02
      CALL GVIEW(1)
      CALL XYPLOT (X1,-X1,X1,I3,0.02,I2+I3,X,Y)
C
DATA YTITLE /'INTE','NSIT','Y   '/
DATA XTITLE /'LATE','RAL',' DIM','ENSI','ON (','MICR','ONS)'/
DATA PTITLE /'LATE','RAL ',' FIE','LD P','ROFI','LE  '/
C
      CALL TITLE3 (4,28,14,XTITLE,0.,1.,0.)
      CALL TITLE3 (3,9,14,YTITLE,-1.,0.,0.)
      CALL TITLE3 (2,22,22,PTITLE,0.,1.,0.)
C
      CALL DISPLA(1)
C
```

```
C*********************************************************************
C
C  THIS SUBROUTINE WILL DO X-Y PLOTS FOR THE MODAL FIELD DISTRIBUTIONS
C
      SUBROUTINE XYPLOT (XP1,XP2,XP3,M,S,N,X,Y)
C
C*********************************************************************
C
      REAL X(N),Y(N),Z(1510)
      INTEGER IVARS(9)
C
C
      IVARS (1) =  9
      IVARS (2) = N
      IVARS (3) = 0
      IVARS (4) = 1
      IVARS (5) = 0
      IVARS (6) = 1
      IVARS (7) = 15
      IVARS (8) = 0
      IVARS (9) = N
C
      DO 150 I = 1 , N
          X(I) = (I - M) * S
150   CONTINUE
C
      CALL GVIEW(1)
      CALL GPLOT3(IVARS,X,Y,Z)
C
C
      CALL GRCPF (XP1,0.,0.,'U',0,XC,YC,ZC)
      CALL UPLOT (XP1,1.,0.,'U','A',0,'Y',15)
C
      CALL GRCPF (XP2,0.,0.,'U',0,XC,YC,ZC)
      CALL UPLOT (XP2,1.,0.,'U','A',0,'Y',15)
C
      CALL GRCPF (XP3,0.,0.,'U',0,XC,YC,ZC)
      CALL UPLOT (XP3,1.,0.,'U','A',0,'Y',15)
C
C
      RETURN
      END
C*********************************************************************
```

```
C*********************************************************************
C
      SUBROUTINE VFIELD(BETA,PI,N0,N1,N2,N3,WAVLEN,PHI,PSI,G,GT,FT,Q1)
C
C     THIS SUBROUTINE CALCULATES THE VERTICAL FIELD QUANTITIES
C
C*********************************************************************
C
      INTEGER LIMLO,LIMHI,FT1,FT2,Q1
      REAL N0,N1,N2,N3,EFIELD(500),X1(500)
      DIMENSION XTITLE(7),YTITLE(3),PTITLE(6),TITLE1(4),TITLE2(4)
C
      SCALE = 50000000
C
      H1=SQRT( (2*PI*N1/WAVLEN)**2 - BETA**2)
      Q3=SQRT( BETA**2 - (2*PI*N3/WAVLEN)**2)
      Q2=SQRT( BETA**2 - (2*PI*N2/WAVLEN)**2)
      Q0=SQRT( BETA**2 - (2*PI*N0/WAVLEN)**2)
      PHI=ATAN(Q0/H1)
      X=Q2/Q3
      PSI=0.5*ALOG( (1+X)/(1-X) )
       G=COS(H1*GT - PHI) /SINH(Q2*FT + PSI)
      LIMLO= 1
      LIMHI= INT( (FT+GT)*SCALE) + 50 + 51
C
      FT1 = INT( FT * SCALE + .5)
      FT2 = INT( (FT + GT) * SCALE + .5 )
C
      DO 100 J = LIMLO,LIMHI
          I = J - 51
          IF (I.LT. 0) EFIELD(J)= G*SINH(PSI)*EXP(Q3*I/SCALE)
          IF ((I.GE.0).AND.(I.LT.FT1))EFIELD(J)=G*SINH(Q2*I/SCALE + PSI)
          IF (.NOT.( (I.GE.FT1).AND.(I.LT.FT2)))  GOTO 50
                    X = H1*(I/SCALE - FT - GT)
                    EFIELD(J) =  COS(X + PHI)
                GOTO 55
50        IF (I .LT. FT2) GOTO 55
                    X = Q0 * (GT + FT - I/SCALE)
                    EFIELD(J) = COS(PHI) * EXP(X)
55         EFIELD(J) = EFIELD(J)**2
100       CONTINUE
C
      F1 = FT1  * .02
      F2 = FT2  * .02
      CALL XYPLOT (0.,F1,F2,51,0.02,LIMHI,X1,EFIELD)
C
DATA YTITLE/'INTE','NSIT','Y   '/
DATA XTITLE/'VERT','ICAL',' DIM','ENSI','ON (','MICR','ONS)'/
DATA PTITLE/'VERT','ICAL',' FIE','LD P','ROFI','LE  '/
DATA TITLE2/'    ','RIDG','E RE','GION'/
DATA TITLE1/'    ','OUTE','R RE','GION'/
C
      CALL TITLE3 (3,9,14,YTITLE,-1.,0.,0.)
      CALL TITLE3 (4,28,14,XTITLE,0.,1.,0.)
```

```
      CALL TITLE3 (2,22,22,PTITLE,0.,1.,0.)
      IF (Q1 .EQ. 1) CALL TITLE3(1,16,22,TITLE1,0.,1.,0.)
      IF (Q1 .EQ. 2) CALL TITLE3(1,16,22,TITLE2,0.,1.,0.)
C
C
      CALL DISPLA(1)
      RETURN
      END
C*********************************************************************
```

```
C*************************************************************************
C
C     THIS SUBROUTINE WILL PLOT T_CUTOFF VS. %AL(GUIDE LAYER)
C             FOR BOTH TE AND TM MODES
C
      SUBROUTINE CUTPLT(NL,NC,NR,WAV)
C
C*************************************************************************
C
C                 * NOTE: N1 >N2 > N0
C
      REAL NL,NR,NC,N0,N1,N2
      REAL X(84),TC(84),Z(84)
      INTEGER IVARS(9)
      DIMENSION XTITLE(5),YTITLE(7)
C
      WAVLEN = WAV * 1000000
      N0 = AMIN1(NL,NR)
      N2 = AMAX1(NL,NR)
C
      PI = 2 * ARSIN(1.0)
      K = 2 * PI / WAVLEN
      XC = 0.0
      I = 1
C
      DO 5 J = 1,84
           TC(J) = 0.0
5     CONTINUE
C
10    N1 = ALTON(XC,WAVLEN)
      IF (N1 .LE. N2) GOTO 20
           SQ1 = SQRT(N1**2 - N2**2)
           SQ2 = SQRT(N2**2 - N0**2) / SQ1
           SQ3 = ( (N1/N0)**2 ) * SQ2
           SQ4 = K * SQ1
C
           TC(I) = ATAN(SQ2) / SQ4
           TC(I+21) = (PI + ATAN(SQ2) ) / SQ4
           TC(I+42) = ATAN(SQ3) / SQ4
           TC(I+63) = (PI + ATAN(SQ3) ) /SQ4
C
C
           XC = XC + 1
           I  = I  + 1
      GOTO 10
C
C
20    DO 22 J = 1,84
           IF (TC(J) .GT. 10.) TC(J) = 0.
22    CONTINUE
C
C     PLOT THE CUTOFF CURVES
C
C
```

```
25    DO 30 J = 1,21
            X(J) = J - 1
            X(J+21) = J - 1
            X(J+42) = J - 1
            X(J+63) = J - 1
30    CONTINUE
C
      DATA IVARS/9,84,0,1,0,1,15,0,21/
C
      CALL GVIEW(1)
      CALL GPLOT3(IVARS,X,TC,Z)
C
DATA XTITLE/'%AL ','IN G','UIDE',' LAY','ER  '/
DATA YTITLE/'CUTO','FF T','HICK','NESS',' (MI','CRON','S)  '/
C
      CALL TITLE3(3,26,14,YTITLE,-1.,0.,0.)
      CALL TITLE3(4,18,14,XTITLE,0.,1.,0.)
C
C
      CALL DISPLA(1)
C
1000  RETURN
      END
C
C*************************************************************************
```

```
C*********************************************************************
C
C     THIS SUBROUTINE CALCULATES THE NUMBER OF MODES
C          SUPPORTED IN EITHER TE OR TM MODE
C          USING A 3-LAYER APPROXIMATION
C
C*********************************************************************
C
      FUNCTION NMODES ( NL,N1,NR,T,WAVLEN,PI,FLAG)
C
      REAL NL,NR,N0,N1,N2,T,WAVLEN,PI,K
      INTEGER FLAG
C
      N0 = AMIN1(NL,NR)
      N2 = AMAX1(NL,NR)
C
      SQ1 = SQRT(N1**2 - N2**2)
      SQ2 = SQRT(N2**2 - N0**2) / SQ1
      IF (FLAG .EQ. 1) SQ2 = SQ2 * ( (N1/N0)**2)
C
      IF (FLAG .EQ. 2) GOTO 10
C
      V2 = (PI*T/WAVLEN) * SQ1 * 2.
      NMODES = INT( (V2-ATAN(SQ2))/PI ) + 1
C
      RETURN
C
10    K =    2 * PI / (WAVLEN * 1000000)
      NMODES = 10000 * (PI + ATAN(SQ2)) / (K * SQ1)
C
      RETURN
C
      END
C
C*********************************************************************
```

Appendix D. Coplanar Electrode Field Analysis Program

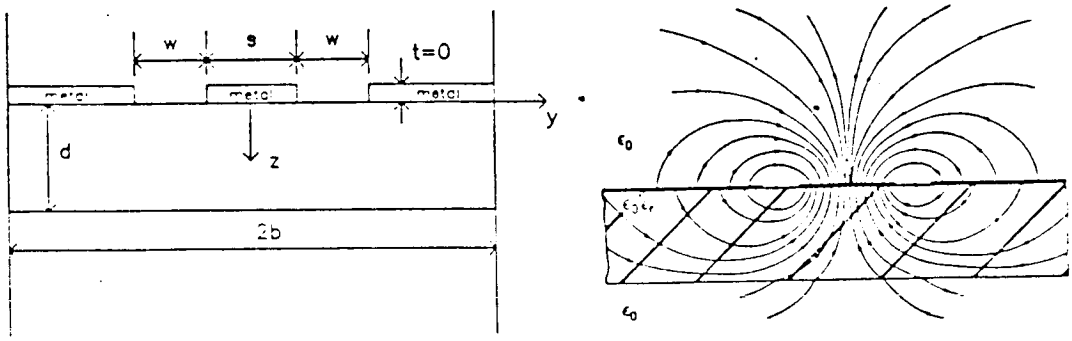

Figure 43. Coplanar Waveguide

Definition of terms: [31]

$$\lambda = c / f \qquad \lambda' = K \lambda$$

$$v = \sqrt{\gamma K^{-2} - 1} \qquad u = \sqrt{\gamma \epsilon_r - K^{-2}}$$

$$\delta = w / b \qquad \bar{\delta} = (s+w) / b$$

$$F_n = \sqrt{1 + \left(\frac{2bv}{n\lambda}\right)^2} \qquad F_{n1} = \sqrt{1 - \left(\frac{2bu}{n\lambda}\right)^2}$$

$$\gamma_n = (F_n \cdot n\pi) / b \qquad \gamma_{n1} = (F_{n1} \cdot n\pi) / b$$

$$r_n = \gamma_{n1} d + \tanh^{-1} (F_{n1} / \epsilon_r F_n)$$

$$q_n = \gamma_{n1} d + \coth^{-1} (F_n / F_{n1})$$

A. Air Side: ($z \leq 0$)

$$E_y = \frac{2V_o}{b} \sum_{n>0}^{\infty} \left\{ \frac{\sin(n\pi\delta/2)}{(n\pi\delta/2)} \sin\left(\frac{n\pi\bar{\delta}}{2}\right) \right\} \sin\left(\frac{n\pi y}{b}\right) e^{-\gamma_n |z|}$$

$$E_z = -\frac{2V_o}{b} \sum_{n>0}^{\infty} \frac{1}{F_n} \left\{ \frac{\sin(n\pi\delta/2)}{(n\pi\delta/2)} \sin\left(\frac{n\pi\bar{\delta}}{2}\right) \right\} \cos\left(\frac{n\pi y}{b}\right) e^{-\gamma |z|}$$

B. Substrate Side of Slot: ($0 \leq z \leq d$)

$$E_x = j \frac{2V_o}{\lambda^+} \sum_{n>0}^{\infty} \frac{2}{n\left[1 + \left(\frac{2b}{n\lambda^+}\right)^2\right]} \left\{ \frac{\sin(n\pi\delta/2)}{(n\pi\delta/2)} \sin\left(\frac{n\pi\bar{\delta}}{2}\right) \right\} \cdot$$

$$\cos\left(\frac{n\pi y}{b}\right) \left[\coth(q_n) - \tanh(r_n)\right] \sinh(\gamma_{n1} z)$$

$$E_y = \frac{2V_o}{b} \sum_{n>0}^{\infty} \left\{ \frac{\sin(n\pi\delta/2)}{(n\pi\delta/2)} \sin\left(\frac{n\pi\bar{\delta}}{2}\right) \right\} \sin\left(\frac{n\pi y}{b}\right) \cdot$$

$$\left[\cosh(\gamma_{n1} z) - \frac{\tanh(r_n) + \left(\frac{2b}{n\lambda^+}\right)^2 \coth(q_n)}{1 + \left(\frac{2b}{n\lambda^+}\right)^2} \sinh(\gamma_{n1} z)\right]$$

$$E_z = -\frac{2V_o}{b} \sum_{n>0}^{\infty} \frac{1}{F_{n1}} \left\{ \frac{\sin(n\pi\delta/2)}{(n\pi\delta/2)} \sin\left(\frac{n\pi\bar{\delta}}{2}\right) \right\} \cos\left(\frac{n\pi y}{b}\right) \cdot$$

$$\left\{\sinh(\gamma_{n1} z) - \tanh(r_n) \cosh(\gamma_{n1} z)\right\}$$

```
C ***************************************************************
C
C   COPLANAR WAVEGUIDE FIELD COMPONENTS
C
C     SUBROUTINES CALLED :
C               1. INPUT : GETS THE WAVEGUIDE DIMENSIONS
C               2. INVCTN : INVERSE HYPERBOLIC COTANGENT
C               3. INVTAN : INVERSE HYPERBOLIC TANGENT
C
C ***************************************************************
C
C  VARIABLE LIST
C
      REAL*8 S,W,D.B,EREL,FREQ,KAPPA,PI,WAVLEN,GDWAVL,U,V
      REAL*8 DELTA,DELTAB,FN,FN1,EX,EY,EZ,X,Y,Z,Z1
      REAL*8 GAMMA,GAMMA1,TEMP1,TEMP2,RN,QN,SIN1,COS1
      REAL*8 YMAX,ZMAX,YINC,ZINC,TEMP,SLOPE
      REAL*8 YPWR,ZPWR,AREA
C
      INTEGER N,NT,NFIN,N0
C
C ***************************************************************
C
C  LOAD THE WAVEGUIDE PARAMETERS
C
      CALL INPUT(S,N,D,B,FREQ,KAPPA)
C
C ***************************************************************
C
C     PUT CONFIGURATION DATA INTO THE FILES
C
      WRITE(91,700)
      WRITE(92,700)
      WRITE(93,700)
      WRITE(91,610) S,W,D,B
      WRITE(92,610) S,W,D,B
      WRITE(93,610) S,W,D,B
      WRITE(91,620) EREL,FREQ,KAPPA
      WRITE(92,620) EREL,FREQ,KAPPA
      WRITE(93,620) EREL,FREQ,KAPPA
      WRITE(91,700)
      WRITE(92,700)
      WRITE(93,700)
610   FORMAT(1X,'S = ',F9.7,'     W = ',F9.7,'     D =',F9.7,'     B =',F9.7)
620   FORMAT(1X,'EREL = ',F5.2,'     FREQ = ',F15.1,'     KAPPA = ',F20.15)
C
C***************************************************************
C
C  INITIALIZE THE CONSTANTS
C
      PI = 4*DATAN(1.0)
      EREL = 13.
      WAVLEN = 2.998E+08 / FREQ
      GDWAVL = KAPPA * WAVLEN
```

```
      V = DSQRT( 1/(KAPPA**2) - 1)
      U = DSQRT( EREL - 1/(KAPPA**2) )
      DELTA = W / B
      DELTAB = (S+W)/B
C
C   INITIALIZE THE USEFUL CONSTANTS
C
      N0 = 3881
      Z1 =  6.299 * 0.000001
      YINC = 25.0 * 0.000001
      ZINC = 5.0 * 0.000001
      YMAX = 500.0 * 0.000001
      ZMAX = 100.0 * 0.000001
      AREA = 125. * 1D-12
C
C
C*****************************************************************
C
C     ZERO THE POWER SUMMATIONS
C
      YPWR = 0.
      ZPWR = 0.
C
C*****************************************************************
C
C
C
C  ZERO THE FIELDS
C
200   Z = 100. * 0.000001
210   Y = 0. *  0.000001
220   EX = 0.
      EY = 0.
      EZ = 0.
C
      NT = N0 / (1 + (Z/Z1) )
C
C*****************************************************************
C  CALCULATE THE FIELDS
C
C
      M = 0
105   M = M + 1
          FN = DSQRT(1 + (2*B*V/(M*WAVLEN))**2 )
          FN1 = DSQRT(1 - (2*B*U/(M*WAVLEN))**2 )
          GAMMA = FN*M*PI/B
          GAMMA1 = FN1*M*PI/B
          TEMP1 = FN1/(EREL*FN)
          CALL INVTAN(TEMP1,RN)
          IF (RN .EQ. -10.) GOTO 30
          TEMP1 = FN/FN1
          CALL INVCTN(TEMP1,QN)
          IF (QN .EQ. -10.) GOTO 30
          GOTO 35
```

```
C
30        WRITE (43,725)
725       FORMAT(1X,'********************')
          NFIN=M
          GOTO 100
C
35        NFIN = M
          RN = RN + GAMMA1*D
          QN = QN + GAMMA1*D
C
      IF (Z .GT. 0.) GOTO 50
          TEMP = M*PI*DELTA/2
          SINC1=DSIN(TEMP)/TEMP
          SIN1=DSIN(M*PI*DELTAB/2)
          SIN2=DSIN(M*PI*Y/B)
          EY = EY + (SINC1*SIN1*SIN2*DEXP(GAMMA*Z))
          COS2=DCOS(M*PI*Y/B)
          EZ = EZ + (SINC1*SIN1*COS2*DEXP(GAMMA*Z)/FN)
          EX = 0.
          GOTO 100
C
50    IF (Z .GT. D) GOTO  75
          TEMP = M*PI*DELTA/2
          SINC1 = DSIN(TEMP)/TEMP
          SIN1 = DSIN(M*PI*DELTAB/2)
          COS2 = DCOS(M*PI*Y/B)
          TEMP1 = ( (1/DTANH(QN))-DTANH(RN))*DSINH(GAMMA1*Z)
          TEMP2 = (2*B/(M*GDWAVL))**2 + 1
          EX = EX + (SINC1*SIN1*COS2*TEMP1/(M*TEMP2))
C
          SIN2 = DSIN(M*PI*Y/B)
          TEMP1 = (2*B/(M*GDWAVL))**2
          TEMP2 = DTANH(RN) + (TEMP1/DTANH(QN))
          TEMP2 = DCOSH(GAMMA1*Z) - (DSINH(GAMMA1*Z)*TEMP2/(1+TEMP1))
          EY = EY + (SINC1*SIN1*SIN2*TEMP2)
C
          TEMP1 = DSINH(GAMMA1*Z) - (DTANH(RN)*DCOSH(GAMMA1*Z))
          EZ =EZ + (SINC1*SIN1*COS2*TEMP1/FN)
          GOTO 100
C
75    ZTEMP = Z
      Z = D
C
          TEMP = M*PI*DELTA/2
          SINC1 = DSIN(TEMP)/TEMP
          SIN1 = DSIN(M*PI*DELTAB/2)
          COS2 = DCOS(M*PI*Y/B)
          TEMP1 = ( (1/DTANH(QN))-DTANH(RN))*DSINH(GAMMA1*Z)
          TEMP2 = (2*B/(M*GDWAVL))**2 + 1
          EX = EX + (SINC1*SIN1*COS2*TEMP1/(M*TEMP2))
C
          SIN2 = DSIN(M*PI*Y/B)
          TEMP1 = (2*B/(M*GDWAVL))**2
          TEMP2 = DTANH(RN) + (TEMP1/DTANH(QN))
```

```
          TEMP2 = DCOSH(GAMMA1*Z) - (DSINH(GAMMA1*Z)*TEMP2/(1+TEMP1))
          EY = EY + (SINC1*SIN1*SIN2*TEMP2)
C
          TEMP1 = DSINH(GAMMA1*Z) - (DTANH(RN)*DCOSH(GAMMA1*Z))
          EZ =EZ + (SINC1*SIN1*COS2*TEMP1/FN)
C
      TEMP1 = DEXP( -GAMMA*(Z-D) )
      EX = EX * TEMP1
      EY = EY * TEMP1
      EZ = EZ * TEMP1
C
      Z = ZTEMP
C
100    CONTINUE
80    FORMAT(1X,'M = ',I4)
C
      IF (M .LT. NT) GOTO 105
C
      IF (NT .EQ. NFIN) GOTO 125
          WRITE(91,717)NFIN,NT
          WRITE(92,717)NFIN,NT
          WRITE(93,717)NFIN,NT
C
C
C
125   EX = 2*EX/CDWAVL
      EY =  2*EY/B
      EZ =  -2*EZ/B
      SLOPE = EY / EZ
      YPWR = YPWR + (AREA * (EY**2))
      ZPWR = ZPWR + (AREA * (EZ**2))
C
      WRITE(43,740) Y,Z,NFIN
C
C*****************************************************************************
C
C     WRITE DATA TO FILES AND SCREEN
C
      WRITE(43,700)
C
      WRITE(91,710) Y,Z,EY,YPWR,NFIN
      WRITE(92,715) Y,Z,EZ,ZPWR,NFIN
      WRITE(93,716) Y,Z,SLOPE,NFIN
C
      Y = Y + YINC
      IF (Y .LE. YMAX) GOTO 220
C
      WRITE(91,700)
      WRITE(91,702)
      WRITE(91,700)
      WRITE(92,700)
      WRITE(92,702)
      WRITE(92,700)
     WRITE(93,700)
```

```
      WRITE(93,702)
      WRITE(93,700)
       Z = Z + ZINC
       IF (Z .LE. ZMAX) GOTO 210
C
C
700    FORMAT(1X)
702    FORMAT(1X,'***   ***   ***   ***   ***   ***   ***   ***   *** ')
710    FORMAT(1X,'Y = ',F10.7,'     Z = ',F10.7,'     EY = ',F25.15,     -
     1 '     YPWR = ',F25.15,'     NT = ',I5)
715    FORMAT(1X,'Y = ',F10.7,'     Z = ',F10.7,'     EZ = ',F25.15,     -
     1 '     ZPWR = ',F25.15,'     NT = ',I5)
716    FORMAT(1X,'Y = ',F10.7,'     Z = ',F10.7,'     SLOPE = ',F20.10,  -
     1 '      NT = ',I5)
717    FORMAT(1X,'NEXT LINE:   NFINAL = ',I4,'     THEORY NTERM = ',I4)
720    FORMAT(1X,'EY = ',F25.15)
730    FORMAT(1X,'EZ = ',F25.15)
740    FORMAT(1X,'Y = ',F10.7,'     Z = ',F10.7,'     NFIN = ',I5)
C
C
       STOP
       END
C
C*************************************************************************
```

```
C*************************************************************************
C
C      THIS SUBROUTINE GETS THE COPLANAR WAVEGUIDE PARAMETERS
C
C*************************************************************************
C
      SUBROUTINE INPUT(S,W,D,B,FREQ,KAPPA)
C
      REAL*8  S,W,D,B,FREQ,KAPPA
C
      DATA Y/'Y   '/
C
5     WRITE(43,10)
      WRITE(43,20)
      READ(90,100) S
      S = S * .000001
      WRITE(43,30)
      READ(90,100) W
      W = W * .000001
      WRITE(43,40)
      READ(90,100) D
      D = D * .000001
      WRITE(43,50)
      READ(90,100) B
      B = B * .001
      WRITE(43,60)
      READ(90,100) FREQ
      FREQ = FREQ * 1000000000
      WRITE(43,70)
      READ(90,100) KAPPA
      WRITE(43,80)
      READ(90,110) QUES
C
      IF (QUES .EQ. Y) GOTO 5
      RETURN
C
10    FORMAT(1X)
20    FORMAT(1X,'ENTER SLOT WIDTH (MICRONS) : ')
30    FORMAT(1X,'ENTER GAP WIDTH (MICRONS) : ')
40    FORMAT(1X,'ENTER WAFER THICKNESS (MICRONS) : ')
50    FORMAT(1X,'ENTER B (MILLIMETERS) : ')
60    FORMAT(1X,'ENTER FREQUENCY (GHZ) : ')
70    FORMAT(1X,'ENTER KAPPA : ')
80    FORMAT(1X,'CHANGE PARAMETERS (Y/N) ? ')
C
100   FORMAT(G11.5)
110   FORMAT(A1)
C
      END
C
C*************************************************************************
```

```
C*************************************************************************
C
C       INVERSE HYPERBOLIC   TANGENT
C
C*************************************************************************
      SUBROUTINE INVTAN(X,Y)
C
      REAL*8  X,Y
C
      IF (1 .LE. X**2) GOTO 100
C
      Y = 0.5*ALOG( (1+X)/(1-X) )
      RETURN
C
100   WRITE(43,110)
      WRITE(43,115) X
      WRITE(43,120)
      WRITE(43,110)
      Y = -10.
      RETURN
C
110   FORMAT(1X)
115   FORMAT(1X,' X = ',F25.15)
120   FORMAT(1X,'****  INVALID ARCTANH  ****')
C
      END
C
C*************************************************************************
```

```
C*************************************************************************
C
C      INVERSE HYPERBOLIC COTANGENT
C
C*************************************************************************
C
      SUBROUTINE INVCTN(X,Y)
C
      REAL*8  X,Y
C
      IF (1 .GE. X**2) GOTO 100
C
      Y = 0.5*ALOG( (X+1)/(X-1) )
      RETURN
C
100   WRITE(43,110)
      WRITE(43,115) X
      WRITE(43,120)
      WRITE(43,110)
      Y = -10.
      RETURN
C
110   FORMAT(1X)
115   FORMAT(1X,' X = ',F25.15)
120   FORMAT(1X,'****  INVALID INVCTNH  ****')
C
      END
C
C*************************************************************************
```

Appendix E. Drawings of the Modulator Test Fixture

Modulator Test Fixture

Sketch of assembled fixture (7 pieces)

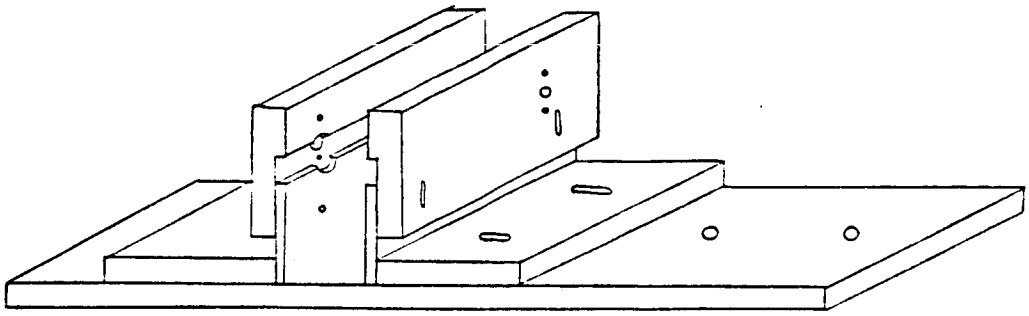

Drawn By: D. Materna 3-3379

Date: 9-24-86

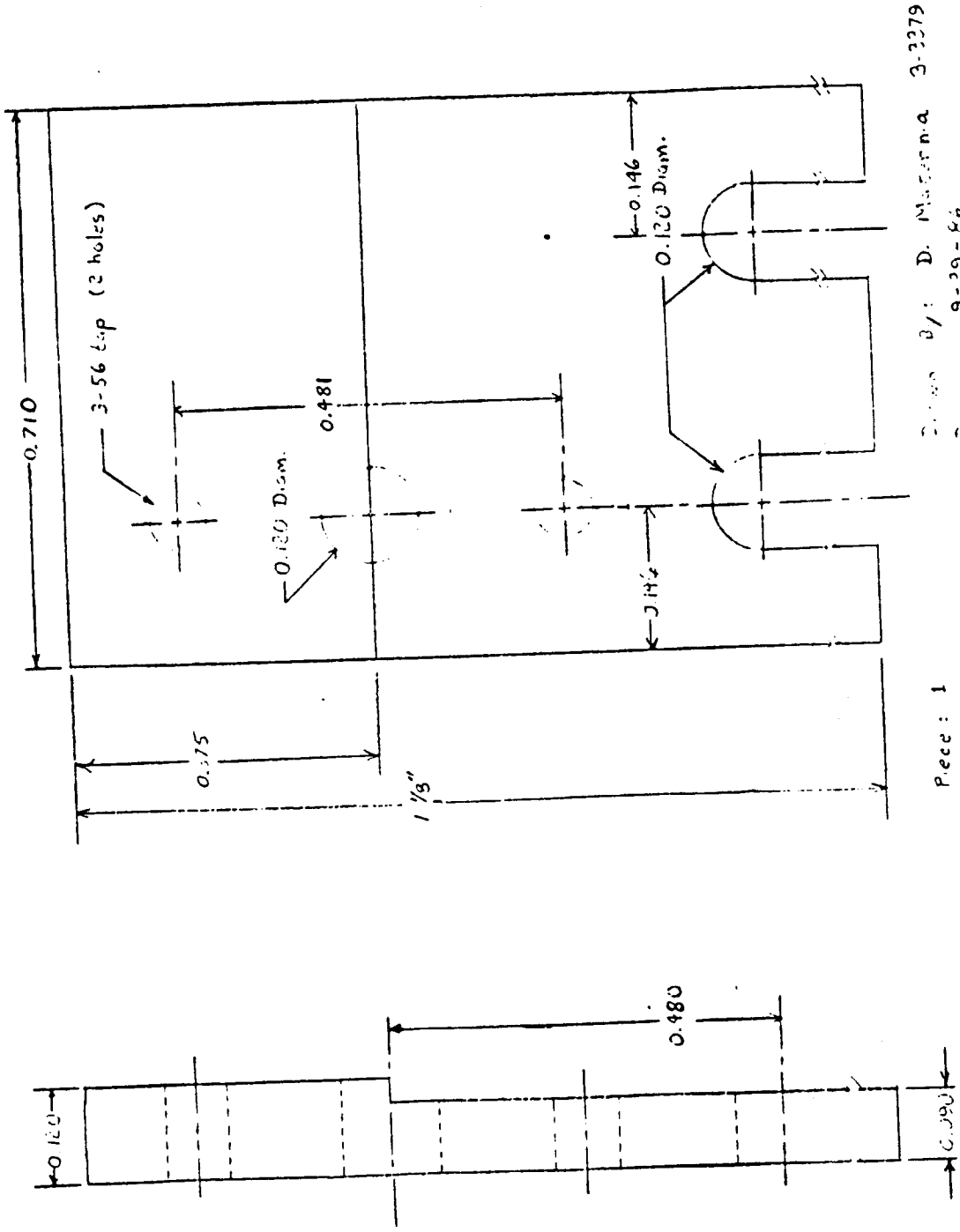

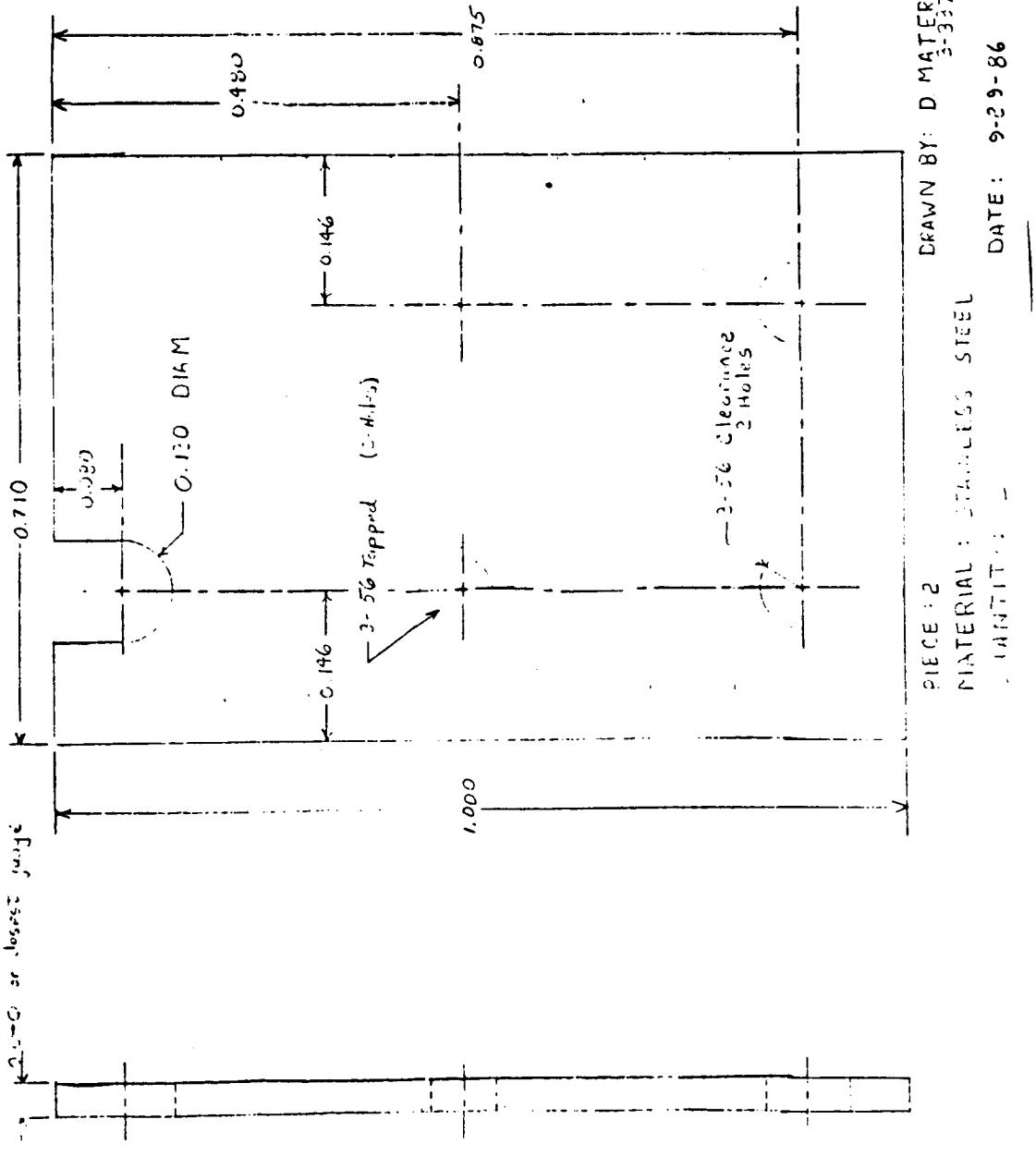

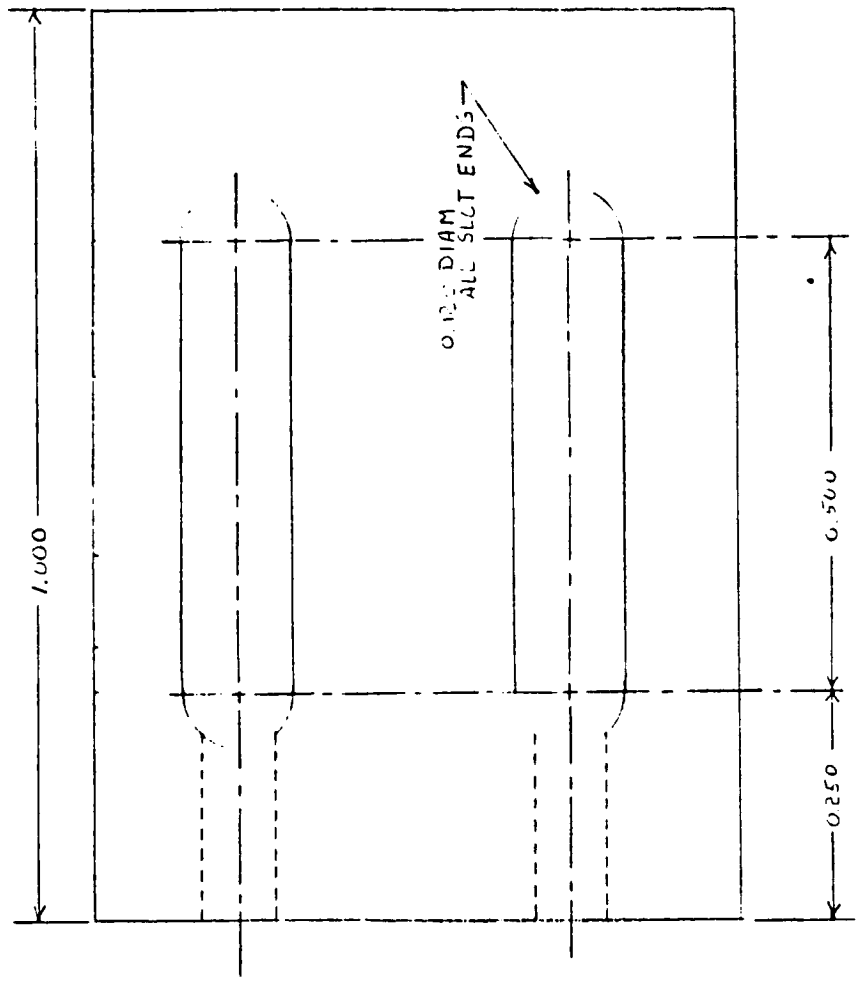

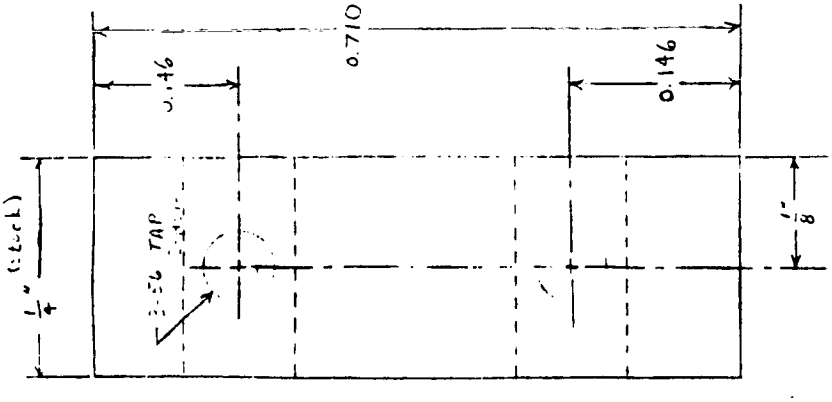

PIECE: 2
MATERIAL: BRASS
QUANTITY: 2

DRAWN BY: D. MATERNA 3-3379
DATE: 9-30-86

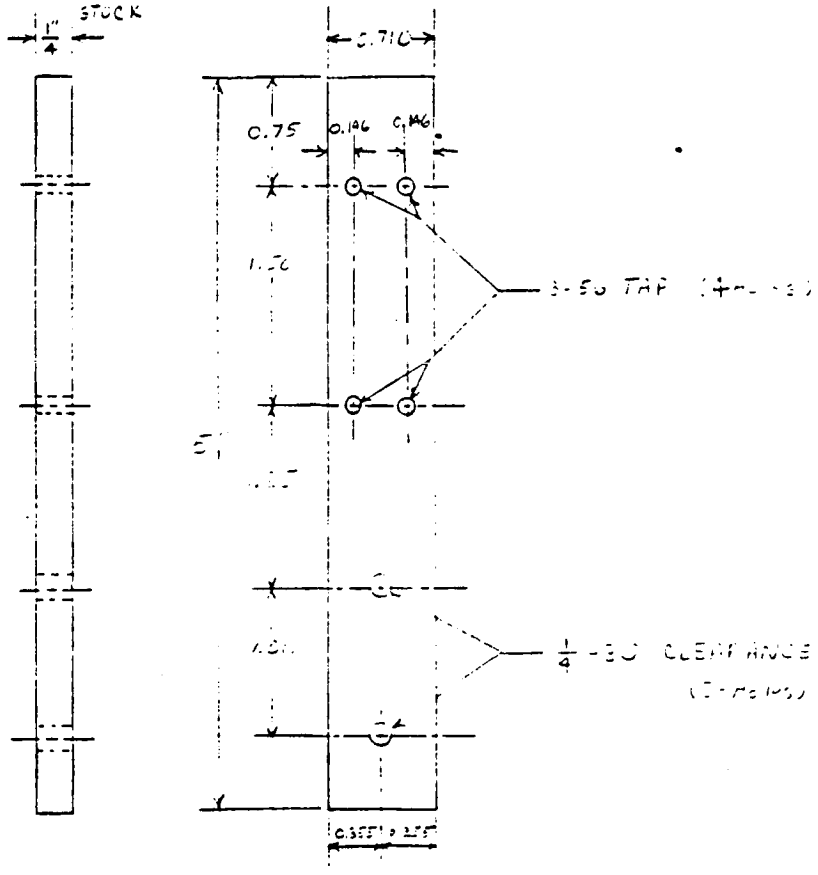

PIECE: 4
MATERIAL: BRASS
QUANTITY: 1

DRAWN BY: D. MATERNA (3-83)
DATE: 9-30-83

REFERENCES

1. H. Blauvelt and H. Yen, "Transmitter and Reciever Design for Microwave Fiber Optic Links", SPIE, vol. 477, Optical Technology for Microwave Applications, pp. 44-51, 1984.

2. C. M. Gee, G. D. Thurmond, and H. W. Yen, "Travelling Wave Electro-Optic Modulator", Applied Optics, vol. 22, no. 13, pp. 2034-37, July 1983.

3. C. M. Gee, G. D. Thurmond, and H. W. Yen, "17-GHz Bandwidth Electro-Optic Modulator", Applied Physics Letters, vol. 43, no. 1, pp. 998-1000, Dec. 1983.

4. C. M. Gee and G. D. Thurmond, "Wideband Travelling-Wave Electro-Optic Modulator", SPIE,

5. P. Buchmann, H. Kaufman, H. Melchoir, and G. Guekos, "Broadband Y-Branch Electro-Optic GaAs Waveguide Interferometer for 1.3 um", Appl. Phys. Lett., vol. 46, no. 5, pp. 462-464, 1 March 1985.

6. J. P. Donelly, N. L. DeMeo, G. A. Ferrante, and K. B. Nichols, "A High Frequency GaAs Optical Guided-Wave Electro-Optic Interferometric Modulator", IEEE J. Quantum Electron., vol. QE-21, no. 1, pp. 18-21, Jan. 1985.

7. S. H. Lin, S. Y. Wang, and Y. M. Houng, "GaAs PIN Electro-Optic Travelling-Wave Modulator at 1.3 um", Elec. Letts., vol. 22, no. 8. pp. 934-935, Aug. 1986.

8. T. R. Joseph, W. E. Stephens, and B. U. Chen, "Fiber Optic RF Links", SPIE, vol. 477, Optical Technology for Microwave Applications, pp. 52-56, 1984.

9. R. R. Kunath and K. B. Bhasin, "Optically Controlled Phased Array Antenna Concepts Using GaAs Monolithic Microwave Integrated Circuits", International IEEE AP-S/VRSI Symposium, Philadelphia, Pennsylvania, June 9-13, 1986.

10. H. R. Schlossberg, "Semiconductor Lasers, Detectors, and Optical Transmission Systems with Response from DC to Millimeter Waves", CLEO, paper THH1, pp. 262-263, June 1986.

11. J. P. Donelly, N. L. DeMeo, G. A. Ferrante, K. B. Nichols, and F. J. O'Donnell, "Optical Guides-Wave GaAs Monolithic Interferometer", Appl. Phys. Lett., vol. 45, no. 4, pp. 360-362, 15 Aug. 1984.

12. R. G. Huntsperger, Integrated Optics: Theory and Technology, 2nd. ed., (Springer Series in Optical Sciences, ed. by T. Tamir), Springer-Verlag, New York, p. 120, 1984.

13. A. Yariv, Optical Electronics, 3rd ed., Holt, Rinehart, and Winston, New York, pp. 274-305, 1985.

14. G. Keiser, Optical Fiber Communications, (McGraw Hill Series in Electrical Engineering, ed. by S. W. Director), McGraw-Hill, New York, p. 6, 1983.

15. S. M. Sze, Physics of Semiconductor Devices, 2nd ed., John Wiley & Sons, New York, pp. 850-851, 1981.

16. G. Lengyel, "GaAlAs p-i-n Junction Waveguide Modulator", IEEE J. Lightwave Tech., vol. LT-1, no. 1, pp. 251-255, March 1983.

17. P. C. Claspy, note set for EEAP 361: Lasers and Optics, Dept. of Electrical Engineering and Applied Physics, Case Western Reserve University, p. Spring 1986.

18. S. Namba, "Electro-Optic Effect of Zincblende", J. Optical Soc. Amer., vol. 51, no. 1, pp. 76-79, Jan. 1951.

19. H. A Haus, Waves and Fields in Optoelectronics, (Prentice-Hall Series in Solid State Physical Electronics, ed. by N. Holonyak, Jr.), Prentice-Hall, Engelwood Cliffs, New Jersey, pp. 327-338, 1984.

20. R. C. Alferness, "Waveguide Electro-Optic Modulators", IEEE Trans. Microwave Theory Tech., vol. MTT-30, no. 8, pp. 1121-37, Aug. 1982.

21. M. J. Adams, An Introduction to Optical Waveguides, John Wiley & Sons, New York, Chapters 2 and 6, 1981.

22. S. H. Lin, "Optimization of Optical Characteristics of Travelling-Wave Modulators", M.S. Thesis, Dept. of Electrical Engineering and Computer Science, Mass. Inst. of Tech., Boston, Mass., Jan. 1985.

23. C. Radens and J. T. Boyd, Dept. of Electrical and Computer Engineering, Univ. of Cincinnatti, Private Discussions, Mar.-Nov. 1986.

24. M. J. Sun and M. W. Muller, "Measurements on Four-Layer Isotropic Waveguides", Applied Optics, vol. 16, no. 4, pp. 814-815, April 1977.

25. L. D. Harris, Numerical Methods Using Fortran, Charles E. Merrill Books, Inc., Columbus, Ohio, pp.129-133, 1964.

26. C. Radens, Letter of 6 May 1986.

27. J. T. Boyd, "Theory of Parametric Oscillation Phase Matched in GaAs Thin Film Waveguides", IEEE J. of Quantum Elec., vol. QE-8, no. 10, pp. 788-796, Oct. 1972.

28. H. Sasak and N. Mikoshiba, "Normalized Power Transmission in Single Mode Optical Branching Waveguides", Elec. Letts., vol. 17, no. 3, pp. 136-138, 5 Feb. 1981.

29. R. N. Simons, NRC Fellow, NASA Lewis Research Center, Cleveland, Ohio, Private Communications, Jan.-Nov. 1986.

30. R. N. Simons, "Suspended Coupled Slot-Line Using Double Layer Dielectric", IEEE Trans. Microwave Theory Tech., vol. MTT-29, pp. 162-165, Feb. 1981.

31. R. N. Simons and R. K. Arora, "Coupled Slot Line Field Components", IEEE Trans. Microwave Theory Tech., vol. MTT-30, no. 7, pp. 1094-1099, July 1982.

32. J. L. Mertz and A. Y. Cho, "Low-Loss AlGaAs Waveguides Grown by Molecular Beam Epitaxy", Appl. Phys. Lett., vol. 28, no. 8, pp. 456-458, 15 April 1976.

33. W. T. Tsang,"MBE for III-V Semiconductors", Semiconductors and Semimetals, ed. by R. K. Willardson and A. C. Beer, Academic Press, New York, 1985.

34. S. M. Sze, VLSI Technology, (McGraw-Hill Series in Electrical Engineering, ed. by S. W. Director), McGraw Hill Book Co., New York, Chapters 7-9, 1983.

35. K. Inoue and H. Sakaki, "A New Highly Conductive (AlGa)As Selectively-Doped Double-Heterostructure Field-Effect Transistor (SD-DH-FET)", Japan Journ. Appl. Phys. Lett., vol. 23, no. 2, pp. L61-L63, Feb. 1984.

36. S. Schiller, U. Heisig, and S. Panzer, Electron Beam Technology, John Wiley & Sons, New York, Chapter 3, pp. 150-253, 1982.

37. W. D. Johnston and I. P. Kaminow, "Contributions to Optical Nonlinearity on GaAs as Determined from Raman Scattering Efficiencies", An Introduction to Electro-Optic Devices, ed. by I. P. Kaminow, Academic Press, New York, Chapter 11, p. 384, 1974.

38. W. C. Borland, D. E. Zelmon, C. J. Radens, J. T. Boyd, and H. E. Jackson, "Properties of Four-Layer Planar Optical Waveguides Near Cutoff", to be published.

39. R. E. Collin, Foundations for Microwave Engineering, (McGraw-Hill Physical and Quantum Electronics Series, ed. by H. Heffner and A. E. Siegman), McGraw-Hill Book Company, New York, p. 69, 1966.

1. Report No.	2. Government Accession No.	3. Recipient's Catalog No.
NASA CR-179573		

4. Title and Subtitle	5. Report Date
Investigation of a GaAlAs Mach-Zehnder Electro-Optic Modulator	January 1987
	6. Performing Organization Code

7. Author(s)	8. Performing Organization Report No.
David M. Materna	None
	10. Work Unit No. 506-44-21 307-51-00

9. Performing Organization Name and Address	11. Contract or Grant No.
Case Western Reserve University Dept. of Electrical Engineering and Applied Physics Cleveland, Ohio 44106	NCC 3-54
	13. Type of Report and Period Covered: Contractor Report Final

12. Sponsoring Agency Name and Address	14. Sponsoring Agency Code
National Aeronautics and Space Administration Lewis Research Center Cleveland, Ohio 44135	

15. Supplementary Notes

Project Manager, Kul B. Bhasin, Space Communications Division, NASA Lewis Research Center. This report was submitted as a thesis in partial fulfillment of the requirements for the Degree of Master of Science to Case Western Reserve University in January 1987.

16. Abstract

A GaAs modulator operating at 0.78-0.88 micron wavelength has the potential to be integrated with a GaAs/GaAlAs laser diode for an integrated fiber-optic transmitter. A travelling-wave Mach-Zehnder modulator using the electro-optic effect of GaAs and operating at a wavelength of 0.82 um has been investigated for the first time. A four layer Strip-loaded ridge optical waveguide has been analyzed using the effective index method and single mode waveguides have been designed. The electro-optic effect of GaAs has also been analyzed and a modulator using the geometry producing the maximum phase shift has been designed. A coplanar transmission line structure is used in an effort to tap the potentially higher bandwidth of travelling-wave electrodes. The modulator bandwidth has been calculated at 11.95 GHz with a required drive power of 2.335 Watts for full intensity modulation. Finally, some preliminary experiments were performed to characterize a fabrication process for the modulator.

17. Key Words (Suggested by Author(s))	18. Distribution Statement
Gallium arsenide; Gallium aluminum arsenide; Electro-optic; Modulation; Optical wave-guiding; Mach-Zehnder interferometers	Unclassified - unlimited STAR Category 32

19. Security Classif. (of this report)	20. Security Classif. (of this page)	21. No. of pages	22. Price*
Unclassified	Unclassified	167	A08

*For sale by the National Technical Information Service, Springfield, Virginia 22161